Edwards Statistical Mechanics for Jammed Granular Matter

Adrian Baule[1], Flaviano Morone[2], Hans J. Herrmann[3], and Hernán A. Makse[2]

[1] *School of Mathematical Sciences, Queen Mary University of London, London E1 4NS, UK*
[2] *Levich Institute and Physics Department, City College of New York, New York, New York 10031, USA*
[3] *ETH Zürich, Computational Physics for Engineering Materials, Institute for Building Materials, Wolfgang-Pauli-Str. 27, HIT, CH-8093 Zürich, Switzerland*

(Dated: June 14, 2016)

In 1989, Sir Sam Edwards made the visionary proposition to treat jammed granular materials using a volume ensemble of equiprobable jammed states in analogy to thermal equilibrium statistical mechanics, despite their inherent athermal features. Since then, the statistical mechanics approach to jammed matter – one of the very few generalizations of Gibbs-Boltzmann statistical mechanics – has garnered an extraordinary amount of attention by both theorists and experimentalists. Its importance stems from the fact that jammed states of matter are ubiquitous in nature appearing in a broad range of contexts such as granular materials, colloids, glasses, soft- and biomatter. Indeed, despite being one of the simplest states of matter – primarily governed by the steric interactions between the constitutive particles – a theoretical understanding based on first principles has proved exceedingly challenging. Here, we review a systematic approach to jammed matter based on the Edwards statistical mechanical ensemble. We discuss the construction of microcanonical and canonical ensembles based on the volume function, which replaces the Hamiltonian in jammed systems. The importance of approximation schemes at various levels is emphasized leading to quantitative predictions for ensemble averaged quantities such as packing fractions and contact force distributions. An overview of experiments, simulations, and theoretical models scrutinizing the strong assumptions underlying Edwards' approach is given, including tests of ergodicity, equiprobability of jammed microstates and extensivity of the associated granular entropy. A theoretical framework for packings whose constitutive particles range from spherical to non-spherical shapes like dimers, polymers, ellipsoids, spherocylinders or tetrahedra, hard and soft, frictional, frictionless and adhesive, monodisperse and polydisperse particles in any dimensions is discussed providing insight into an unifying phase diagram for all jammed matter. Furthermore, the connection between the Edwards' ensemble of metastable jammed states and metastability in spin-glasses is established. This highlights that the packing problem can be understood as a constraint satisfaction problem for excluded volume and force and torque balance leading to a unifying framework between the Edwards ensemble of equiprobable jammed states and out-of-equilibrium spin-glasses.

arXiv:1602.04369v3 [cond-mat.soft] 13 Jun 2016

CONTENTS

I. Introduction 2

II. Statistical Mechanics for jammed granular matter 4
- A. Definition of jammed states 5
- B. Metastability of the jammed states 5
- C. Edwards statistical ensemble for granular matter 7
- D. Volume ensemble 10
  1. Conventions for space tessellation 10
  2. Statistical mechanics of planar assemblies using quadrons 13
  3. Γ-distribution of volume cells 13
- E. Stress and force ensemble 15
  1. Force tilings 15
  2. Information entropy 15
  3. Maximum entropy of modified Edwards ensemble 16
  4. Force network ensemble 17
  5. Stress ensemble 17

III. Phenomenology of the jammed states and scrutinization of the Edwards ensemble 19
- A. Jamming in soft and hard sphere systems 19
  1. Isostaticity in jammed packings 19
  2. Packing of soft spheres 20
  3. Packing of hard spheres 22
  4. The nature of random close packing 24
  5. Force statistics 27
- B. Test of ergodicity and the flat assumption in Edwards ensemble 27
- C. Are there alternatives to Edwards' approach? 29

IV. Edwards volume ensemble 30
- A. Mean-field calculation of the microscopic volume function 30
- B. Packing of jammed spheres 33
- C. Packing of high-dimensional spheres 36
- D. Packing of discs 38
- E. Packing of bidisperse spheres 40

F. Packing of attractive colloids 42
G. Packing of non-spherical particles 44
1. Coarse-grained Voronoi volume of non-spherical shapes 46
2. Parametrization of non-spherical shapes 48
3. Dependence of coordination number on particle shape 48
H. Towards an Edwards phase diagram for all jammed matter 50

V. Jamming Satisfaction Problem, JSP 52
A. Cavity approach to JSP 53
B. Edwards flat hypothesis in the Edwards-Anderson spin-glass model 55
C. Opening Pandora's box: Test of Edwards flat hypothesis in the Sherrington-Kirkpatrick spin-glass model 58

VI. Conclusions and outlook 60

Acknowledgments 63

References 63

I. INTRODUCTION

Materials composed of macroscopic grains such as sand, sugar, and ball bearings are ubiquitous in our everyday experience. Nevertheless, a fundamental description of both static and dynamic properties of granular matter has proven exceedingly challenging. Take for example the pouring of sand into a sandpile, Fig. 1a. This process can be considered as a simple example of a fluid-to-solid phase transition of a multi-particle system. However, it is not clear whether this transition is governed by a variational principle of an associated thermodynamic quantity like the free energy in equilibrium systems. Granular materials do not explore different configurations in the absence of external driving because thermal fluctuations induce negligible particle motion at room temperature and inter-grain dissipation and friction quickly drain the kinetic energy from the system. On the other hand, the *jammed* state of granular matter bears a remarkable resemblance with an amorphous solid in thermal equilibrium: both are able to sustain a non-zero shear stress; the phase transition from liquid to solid states and the analogous *jamming transition* in grains are both governed by one or a few macroscopic control parameters; and, when using certain packing-generation protocols, macroscopic observables, such as the packing fraction, are largely reproducible.

Jamming transitions not only occur in granular media, but in many other soft materials such as colloids, emulsions, foams, structural glasses (e.g. silica glass), spin-glasses and biological materials. Even more broadly, the jamming transition pertains to a larger family of problems named Constraint Satisfaction Problems (CSP) (Krzakala and Kurchan, 2007). These problems involve finding the values of a set of variables satisfying simultaneously all the constraints imposed on those variables and maximizing (or minimizing) an objective function. For example, in the problem of sphere packings, the goal is to minimize the volume occupied by the packing subject to the geometrical constraint of non-overlapping particles and the mechanical constraints of force and torque balance at mechanical equilibrium. In general, packing problems play a central role in various fields of science in addition to physics, such as discrete mathematics, number theory and information theory. An example of utmost practical interest is the problem of efficient data transmission through error-correcting codes, which is deeply related to the optimal packing of (Hamming) spheres in a high-dimensional space (Conway and Sloane, 1999). The common feature of all packing problems is the existence of a phase transition, the jamming transition, separating the phase where the constraints are satisfiable from a phase where they are unsatisfiable.

The existence of constraints in physical systems causes, in general, a significant metastability, i.e., the phenomenon by which the system remains confined for a relatively long time in suboptimal regions of the phase space is related to the rough energy (or free energy) landscape, i.e. the presence of many non-trivially related minima as a function of the microscopic configurations (or the macroscopic states). Metastability is, indeed, the *leitmotiv* in most complex physical systems, whatever its origin. For example, in granular materials metastability arises from geometrical and mechanical constraints, but it is found also in spin glasses, which are magnetic systems with competing ferromagnetic and antiferromagnetic exchange interactions. In spin glasses, the emergence of metastability is due to frustration, which is the inability of the system to satisfy simultaneously all local ordering requirements. Notwithstanding their differences, these two physical systems, jammed grains and spin-glasses exhibit a remarkably similar organization of their metastable states, a fact that stimulates the search for further analogies within these systems and common explanations. It is, indeed, this analogue approach, as best exemplified by the encompassing vision of Sir Sam Edwards (Goldbart *et al.*, 2005), that may shed new light on the solution to jamming problems otherwise doomed to remain obscure.

Due to their substantial metastability, these systems are fundamentally out-of-equilibrium even in a macroscopically quiescent state. Nevertheless, the commonalities with equilibrium many body systems suggest that ideas from equilibrium statistical mechanics might be useful. In this review, we consider theories for jammed matter based on generalizations of equilibrium ensembles. These statistical mechanics-based approaches were pioneered by Sir Sam F. Edwards in the late 1980s (Fig. 1b).

Investigations of the structural properties of jammed packings are much older. In fact, the related problem of identifying the densest packing of objects with a par-

(a)

(b)

FIG. 1 **(a)** Pouring grains into a sandpile is the simplest example of a jamming transition from a flowing state to a mechanically stable jammed state. However, this simplicity can be deceiving. In this review we show that building sandpiles is at the core of one of the most profound problems in disordered media. From the glass transition to novel phases in anisotropic colloidal systems, pouring grains in a pile is the emblematic system to master with tremendous implications on all sort of soft materials, from glasses, colloids, foams and emulsions to biomatter. Edwards' endeavour to tame granular matter is condensed in the courageous attempt of measuring the 'temperature' of the sandpile. **(b)** Sir Sam F. Edwards, pictured here, first introduced the intriguing idea that a far-from-equilibrium, jammed granular matter could be described using methods from equilibrium statistical mechanics. In the Edwards' ensemble, macroscopic quantities are computed as flat averages over force- and torque-balanced configurations, which leads to a natural definition of a configurational 'granular' temperature known as the compactivity.

ticular shape represents one of the oldest scientific endeavours (Kepler, 1611; Weaire and Aste, 2008). Exact mathematical proofs of the densest packings are extremely challenging even for spherical particles. The Kepler conjecture of 1611 stating that the densest arrangement of spheres in three spatial dimensions (3d) is a face-centered-cubic (FCC) crystal with a packing volume fraction $\phi_{\rm fcc} = \pi/(3\sqrt{2}) \approx 0.74048...$ remained an unsolved mathematical problem for almost four centuries (Hales, 2005; Kepler, 1611). Systematic experiments on disordered hard-sphere packings began in the 1960s with the work by Bernal (Bernal, 1964; Bernal and Mason, 1960). These experiments are conceptually simple, yet give fundamental insight into the structure of dense liquids, glasses, and jammed systems. Equally sized spherical particles were placed into a container and compactified by shaking or tapping the system until no further volume reduction was detected. These experiments typically yielded configurations with packing fraction $\phi_{\rm rcp} \approx 0.64$, which is historically referred to as random close packing (RCP).

In order to apply a statistical mechanical framework to these jammed systems, it is first necessary to identify the variables characterizing the state of the system macroscopically. Clearly, the system energy is not suitable, since it may either not be conserved (for frictional dissipative particles) or not be relevant (for hard particles). On the other hand, an obvious state variable is the packing fraction, or, equivalently, the system volume. In fact, unlike in equilibrium systems, the volume in jammed systems is not an externally imposed fixed variable, but rather depends on the microscopic configuration of the grains. Edwards first extraordinary insight was to parametrize the ensemble of jammed states by the volume function $\mathcal{W}(\{\mathbf{r}_i, \hat{\mathbf{t}}_i\})$, as a function of the N particles' positions $\{\mathbf{r}_i\}$ and orientations $\{\hat{\mathbf{t}}_i\}$, as a replacement for the Hamiltonian in the equilibrium ensembles (Edwards and Oakeshott, 1989; Edwards, 1991, 1994; Mehta and Edwards, 1990).

A second crucial point in the development of the Edwards granular statistical mechanics is a proper definition of the jammed state. It is important to note that only jammed configurations $\{\mathbf{r}_i, \hat{\mathbf{t}}_i\}$ are included in the ensemble. A definition of what we mean by jammed state is not a trivial task and will be treated rigorously in the next section. Briefly, a jammed state satisfies the geometrical constraints imposed by hard-core interactions, force and torque balance of mechanical equilibrium and stability conditions on particle displacements defining a hierarchy of metastable jammed states. Assuming that an unambiguous definition of metastable jammed state can be expressed analytically, then a statistical mechan-

ics approach to granular matter proceeds by analogy with equilibrium systems. In this case, the volume function allows for the definition of a granular entropy leading to both microcanonical and canonical formulations of the volume ensembles. This implies, in particular, the existence of an intensive parameter conjugate to the volume. This temperature-like parameter was called *compactivity* by Edwards.

The Edwards ensemble is characterized by the macroscopic volume and stress of the packing. Since analytical treatments of the full ensemble are challenging, one typically considers suitable approximations. Neglecting correlations between the volume and the stress leads to a volume ensemble under the condition of isostaticity (Song *et al.*, 2008). The core of this review will be devoted to elaborate on a mean-field formulation of the Edwards volume ensemble that can potentially lead to a unifying phase diagram encompassing all jammed matter ranging from systems made of spherical to non-spherical particles, with friction or adhesion to frictionless particles, monodisperse and polydisperse systems and in any dimension. Likewise, we describe frameworks for stress and force statistics alone, such as the stress ensemble (Chakraborty, 2010; Henkes *et al.*, 2007), force network ensemble (Bouchaud, 2002; Snoeijer *et al.*, 2004; Tighe *et al.*, 2010), and belief propagation for force transmission (Bo *et al.*, 2014).

Edwards statistical mechanical ensemble rely on two assumptions: (i) Ergodicity and (ii) Equiprobability of microstates. These assumptions have been scrutinized in the literature, and the questions raised in this context will be reviewed here.

Despite these critiques, the Edwards' approach has been used to describe a wide range of jammed and glassy materials. Early works adopted the concept of inherent structures from glasses (Coniglio *et al.*, 2002; Coniglio and Herrmann, 1996; Coniglio and Nicodemi, 2000, 2001; Fierro *et al.*, 2002b) and effective temperatures (Ciamarra *et al.*, 2006; Cugliandolo, 2011; Kurchan, 2000, 2001; Makse and Kurchan, 2002; O'Hern *et al.*, 2004; Ono *et al.*, 2002) with applications to plasticity (Lieou and Langer, 2012). More recent approaches are based on replica theory for hard-sphere glasses (Parisi and Zamponi, 2010). Valuable insight is gained from models that exhibit both jamming and glass transitions (Ikeda *et al.*, 2012; Krzakala and Kurchan, 2007; Mari *et al.*, 2009). In this review, we also emphasize that the Edwards ensemble can be recast as a constraint satisfaction problems, which would allow for an unifying view of hard-sphere glasses and spin-glasses through a synthesis applied at the foundation of granular statistical mechanics.

This review is organized as follows. In Sec. II we discuss the foundations of the ensemble approach via the rigorous definition of metastable jammed states, and the construction of microcanonical and canonical ensembles based on the volume function and stress-moment tensor, which play the role of the Hamiltonian in jammed systems. In Sec. III results from experiments, simulations, and theoretical models that test the ergodic and flat assumptions underlying the ensemble approach are reviewed. In Sec. IV, we consider volume ensembles and their mean-field description, which provides quantitative predictions for ensemble averaged quantities such as the packing fraction of spherical and non-spherical particles. In Sec. V we elucidate a possible unification between the Edwards ensemble of jammed matter and theories based on ideas from glass/spin glass theories under the CSP paradigm. In Sec. VI we finally close with a summary and a collection of open questions for future work.

In recent years a number of reviews have appeared dealing with more specific aspects of granular matter: (Richard *et al.*, 2005) (granular compaction), (Makse *et al.*, 2005) (jammed emulsions), (Bi *et al.*, 2015; Chakraborty, 2010) (stress ensembles), (Tighe *et al.*, 2010) (force network ensemble), (Cugliandolo, 2011; Qiong and Mei-Ying, 2014) (effective temperatures). The present review is also complementary to other reviews on jammed granular matter, which do not specifically discuss the Edwards thermodynamics: (Alexander, 1998; Borzsonyi and Stannarius, 2013; van Hecke, 2010; Jaeger *et al.*, 1996; Kadanoff, 1999; Liu and Nagel, 2010; Parisi and Zamponi, 2010; Torquato and Stillinger, 2010). Rather than replacing these reviews, our work puts these topics into the general context of Edwards statistical mechanics and provides, in particular, an overview of the immense amount of literature related to Edwards ensemble approaches.

II. STATISTICAL MECHANICS FOR JAMMED GRANULAR MATTER

In a jammed system all particle motion is prevented due to the confinement by the neighbouring particles. The transition to a jammed state is thus not controlled by the temperature as conventional phase transitions in systems at thermal equilibrium, but by geometrical and mechanical constraints imposed by all particles in the system. Therefore, jammed states can be regarded as the set of solutions in the general class of Constraint Satisfaction Problems (CSP), which we term *Jamming Satisfaction Problem* (JSP), where the constraints are fixed by the mechanical stability of the blocked configurations of grains. From this standpoint, the jamming problem has a wider scope than the pure physical significance, encompassing the broader class of CSPs: the unique feature of the packing problem in the large universe of CSPs is that this system allows for a direct and relatively simple experimental test of theoretical predictions.

Thus, we formulate the Edwards ensemble of jammed states in the more general and modern framework of CSP, and we discuss how to construct specific solutions to the

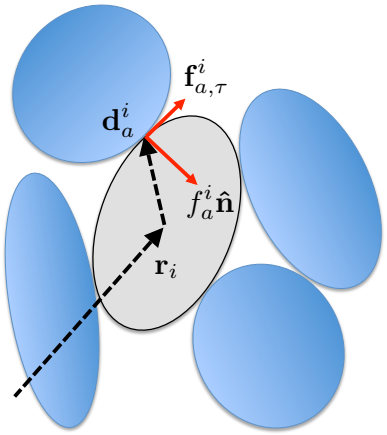

FIG. 2 Parametrization of a jammed configuration involving 5 non-spherical grains. The tangential $\mathbf{f}^i_{a,\tau}$ and normal force vectors $f^i_{a,n}\hat{n}^i_a$ at contact a on particle i are shown. d^i_a indicates the vector from the center of particle i to the contact point a between one of its neighbours. r_i gives the location of the center of particle i. The grey-shaded particle is mechanically stable if all forces and torques generated at the four contact points cancel (see Eqs. (2,3)).

granular case by reviewing several theories for jammed assemblies of athermal particles under the umbrella of the general statistical mechanical framework.

A. Definition of jammed states

We consider an assembly of N (for the sake of simplicity) monodisperse particles described by the configurations of the particles $\{\mathbf{r}_1, \hat{\mathbf{t}}_1; ...; \mathbf{r}_N, \hat{\mathbf{t}}_N\}$, where $\mathbf{r}_i$ denotes the ith particle's position (of its center of mass) and $\hat{\mathbf{t}}_i$ its orientation. The first problem we address concerns the definition of a blocked configuration of the particles, i.e, the jammed states. To be jammed the system has to satisfy both excluded volume and mechanical constraints. The excluded volume constraint enforces that particles do not overlap, and its mathematical implementation depends on the shape of the particles. For a system of monodisperse hard-spheres, this constraint takes on the following form:

$$|\mathbf{r}_i - \mathbf{r}_j| \geq 2R\ , \qquad \text{(equal-size spheres)} \qquad (1)$$

which means that the centers of any pair of particles i and j must be at a distance twice as large as their radius R. The hard-core constraint in Eq. (1) is valid only for monodisperse spheres, but it can be generalized to polydisperse and nonspherical particles.

The excluded volume constraint is necessary but not sufficient by itself to determine whether a configuration of particles is jammed. Indeed, it has to be supplemented by a constraint enforcing the mechanical stability of the system, requiring that particles satisfy the force and torque balance conditions. We denote by $\mathbf{d}^i_a$ the vector connecting $\mathbf{r}_i$ and the ath contact on the ith particle (Fig. 2). At this contact there is a corresponding force vector $\mathbf{f}^i_a$ on particle i arising from the contacting particle. With this notation we can formulate the conditions of force and torque balances for a particle of general shape:

$$\sum_{a\in\partial i} \mathbf{f}^i_a = 0, \qquad i = 1, ..., N \qquad (2)$$

$$\sum_{a\in\partial i} \mathbf{d}^i_a \times \mathbf{f}^i_a = 0, \qquad i = 1, ..., N \qquad (3)$$

where the notation ∂i denotes the set of contacts of particle i. Equations (2–3) apply to both frictional and frictionless particles. In the latter case there is only one single force component in the normal direction

$$\mathbf{f}^i_a = -f^i_a\hat{\mathbf{n}}^i_a \qquad \text{(frictionless)}, \qquad (4)$$

where $\hat{\mathbf{n}}^i_a$ denotes the normal unit vector at the contact point, which depends on the particle shape. For frictional particles, we can decompose $\mathbf{f}^i_a$ into a normal component $f^i_{a,n}$ and a force vector in the tangent plane $\mathbf{f}^i_{a,\tau}$ (see Fig. 2). Coulomb's law with friction coefficient μ is then expressed by the inequality

$$|\mathbf{f}^i_{a,\tau}| \leq \mu f^i_{a,n} \qquad \text{(frictional)}. \qquad (5)$$

If the interparticle forces are purely repulsive, as in most of the cases treated in this review, we also have the condition:

$$\mathbf{d}^i_a \cdot \mathbf{f}^i_a < 0. \qquad (6)$$

Finally, Newton's third law implies, that two particles i, j in contact at a satisfy:

$$\mathbf{f}^i_a = -\mathbf{f}^j_a. \qquad (7)$$

B. Metastability of the jammed states

Having defined the necessary and sufficient conditions for a granular system to be jammed, we now provide a finer description of jammed states, based on the concept of metastability, i.e., their stability with respect to particles displacements. A characterization similar to the one proposed here appeared already in (Torquato and Stillinger, 2001), where the authors defined the concept of jamming categories for metastable packings. The similarities with the classification of the jammed states in (Torquato and Stillinger, 2001) are discussed in parallel with the classification presented next.

To define properly the metastable jammed states we need to specify with respect to what type of displacements they are metastable. More precisely, if we start from an initially jammed state satisfying Eqs. (1)–(7) and

then displace a set of particles, how do we decide if the initial state is stable under this move? A helpful discriminant is the volume V or equivalently the volume fraction of the packing ϕ defined as the ratio of the volume occupied by the particles to the total volume of the system. Thus, consider again an initially jammed state, and assume you can displace only one particle at a time. If the volume fraction of the packing is not increasing whatever particle you move, then we may assert that the packing is stable against any single particle displacement. We call this type of jammed state a 1-Particle-Displacement (1-PD) metastable jammed state, which is defined as a configuration whose volume fraction cannot be increased by the displacement of one single particle, Fig. 3a. The definition of 1-PD metastable jammed states is similar to the definition of the *local* jamming category in (Torquato and Stillinger, 2001), stating that in a locally jammed configuration no particle can be displaced while keeping the positions of all other particles fixed.

We can now extend this definition to jammed states which are stable with respect to the simultaneous displacement of multiple particles. Specifically, we define a k-Particle-Displacement (kPD) metastable jammed state as a configuration whose volume fraction cannot be increased by the simultaneous displacement of any contacting subset of $1, 2, \ldots, k$ particles. Again, we find this definition quite similar to the definition of the *collective* jamming category in (Torquato and Stillinger, 2001), which states that in collectively jammed configurations no subset of particles can be simultaneously displaced so that its members move out of contact with one another and with the remaining set. Following the definitions given above a ground state of the system is a configuration whose volume fraction cannot be increased by the simultaneous displacement of any finite number of particles. A ground state of jamming corresponds to the $k \to \infty$ limit of a kPD metastable jammed state, the ∞-PD jammed ground state.

In the following section we will introduce the concept of volume function $\mathcal{W}(\mathbf{r})$ to parametrize the system volume as a function of the particles' positions. It is useful then to classify the kPD metastable jammed states in terms of the minima of this function. More precisely, we identify the kPD metastable jammed states as those states that satisfy the geometrical and mechanical constraints and are local minima of $\mathcal{W}(\mathbf{r})$. For example, 1PD metastable states are those configurations $\mathbf{r}^*$ for which $\mathcal{W}(\mathbf{r})$ is convex around $\mathbf{r}^*$ under 1-Particle-Displacements, but non-convex under k-Particle-Displacements with $k > 1$. Here, convex means that all the eigenvalues of the Hessian of $\mathcal{W}(\mathbf{r})$ evaluated at the configurations $\mathbf{r}^*$ are positive, while non-convex means that there exists at least one negative eigenvalue in the spectrum of the Hessian. Similarly, kPD metastable states are those configurations $\mathbf{r}^*$ for which $\mathcal{W}(\mathbf{r})$ is convex around $\mathbf{r}^*$ under any k'-Particle-Displacements with $k' \leq k$, and non-convex under any k'-Particle-Displacements with $k' > k$. A simple example of a 1-PD metastable jammed state is shown in Fig. 3(a).

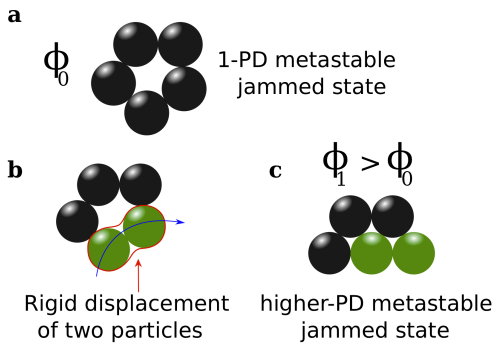

FIG. 3 (a) Example of a 1-Particle-Displacement jammed state: no particle can increase the volume fraction by displacing itself while keeping the others fixed in their positions. It is assumed that a membrane is keeping the particles in place or that they are surrounded and kept in place by a rigid container. (b) Simultaneous displacement of two particles: to escape the 1-PD metastable trap, two contacting particles must be displaced while keeping the others fixed in their positions. (c) Higher order metastable jammed state: after the move in (b), a new metastable jammed state is reached having higher stability than the original one in (a).

Interestingly, in spin-glass systems the (energetically) metastable states can be defined in a similar way, not with respect to volume but with respect to energy. The analog of the 1PD metastable jammed state is, for a spin glass, the 1-spin-flip (1SF) metastable state, defined as a configuration whose energy cannot be lowered by the flip of any single spin. Similarly the k-spin-flip (kSF) metastable state, akin to the kPD metastable jammed state, is a configuration whose energy cannot be lowered by the flip of any cluster of $1, 2, \ldots, k$ spins. Moreover, for spin glasses, several rigorous results on metastable states are known, including their probabilities, basins of attraction, and how they are sampled by various dynamics (Newman and Stein, 1999). These results are explained in detail in Section V along with their granular counterpart. The analogy between grains, hard-sphere glasses, and spin glasses has been nicely reviewed in (Dauchot, 2007) and is described in Table I.

Now that we have a rigorous definition for the jammed states and their metastable classification, we address the crucial problem of how to describe their statistical properties. Consider a granular material undergoing vertical tapping. After tapping, the system relaxes into a jammed state. Subsequent tapping will allow the system to explore other jammed states. An important question is: how does the tapping dynamics sample jammed states, or what is the probability measure for jammed states obtained from tapping? We will discuss the Edwards hypothesis of a flat probability measure for jammed states

in the next section.

C. Edwards statistical ensemble for granular matter

In 1989 Edwards made the remarkable proposal that the macroscopic properties of static granular matter can be calculated as ensemble averages over equiprobable jammed microstates controlled by the system volume (Edwards and Oakeshott, 1989). The thermodynamics of powders was created with this claim (Edwards, 1994): *"We assume that when N grains occupy a volume V they do so in such a way that all configurations are equally weighted. We assume this; it is the analog of the ergodic hypothesis of conventional thermal physics."*

This idea is very suggestive because it turns a complicated dynamical problem into a relatively simpler equilibrium problem. Indeed Edwards idea of using a thermodynamic approach to study amorphous states of condensed matter has been also adopted by several authors in the glass community to study amorphous packings as the infinite pressure limit of metastable glassy states described by equilibrium statistical mechanics (Parisi and Zamponi, 2010). In a sense this amounts to make an assumption á la Edwards at the (supercooled) liquid level, i.e. taking flat averages over metastable glassy states, supplemented by the additional assumption that each metastable glassy state can be followed down to the jammed state by compressing very fast. Even more, it turns out that mean-field glass models relaxing at zero temperature have exactly Edwards ergodicity property (Kurchan, 2001): at long times any nonequilibrium observable is correctly given by the typical value it takes over all local energy minima of the appropriate energy density.

The original idea put forward by Edwards was basically to take the flat average at the end, i.e., in the jammed state. After all we have no liquid state in granular matter, we just pour grains and they immediately jam.

Therefore, granular matter should be amenable to an equilibrium statistical mechanical treatment, where the role of energy is played by the volume, and all the jammed states at a fixed volume are equally probable. In granular assemblies consisting of dry particles in a size range above a few microns, the thermal energy at room temperature can be neglected and neither equilibrium entropy nor free energy can be used as thermodynamic potentials to describe the system. Nevertheless, for large enough particle numbers, statistical ideas seem relevant: Macroscopic observables such as the packing fraction are robustly reproduced. If operations manipulating individual particles are neglected, granular assemblies are thus described by well defined macrostates that correspond to many different microscopic configurations. Instead of the energy, one can equivalently take the volume as the key variable characterizing the macrostate of a static assembly. S. F. Edwards insight has suggested to consider the volume of a granular assembly analogous to the energy of an equilibrium system: Unlike in typical equilibrium systems, the volume is not an externally fixed parameter, but depends on the microscopic configuration of the particles including positions and orientations. This suggests to introduce a volume function $\mathcal{W}(\{\mathbf{r}_i, \hat{\mathbf{t}}_i\})$ giving the system volume as a function of the particles' positions $\mathbf{r}_i$ and orientations $\hat{\mathbf{t}}_i$ equivalent to the Hamiltonian $\mathcal{H}(\{\mathbf{p}_i, \mathbf{r}_i\})$, $i = 1, ..., N$.

With this analogy, all concepts of equilibrium statistical mechanics can be carried over into the realm of non-thermal static granular systems opening the door for the use of thermal concepts for athermal systems, i.e., there is a whole new statistical mechanics emerging from the point which, in conventional, thermal, statistical mechanics corresponds to $T = 0$, $S = 0$ (Edwards, 2008).

This review is devoted to the consequences of this idea emanating from the great insight of Sir Sam Edwards. For an in-depth treatment of equilibrium statistical mechanics we refer to standard textbooks (Huang, 1987; Landau and Lifshitz, 1980; Pathria and Beale, 2011). In particular, one can introduce the concept of a granular entropy $S(V)$ as a measure of the number of microstates $\Omega(V)$ for a given fixed volume V

$$S(V) = \lambda \log \Omega(V), \tag{8}$$

$$\Omega(V) = \int \mathrm{d}\mathbf{q}\, \delta(V - \mathcal{W}(\mathbf{q}))\Theta_{\mathrm{jam}}. \tag{9}$$

Here, we use the shorthand notation $\mathbf{q} = \{\mathbf{r}_i, \hat{\mathbf{t}}_i\}$ and $\int \mathrm{d}\mathbf{q} = \prod_{i=1}^{N} \int \mathrm{d}\mathbf{r}_i \oint \mathrm{d}\hat{\mathbf{t}}_i$. The parameter λ ensures the correct dimension of S as volume (set to unity in the following).

The function Θ_{jam} in Eq. (9) is crucial. It is there to admit only microstates in the ensemble that are jammed by enforcing the excluded volume and mechanical stability constraints in Eqs. (1)-(7). Only these rigid states lead to a static assembly at fixed volume. While this function has been treated lightly in earlier studies of Edwards thermodynamics, it contains most of the interesting physics of the problem and therefore will be treated carefully in the remaining of this review.

The Edwards' measure Θ_{jam} is exactly the uniform measure over the solutions of the Jamming Satisfaction

	Granular matter	Hard-Sphere Glasses	Spin-Glasses
Thermodynamic descriptor	Volume function $\mathcal{W}(\mathbf{q})$	Density functional $\mathcal{S}[\rho(\mathbf{r})]$	Hamiltonian $\mathcal{H}(\boldsymbol{\sigma})$
Lagrange multiplier	Compactivity X	Replica number m	Temperature T
Entropy	Edwards entropy $S(V)$	Configurational entropy Σ	Complexity Σ
Metastable states	Minima of $\mathcal{W}(\mathbf{q})$ + jamming constraint	Minima of $\mathcal{S}[\rho(\mathbf{r})]$	Minima of $\mathcal{H}(\boldsymbol{\sigma})$
Local metastable	1-Particle-Displacement	$\phi_{\rm th}$	1-Spin-Flip
Collective metastable	k-Particle-Displacement	$\phi \in (\phi_{\rm th}, \phi_{\rm gcp})$	k-Spin-Flip
Global (ground state)	∞-Particle-Displacement	$\phi_{\rm gcp}$	∞-Spin-Flip

TABLE I Synoptic view of unifying framework to understand the thermodynamics, relevant observables and classification of metastable states in granular matter, hard-sphere glasses and spin-glasses.

Problem (JSP), which reads (Bouchaud, 2002):

$$\begin{aligned}
\Theta_{\rm jam} = & \prod_{i,j=1}^{N} \theta\Big(|\mathbf{r}_i - \mathbf{r}_j| - 2R\Big) && \text{hard}-\text{core (spherical)} \\
& \times \prod_{i=1}^{N} \delta\left(\sum_{a\in\partial i} \mathbf{f}_a^i\right) && \text{force balance} \\
& \times \prod_{i=1}^{N} \delta\left(\sum_{a\in\partial i} \mathbf{d}_a^i \times \mathbf{f}_a^i\right) && \text{torque balance} \\
& \times \prod_{i=1}^{N} \prod_{a\in\partial i} \theta\left(\mu f_{a,n}^i - |\mathbf{f}_{a,\tau}^i|\right) && \text{Coulomb friction} \\
& \times \prod_{i=1}^{N} \prod_{a\in\partial i} \theta\left(-\mathbf{d}_a^i \cdot \mathbf{f}_a^i\right) && \text{repulsive forces} \\
& \times \prod_{\text{all contacts } a} \delta(\mathbf{f}_a^i + \mathbf{f}_a^j) && \text{Newton } 3^{\rm rd} \text{ law} .
\end{aligned} \tag{10}$$

Implicit in this microcanonical description is again the underlying assumption of equiprobability: The distribution of jammed configurations $\mathbf{q}$ at a given volume is uniform:

$$P_{\rm mic}(\mathbf{q}) = \Omega(V)^{-1}\delta(V - \mathcal{W}(\mathbf{q}))\Theta_{\rm jam}. \tag{11}$$

The definition of $\Theta_{\rm jam}$ deserves a crucial clarification. According to the classification of metastable jammed states given previously, when constructing the volume ensemble we have to specify what type of metastable jammed states we are considering at the fixed volume V. The crucial point is that k-PD jammed states are fundamentally different for different values of k, and hence there is no reason, in principle, to assign them the same statistical weight across all the values of k. In other words, when we fix the volume V, we consider as equiprobable only the jammed state corresponding to the same metastable class, i.e., with the same k. This is evident in the language of jammed categories: a locally jammed state (=1-PD) is substantially different from a collectively jammed state (=k-PD), and cannot be claimed, *a priori*, that they are found with equal probability in a tapping experiment, even if they may have the same density. Identical situation applies to metastable states in spin-glasses and disordered ferromagnets where the equiprobability of the metastable states has been rigorously studied (Newman and Stein, 1999).

This clarification is very important, and indeed it is at the origin of many headaches when trying to prove or disprove Edwards conjecture. Even if this condition did not appear in the original formulation by Edwards, it is nevertheless a quite obvious requirement, specially in

light of analogous exact results in spin-glasses and hard-sphere glasses (Newman and Stein, 1999; Parisi and Zamponi, 2010). The reason to not make explicit this further condition was presumably the feeling of Edwards that the jammed states that only matter in granular media are the ones corresponding to $k = \infty$, i.e. the "ground states" (see however (Edwards *et al.*, 2004) for a more detailed discussion). Here, we extend Edwards idea also to jammed states with $k < \infty$. Summing it up, the correct reading of the assumption about the probability measure over jammed states must take into account the restriction to the states within the same k-PD class, a condition that must be included in the definition of $\Theta_{\rm jam}$ as an additional constraint. In practice this can be done after having defined the volume function of the system, which provides an unambiguous definition of mechanically metastable states via its convexity, much in the same way as for spin-glasses, the Hamiltonian allows one to properly define the energetically metastable states, i.e. its local minima (Newman and Stein, 1999). This topic will be discussed in detail in Section V.

In principle the Edwards conjecture can be correct or not, and a case-by-case analysis is required to establish its validity. This is due to the fact that granular matter is profoundly out of equilibrium, since thermal fluctuations are essentially absent for the macroscopic length scales considered. The difference with equilibrium Hamiltonian systems is that Liouville's theorem for the conservation of phase space volume under time evolution (the cornerstone of conventional equilibrium statistical mechanics) does not hold for granular systems, which are in general characterized by nonzero phase space compressibility. The reason is the strongly dissipative nature of granular assemblies, which are dominated by static frictional forces; although an intuitive proof for the use of $\mathcal{W}$ in granular thermodynamics has been sketched by the analogous proof of the Boltzmann equation (H-theorem) (Edwards *et al.*, 2004).

Nevertheless, the Edwards ensemble approach has proven exceedingly useful in characterizing the properties of these athermal states of matter and continues to intrigue both experimentalists and theoreticians alike.

In this ensemble, statistical averages of observables are assumed to be equal to time averages over single trajectories, provided the actual dynamics is ergodic. This can be induced by some external drive, such as infinitesimally small tapping or very slow shearing. Since the drive induces fluctuations of the packing configuration, and thus fluctuations of the volume, one can similarly introduce a canonical picture (without change in particle number). The analogue of temperature is called compactivity X, whose inverse is the derivative of the granular entropy

$$X^{-1} = \frac{\partial S(V)}{\partial V}. \tag{12}$$

For a real granular system, the compactivity can be thought of as a measure of how more compact the system can possibly be. Large values of X indicate a loose or "fluffy" (but mechanically stable) configuration, whose volume could be reduced further under rearrangement.

The canonical distribution follows from the maximization of the Gibbs entropy just as in thermal equilibrium under the constraint of a fixed average volume

$$V = \int \mathrm{d}\mathbf{q}\, \mathcal{W}(\mathbf{q})\, P_{\rm can}(\mathbf{q}) \ , \tag{13}$$

and has the standard Gibbs form and canonical partition function:

$$P_{\rm can}(\mathbf{q}) = \frac{1}{\mathcal{Z}} e^{-\mathcal{W}(\mathbf{q})/X} \Theta_{\rm jam}, \tag{14}$$

$$\mathcal{Z} = \int \mathrm{d}\mathbf{q}\, e^{-\mathcal{W}(\mathbf{q})/X} \Theta_{\rm jam}. \tag{15}$$

If we follow the analogy with equilibrium thermodynamics, the concepts of granular entropy and compactivity translate into postulated laws of a granular thermodynamics (Edwards *et al.*, 2004):

Zeroth law. A consistent picture of compactivity as a temperature-like parameter requires the notion of equilibration: Two systems in physical contact should equilibrate to the same compactivity. The required "volume" transfer is achieved by the external drive, but needs to avoid any mixing of the particles.

First law. The analogy with granular matter is not clear as a distinction between heat and work is not useful for jammed granular materials.

Second law. In any natural process, the granular entropy always increases. The second law forms the basis of Edwards statistical mechanics.

Third law. Our qualitative discussion of compactivity suggests that entropy should thus be a monotonically increasing function of X: Loose packings at high X can be realized in many more configurations than dense packings at low X. In the limit $X \to 0$ we can thus postulate that $S(V) \to$ const. The limiting entropy will be finite for any disordered arrangement, while $S(V) = 0$ is only achieved for a fully ordered crystal structure.

Up to know we have considered only the volume V as the relevant variable to characterize the jammed state of a granular system. However, this is not the general case. Indeed, when the system is shaken the grains will fill a volume V and exert a stress $\hat{\Sigma}$ on the boundary. Shaking after shaking, the system explores presumably typical configurations in the configuration phase space, which are subject to the constraint on V and also on $\hat{\Sigma}$. Consequently, the entropy of the system $S(V, \hat{\Sigma})$ must then be computed as a function of those observables, which in the microcanonical ensemble can be defined as

$$S(V, \hat{\Sigma}) = \log \int \mathrm{d}\mathbf{q}\, \delta(V - \mathcal{W}(\mathbf{q}))\, \delta(V\hat{\Sigma} - \hat{\Phi}(\mathbf{q}))\Theta_{\rm jam} \tag{16}$$

where

$$\hat{\sigma}_i = \sum_{a\in\partial i} \mathbf{d}_a^i \otimes \mathbf{f}_a^i \tag{17}$$

is the stress tensor associated with particle i and the sum

$$\hat{\Phi} = \sum_{i=1}^{N} \hat{\sigma}_i = \sum_{i=1}^{N}\sum_{a\in\partial i} \mathbf{d}_a^i \otimes \mathbf{f}_a^i. \tag{18}$$

is the macroscopic force-moment tensor.

In analogy to the volume ensemble, there should thus exist a temperature-like Lagrange multiplier associated with the stress. Since $\hat{\Sigma}$ is a tensor, this quantity is also a tensor, which can be defined as

$$\hat{\Lambda}_{ij} = V\frac{\partial\hat{\Sigma}_{ij}}{\partial S}. \tag{19}$$

The tensor $\hat{\Lambda}$ is referred to as angoricity from the Greek word *ankhos* for stress (Blumenfeld and Edwards, 2009).

A simplification occurs if the stress $\hat{\Sigma}$ is a simple hydrostatic pressure $\hat{\Sigma} = p$. In this case the angoricity degenerates to the scalar quantity $\Lambda = V\partial p/\partial S$.

Considerable progress in a theoretical description of granular matter could be achieved from pure volume and stress/force ensembles, which appear as limits of the full description Eq. (16). We discuss these in detail in the following. Recently, it has been suggested that volume and stress ensembles are necessarily interdependent, which would require more sophisticated approaches to deal with their correlations (Blumenfeld *et al.*, 2012). It has also been suggested that the the volume function is not suitable as the central concept for a statistical mechanical approach, since it neglects structural degrees of freedom. An alternative connectivity function has been proposed in (Blumenfeld *et al.*, 2016).

D. Volume ensemble

Pure volume ensembles neglect the force degrees of freedom. This is reasonable, e.g., in isostatic systems, where all forces are uniquely determined from the configurational degrees of freedom. In this case, the statistical volume ensemble is fully specified by the volume function Eq. (14), which relies on a suitable space tessellation. The most natural tesselation of the space is the Voronoi construction, which is the base of most of the work developed here. Below, we also review other approaches of relevance in historical order.

1. Conventions for space tessellation

The Edwards ensemble is centred around the concept of a volume function playing the role of the Hamiltonian. In the case of a Hamiltonian there is a unique way to define the energy as a function of the particle configurations, typically in terms of a superposition of all particles' individual kinetic and potential energy plus the energy contribution due to interactions. Such a decomposition is not straightforward in the case of the volume function. Nevertheless, it is natural to express $\mathcal{W}$ in the form of a superposition

$$\mathcal{W}(\mathbf{q}) = \sum_{i=1}^{N} \mathcal{W}_i(\mathbf{q}) \tag{20}$$

of non-overlapping volume elements that tesselate the space occupied by the packing. $\mathcal{W}_i$ is the volume associated with each of the N particles. Crucially, this volume is not a function of the configuration of the ith particle only. Naively, one could imagine that $\mathcal{W}_i$ depends solely on the configurations of particles in the first coordination shell. However, such a restriction is mathematically not sufficient and does not apply in general, e.g., in the Voronoi tesselation. The collective nature of the systems' response to perturbations induces dependencies on particles further away. Moreover, even if one considers only particles in the first coordination shell as a first approximation, a precise definition of $\mathcal{W}_i$ is not straightforward. The key problem is to reference individual particles, so that their neighbours can be defined. While this is easily achieved in a regular crystalline packing, the difficulties originating from a disordered contact network have been realized early on in Refs. (Edwards and Oakeshott, 1989; Mounfield and Edwards, 1994). Below we review the different definitions of $\mathcal{W}_i$ in historical order.

a. Tensorial formulation A first solution to the problem of defining $\mathcal{W}(\mathbf{q})$ was proposed in (Edwards and Grinev, 2001a). Introducing the tensor (Edwards and Grinev, 1999a,b)

$$\hat{F}_i = \sum_{j\in\partial i} \mathbf{r}_{ij} \otimes \mathbf{r}_{ij}, \tag{21}$$

where $\mathbf{r}_{ij}$ is the separation vector of particles i and j, we can define the volume associated with particle i as

$$\mathcal{W}_i = 2\sqrt{\det \hat{F}_i}. \tag{22}$$

Equation (22) only involves contacting particles. The resulting total volume $\mathcal{W} = \sum_{i=1}^{N} \mathcal{W}_i$ is thus only an approximation of the exact volume occupied by all N particles. Formal corrections that allow for an exact definition of $\mathcal{W}$ have been suggested, but the quantities specifying correlations of tensors belonging to nearest neighbours are intractable for any practical purposes (Edwards and Grinev, 2001a).

b. Quadrons In 2d, a definition of $\mathcal{W}_i$, such that Eq. (20) is exact (it has been noted that this is only true in the absence of non-convex voids, which are actually present in

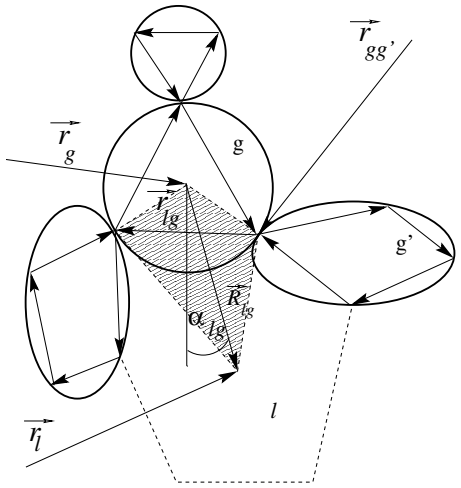

FIG. 4 Illustration of grain and void loops. The vector $\mathbf{r}_{lg}$ denotes the part of the grain loop connecting the contact points of particle g. $\mathbf{r}_{lg}$ is also part of the void loop l centred at $\mathbf{r}_l$. The vector $\mathbf{R}_{lg}$ connects the center of particle g and the center of the void l. The grey area denotes the quadrilateral (quadron) formed by $\mathbf{r}_{lg}$ and $\mathbf{R}_{lg}$. Its area can be expressed in terms of the angle α_{lg}. The collection of all quadrons tesselates the total area of a 2d packing. Figure reprinted with permission from (Blumenfeld and Edwards, 2003).

a gravitational field (Ciamarra, 2007)), can be obtained by analysing planar packings in terms of loops and voids (Ball and Blumenfeld, 2002; Blumenfeld and Edwards, 2003). In (Ball and Blumenfeld, 2002) two types of loops have been defined: *(i)* Grain loops defined by the vectors connecting adjacent contact points in a clockwise way; *(ii)* The vectors defining the grain loops also define loops in an anticlockwise way around the voids of the packing (void loops, see Fig. 4). We then denote by $\mathbf{r}_{lg}$ the vector that is part of the grain loop of particle g and adjacent void loop l, and by $\mathbf{R}_{lg}$ the vector connecting the center of particle g and the center of the void l. With these conventions we define the tensor (Ball and Blumenfeld, 2002)

$$\hat{C}_g = \sum_l \mathbf{r}_{lg} \otimes \mathbf{R}_{lg}. \tag{23}$$

The antisymmetric part of $\hat{C}_g$ can then be expressed as $\mathcal{W}_g\hat{\epsilon}$, where $\hat{\epsilon} = \begin{pmatrix} 0 & 1 \\ -1 & 0 \end{pmatrix}$. The particle volumes $\mathcal{W}_g$ defined in this way tessellate the plane. More specifically, we can write $\mathcal{W}_g = \sum_{l=1}^{z_g} A_{lg}$, where A_{lg} is the area of the quadrilateral formed by $\mathbf{r}_{lg}$ and $\mathbf{R}_{lg}$: $A_{lg} = \mathbf{r}_{lg} \times \mathbf{R}_{lg}/2$ and z_g is the coordination number of the grain.

If we introduce an index n that labels each of the quadrilaterals A_{lg}, we can also express the total volume as (Blumenfeld and Edwards, 2003)

$$\mathcal{W} = \frac{1}{2}\sum_n \mathbf{r}_n \times \mathbf{R}_n = \frac{1}{2}\sum_n r_n R_n \cos(\alpha_n), \tag{24}$$

where the angle $\alpha_n = \alpha_{lg}$ is defined in Fig. 4. The elementary area tesselating quadrilateral elements are also referred to as quadrons.

In 2d one can show that the number of quadrons is identical to the number of configurational degrees of freedoms (Blumenfeld and Edwards, 2003, 2006), motivating the use of the quadrons as the elementary "particles" of the system on which the statistical mechanics is based. In 3d this coincidence is no longer valid (Blumenfeld and Edwards, 2006), thus limiting the applicability of the quadrons to realistic systems.

c. Delaunay tessellation For a set of points specifying, e.g., the centres of spheres in a packing, elementary Delaunay cells are simplexes with vertices at the centres of neighbouring particles. In 2d the simplexes are triangles defined such that no other point lies inside the circumcircle of a given triangle. In 3d the simplexes are likewise tetrahedra defined such that no other point lies inside the circumsphere of a given tetrahedron. In both cases a space filling set of cells is obtained, which, however, is not uniquely associated with a given set of particles. Thus, it is not possible to cast this tesselation into the form of Eq. (20), reducing its applicability to realistic systems. The Delaunay tessellation has been used to analyse the volume statistics of disordered sphere packings (Aste, 2005, 2006; Aste *et al.*, 2007; Finney, 1970; Hiwatari *et al.*, 1984; Klumov *et al.*, 2014), and is the cornerstone in Hales' proof of the Kepler conjecture.

d. Voronoi tessellation A straightforward way to tessellate the volume of a packing is to associate that amount of space with particle i that is closer to it than to any other particle (Fig. 5), thus making full use of the form Eq. (20). This defines the Voronoi tesselation, first introduced by the Ukrainian mathematician G. F. Voronoi in 1908, which is now widely used in mathematics and many applied areas (Aurenhammer, 1991; Okabe *et al.*, 2000). The Voronoi tesselation has been used in the Edwards ensemble in the mean-field approximation to obtain the volume fraction of RCP for spheres (Song *et al.*, 2008) and non-spherical particles (Baule *et al.*, 2013) and it is the basis of the main results reviewed here. For a discussion of the concept of RCP, see Sec. III.A.4. In the case of spheres or points, the Voronoi tessellation is dual to the Delaunay decomposition: the centres of the circumspheres are just the vertices of the Voronoi graph.

Before we define the volume $\mathcal{W}_i$, we first introduce the Voronoi boundary (VB). The VB between two particles is defined as the hypersurface that contains all the

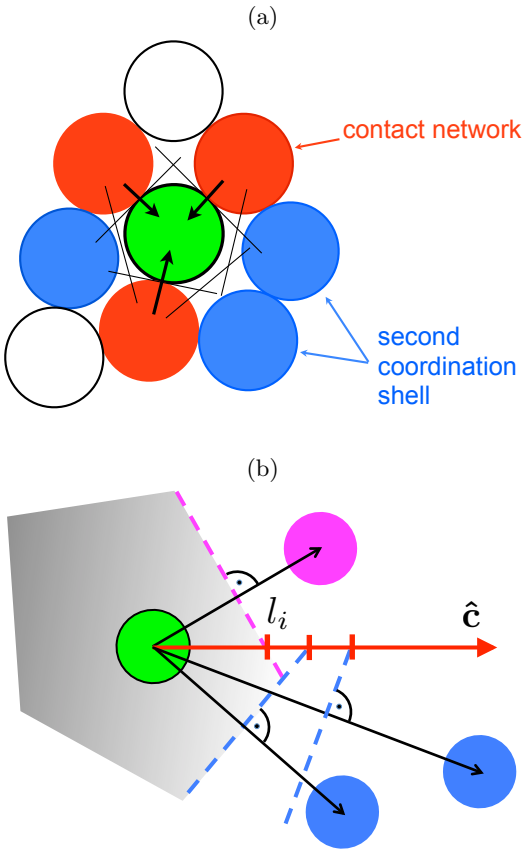

FIG. 5 (Colors online) Illustration of the Voronoi tessellation in a packing of monodisperse disks. (a) In this case the Voronoi boundary (VB) between two particles is the plane perpendicular to the separation vector at half the distance (see Eq. (25)). The VBs of the reference particle (green) with the particles in the first and second coordination shell are indicated with thin black lines. (b) The volume of a Voronoi cell associated with a given particle is defined as the amount of space that is closer to the surface of that particle than to the surface of any other particle. The cell boundary $l_i(\mathbf{q},\hat{\mathbf{c}})$ in a given direction $\hat{\mathbf{c}}$ for a configuration $\mathbf{q}$ thus follows from the global minimization Eq. (28) and the cell volume from the orientational integral Eq. (27). In the figure the contributed VBs of all particles along $\hat{\mathbf{c}}$ are indicated. The pink particle contributes the smallest VB, which thus defines the boundary of the Voronoi cell (indicated in grey). We also refer to this particle as "Voronoi particle" along the direction $\hat{\mathbf{c}}$.

points that are equidistant to the surface of both particles (Baule *et al.*, 2013; Portal *et al.*, 2013; Schaller *et al.*, 2013). If we fix our coordinate system at the centre of mass of particle i (and also assume its orientation fixed), we can parametrize the VB in terms of the direction $\hat{\mathbf{c}}$ from particle i (Fig. 5b). A point on the VB is found at $s\hat{\mathbf{c}}$, where s depends on the relative position $\mathbf{r}_{ij}$ and orientation $\hat{\mathbf{t}}_{ij}$ of the two particles: $s = s(\mathbf{r}_{ij},\hat{\mathbf{t}}_{ij};\hat{\mathbf{c}})$. The value of s is obtained from two conditions:

1. The point $s\hat{\mathbf{c}}$ has the minimal distance to the surfaces of each of the two objects along the direction $\hat{\mathbf{c}}$.
2. Both distances are the same.

As an example, the VB between two spheres of equal radii is the same as the VB between two points at the centres of the spheres. Therefore, condition 1 is trivially satisfied for every s and condition 2 translates into the equation $(s\hat{\mathbf{c}})^2 = (s\hat{\mathbf{c}} - \mathbf{r}_{ij})^2$, leading to

$$s = \frac{r_{ij}}{2\hat{\mathbf{c}}\cdot\hat{\mathbf{r}}_{ij}}, \tag{25}$$

i.e., the VB is the plane perpendicular to the separation vector $\mathbf{r}_{ij}$ at half the separation (see Fig. 5a). Already for two spheres of unequal radii, the VB is a curved surface. Taking into account the different radii R_i and R_j, the second condition becomes $s - R_i = \sqrt{(s\hat{\mathbf{c}} - \mathbf{r}_{ij})^2} - R_j$, which has the solution (Danisch *et al.*, 2010):

$$s = \frac{1}{2}\frac{r_{ij}^2 - (R_i - R_j)^2}{\hat{\mathbf{c}}\cdot\hat{\mathbf{r}}_{ij} - (R_i - R_j)}. \tag{26}$$

Finding a solution for both conditions 1. and 2. for general non-spherical objects is non-trivial (Baule *et al.*, 2013; Portal *et al.*, 2013) and will be discussed in detail in Sec. IV.G.2.

The exact mathematical formula for $\mathcal{W}_i(\mathbf{q})$ is then given by the orientational integral:

$$\mathcal{W}_i(\mathbf{q}) = \frac{1}{3}\oint \mathrm{d}\hat{\mathbf{c}}\, l_i(\mathbf{q},\hat{\mathbf{c}})^3, \tag{27}$$

where $l_i(\mathbf{q},\hat{\mathbf{c}})$ is the boundary of the Voronoi cell in the direction $\hat{\mathbf{c}}$. This boundary depends on all N particle configurations $\mathbf{q}$ in terms of a global minimization: $l_i(\mathbf{q},\hat{\mathbf{c}})$ is the minimum among all VBs in the direction $\hat{\mathbf{c}}$ between particle i and all other $N-1$ particles in the packing (see Fig. 5b). Formally,

$$l_i(\mathbf{q},\hat{\mathbf{c}}) = \min_{j:s>0} s(\mathbf{r}_{ij},\hat{\mathbf{t}}_{ij},\hat{\mathbf{c}}). \tag{28}$$

Clearly, the global minimization over all particles j defining $\mathcal{W}_i$ in Eq. (28) is highly difficult to treat analytically. The Voronoi volume of a particle depends on the position of all the other particles in the packing; clearly, a many-body interaction. The precise knowledge of the microscopic configurations of all particles is intractable in the thermodynamic limit. Nevertheless, the Voronoi convention has been shown to be the most useful way of defining the volume function, since it is well defined for any dimension and captures the effect of different particle shapes. The technical challenges can be circumvented by:

(i) Decomposing non-spherical shapes into overlapping and intersecting spheres leading to analytically tractable expressions for the VB;

(ii) Coarse-graining the volume function over a mesoscopic length-scale, which avoids the global minimization problem.

This approach (Baule *et al.*, 2013; Song *et al.*, 2008) turns the volume ensemble into a predictive framework for packings, as discussed in detail in Sec. IV.

Interestingly, the Voronoi cell of a particle can be interpreted as its available volume in the packing. This correspondence can be demonstrated by considering a soft interparticle potential and evaluating the free volume for a given potential energy before taking the hard core limit (Song *et al.*, 2010). Analyzing the statistics of the Voronoi cells also provides deeper insight into structural features of packings, e.g., by quantifying the cell shape anisotropies (Luchnikov *et al.*, 1999; Medvedev and Naberukhin, 1987; Schaller *et al.*, 2015a; Schröder-Turk *et al.*, 2010).

2. Statistical mechanics of planar assemblies using quadrons

The quadron convention of the volume function $\mathcal{W}$ has been used in (Blumenfeld and Edwards, 2003) to calculate the partition function of the volume ensemble explicitly. With Eq. (24) we obtain (Blumenfeld and Edwards, 2003)

$$\begin{aligned}\mathcal{Z} &= \int \mathrm{d}\mathbf{q}\, e^{-\mathcal{W}(\mathbf{q})/X}\Theta_{\mathrm{jam}}(\mathbf{q}) \\ &= \prod_n \int_0^\infty \mathrm{d}r_n \int_0^\infty \mathrm{d}R_n \int_{-\pi/2}^{\pi/2} \mathrm{d}\alpha_n \\ &\quad \times e^{-\frac{1}{2X}\sum_n r_n R_n \cos(\alpha_n)}\Theta(\{r_n\},\{R_n\},\{\alpha_n\}), \end{aligned} \tag{29}$$

where n labels each of the quadrons in the packing (see Fig. 4). As before, the Θ_{jam} function imposes the jamming constraint. This implies that the values of $\{R_n\}$, $\{r_n\}$, $\{\alpha_n\}$ are constrained by minimal and maximal volumes of the assembly: Compactification below the minimal volume would induce overlap, while dilation beyond the maximal volume would lead to a breakdown of mechanical stability.

If correlations between $\{r_n\}$, $\{R_n\}$, and $\{\alpha_n\}$ are neglected, analytical results for $\mathcal{Z}$ can be obtained by introducing suitable approximations for Θ_{jam}. A simple example is

$$\Theta_{\mathrm{jam}} = \prod_{n=1}^{\langle z_g\rangle N} \frac{\delta(R_n - R_0)\delta(\gamma_n - \gamma_0)}{r_{\max} - r_{\min}}, \qquad r_{\min} < r < r_{\max}. \tag{30}$$

Here, z_g is the coordination number of the particle and $r_{\min}$, $r_{\max}$ are related to the minimal and maximal volumes of the quadrons via $v_{\min} = R_0\gamma_0 r_{\min}/2$, $v_{\max} = R_0\gamma_0 r_{\max}/2$ for given reference values of R_0 and γ_0. The angle γ_n is defined as $\gamma_n = \cos(\alpha_n)$. The partition function for a single particle is then

$$\mathcal{Z}^{1/N} = \left[\frac{X e^{-v_{\min}/X}}{\Delta v}(1 - e^{-\Delta v/X})\right]^{z_g}, \tag{31}$$

and the average volume and volume fluctuations per particle are

$$\langle v\rangle = z_g\left[\frac{v_{\min}+v_{\max}}{2} + X + \frac{\Delta v}{2}\coth\left(\frac{\Delta v}{4X}\right)\right] \tag{32}$$

$$\left\langle \delta v^2\right\rangle = z_g\left[X^2 - \left(\frac{\Delta V}{\sinh(\Delta V/X)}\right)^2\right], \tag{33}$$

where $\Delta V = V_{\max} - V_{\min}$. These expressions yield the limits $\langle v\rangle \to z_g v_{\min}$ and $\left\langle \delta v^2\right\rangle \to 0$ for $X \to 0$ and $\langle v\rangle \to z_g(v_{\max} - v_{\min})/2$ and $\left\langle \delta v^2\right\rangle \to \Delta v^2/3$ for $X \to \infty$, capturing the essential behaviour of compaction experiments (see Sec. III).

More realistic forms of Θ_{jam} are captured by the form (Blumenfeld and Edwards, 2003)

$$\Theta_{\mathrm{jam}} = \prod_{n=1}^{\langle z_g\rangle N} P(r_n)\delta(R_n - R_0)C_\gamma e^{-[(\gamma_n-\gamma_0)^2]/(2\sigma_\gamma^2)} \tag{34}$$

Here, a Gaussian distribution of γ_n around γ_0 is assumed with normalization constant C_γ and variance σ_γ^2. It is argued that in general the distribution of R_n is Gaussian-like and narrower than the distribution of the r_n leading to the delta function term. The partition function is then still analytically tractable and leads likewise to predictions for $\langle v\rangle$ and $\left\langle \delta v^2\right\rangle$. Interestingly, the qualitative behaviour of Eqs. (32,33) is still recovered with the more realistic Θ_{jam} assuming a uniform distribution $P(r_n)$.

The quadron approach also allows us to assess the effect of correlations among the $\{R_n\}$, $\{r_n\}$, $\{\alpha_n\}$. The lowest order correlations originate from intergranular loops, since the R_n and γ_n depend on several r_n degrees of freedom and can thus be considered as background fluctuations. In the case of circular particles with three neighbours one finds, that taking into account correlations only due to the intergranular loops reduces the packing density at high compactivity, but increases it at low compactivity. In addition, the difference in density due to correlations is shown to be relatively small at around 2–4%, which suggests that correlation-free models might be sufficiently accurate to capture many packing properties.

3. Γ-distribution of volume cells

The analysis of the statistics of volume cells in sphere packings reveals a striking universality irrespective of different packing methodologies and volume conventions. Experimental packings of $\sim$ 145,000 spherical glass beads were prepared with fluidized bed techniques and observed with X-ray tomography. The resulting PDF of cell volumes in the Delaunay convention shows a clear exponential decay for different packing fractions with coefficients associated with the density (Aste, 2006; Aste *et al.*, 2007). Moreover, a collapse onto a unique master

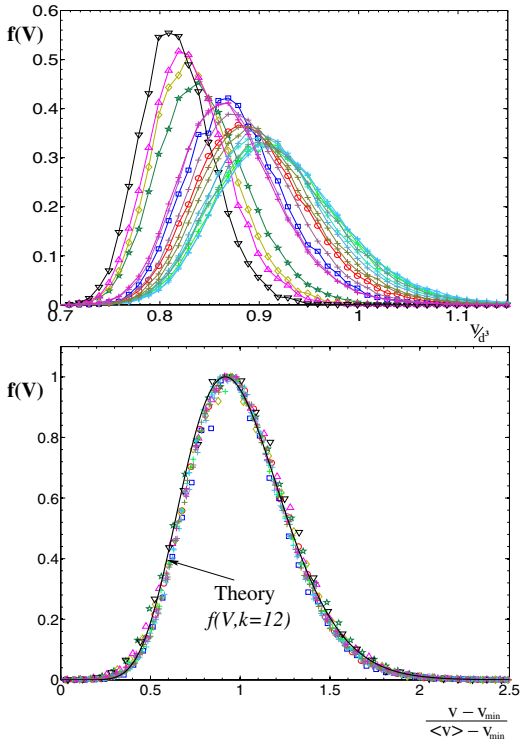

FIG. 6 (Colors online) Top: PDFs of Voronoi cell volumes plotted vs. V/d^3. The data refer to 18 experiments with different protocols using a fluidized bed and observing the particles with X-ray tomography in systems of $\sim 145,000$ spherical glass beads (Aste *et al.*, 2007). Bottom: all the distributions collapse onto a universal curve when plotted vs. $(V-V_{\min})/(\langle V\rangle - V_{\min})$, where $V_{\min} \approx 0.694d^3$ is the smallest Voronoi cell obtained from equal spheres. The theoretical line is $f(V,k=12)$ Eq. (35). Figure reprinted with permission from (Aste *et al.*, 2007).

curve (Fig. 6) is observed upon plotting the PDF against $y = (V-V_{\min})/(\langle V\rangle - V_{\min})$, where $V_{\min} = \sqrt{2}d^3/12$ (d is the sphere diameter) is the volume of the smallest compact tetrahedron with four spheres. The master curve is the Γ-distribution

$$f(V,k) = \frac{(V-V_{\min})^{k-1}}{\Gamma(k)\chi^k} e^{-(V-V_{\min})/\chi}, \qquad (35)$$

with shape parameter k and scale parameter $\chi = (\langle V\rangle - V_{\min})/k$. In the Delaunay convention $k=1$, which describes packings as diverse as dry acrylic bead packs compactified by pouring and tapping, and glass beads in water prepared with fluid pulses (Aste *et al.*, 2007). The data collapse is also observed for the volume cells in the Voronoi convention for the same packing data. In this case, $k=12$ and $V_{\min} \approx 0.694d^3$, which is the smallest Voronoi cell obtained from equal spheres. The value of $k=12$ might be related to the fact that around 12 spheres are expected to be in the close neighbourhood of any given sphere (Aste *et al.*, 2007). Simulation data confirm the data collapse also for the LS algorithm with a wide range of expansion rates (Aste and Di Matteo, 2008).

Numerical investigations of polydisperse frictional disc packings show that also the distributions of quadron volumes and of the grain volumes $\mathcal{W}_g$ are approximately described by a Γ-distribution (Frenkel *et al.*, 2008). Recent simulations have shown that the quadron PDFs collapse onto a single Γ-distribution upon rescaling by the mean volume independent of friction, initial state, the protocol used and the disc size distribution once rattlers are removed (Matsushima and Blumenfeld, 2014). Similarly, it has been found that the conditional PDF $P(A|e)$ of quadron volumes conditional on the number of grains e surrounding the cell in which the quadron resides (the closed loop) is independent of friction (Frenkel *et al.*, 2008; Matsushima and Blumenfeld, 2014). This might be due to the fact that the number of ways to arrange e particles to close the loop depends primarily on the particle shape.

The observed data collapse of the volume statistics and universality of the Γ-distribution is by no means expected apriori and seem to indicate that some structural properties might be largely independent of specific aspects of the packing generation. The emergence of the Γ-distribution Eq. (35) can be motivated by statistical mechanical arguments applied to independent elementary volume cells (Aste and Di Matteo, 2008; Aste *et al.*, 2007). Imagine that the system is divided into C volume cells, which can have any volume v_i $(i=1,...,C)$ with $v_i \geq v_{\min}$, where $v_{\min}$ is a minimal volume. The total volume is the superposition $V = \sum_{i=1}^{C} v_i$. We are interested in the PDF of the volume cells, which can be calculated, assuming that they are uncorrelated, as the ratio

$$f(v) = \frac{Z(v)}{Z} = \frac{C}{V - Cv_{\min}} \left(1 - \frac{v - v_{\min}}{V - Cv_{\min}}\right)^{C-1} \qquad (36)$$

where Z denotes the total number of configurations $Z = (V-Cv_{\min})^C/C!$ and $Z(v)$ the number of configurations containing a cell with volume v: $Z(v) = (V - v - (C-1)v_{\min})^{C-1}/(C-1)!$. In the limit $C \to \infty$ while keeping the ratio V/C finite, we obtain the exponential PDF

$$f(v) = \frac{1}{\langle v\rangle - v_{\min}} \exp\left[-\frac{v - v_{\min}}{\langle v\rangle - v_{\min}}\right], \qquad (37)$$

where $\langle v\rangle$ is just the average cell volume $\langle v\rangle = V/C$. The assumption underlying the combinatorial result Eq. (37) is that any combination of cells yields the total volume and represents a mechanically stable packing. The scale parameter $\langle v\rangle - v_{\min}$ is then akin to an intensive thermodynamic variable accounting for the exchange in volume between the cell and the surrounding volume reservoir.

Crucially, the elementary cells do not necessarily coincide with the cells of a particular volume tessellation, but rather constitute elementary building blocks. The

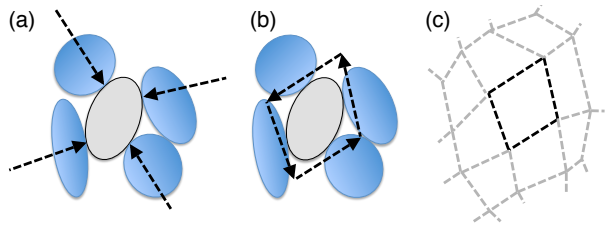

FIG. 7 . Illustration of a Maxwell-Cremona tessellation. (a,b) Rotating the contact force vectors by $\pi/2$ and joining them tip to end leads to a tile that can be associated with an individual particle. (b,c) Due to force balance every tile is closed and the collection of tiles tesselates the plane.

volume of a cell in the tessellation can thus be written as a sum $V = \sum_{i=1}^{k} v_i$ of k elementary cells. The resulting PDF of cell volumes $f(V, k)$ then just becomes the Γ-distribution Eq. (35). The surprising fact is that this result is achieved assuming that the cells are uncorrelated, an assumption that is at odds with the jammed correlated nature of packings. The observed data collapse on a master curve with $k = 1$ for the Delaunay tessellation (Aste *et al.*, 2007) suggests that this convention might generate the elementary cells. However, only in the 1d case is any assembly of the cells (consisting just of the line segments between particle centres) space filling and mechanically stable.

The free volume distribution and compactivity has also been studied experimentally for two-dimensional, bidisperse packings (Lechenault *et al.*, 2006). For the distribution of the free volume per grain, i.e. of its Voronoi cell, they also find a Gamma-distribution like Eq. (35), but interestingly the normalization factor turns out to exhibit a non-extensive scaling for large particle numbers.

E. Stress and force ensemble

1. Force tilings

It has already been noted in the mid 19th century that the contact forces in a 2d packing can be mapped to a tessellation of the plane, the so called Maxwell-Cremona tessellation (Cremona, 1890; Maxwell, 1864). We first discuss how this tessellation is constructed before clarifying their relevance for the statistical ensembles. An individual tile in the tessellation arises from the contact forces acting on a particle i: The boundary of the tile is constructed by rotating all force vectors by $\pi/2$ and joining them tip to end leading to a polygon (see Fig. 7a,b). If the forces on the particle all balance the polygon is closed, because its boundary is the sum of all contact forces. Moreover, due to Newton's third law the tiles of contacting particles always have a side of equal length and orientation, which, for a N particle packing satisfying force balance leads to a tessellation of the plane without any gaps (Fig. 7c). If the packing has periodic boundary conditions, the Maxwell-Cremona tessellation is also periodic. In the presence of boundary stresses, the forces acting on the boundary particles lead to boundaries of the tessellation. Note that the condition of torque balance is not required to construct the tiles. The Maxwell-Cremona tessellation underlies the mapping of contact forces to auxiliary forces such as the void forces (Satake, 1993), loop forces (Ball and Blumenfeld, 2002), and height fields (Henkes and Chakraborty, 2005) (see Sec. II.E.5).

An important observation is that any rearrangement of forces changes the area of individual tiles A_i, but leaves the overall area of the tessellation invariant if force balance is maintained and boundary forces are unchanged. This means that the total area is an invariant under these force rearrangements (Tighe *et al.*, 2008; Tighe and Vlugt, 2010, 2011)

$$\sum_{i=1}^{N} A_i = \text{const}, \tag{38}$$

where the sum runs over all tiles in the tessellation. Another manifestation is the conservation of the stress-moment tensor (Ball and Blumenfeld, 2002; Henkes and Chakraborty, 2005; Henkes *et al.*, 2007). Eq. (38) only holds for frictionless grains. In frictional systems, the force tiles are non-convex and self-intersecting polygons, which makes the tiling graph non planar and the individual tile areas do not sum up to the overall area (Bi *et al.*, 2015).

2. Information entropy

Maximum entropy methods in the spirit of E. D. Jaynes information theoretic approach to statistical mechanics (Jaynes, 1957a,b) have been applied to the problem of force statistics in a number of works (Bagi, 1997, 2003; Goddard, 2004; Kruyt and Rothenburg, 2002; Ngan, 2004, 2003; Radeke *et al.*, 2004; Rothenburg and Kruyt, 2009). Here, there is no need to justify the a priori existence of thermodynamic-like quantities, but rather the method corresponds to a maximum likelihood estimate of the microscopic statistics given some macroscopic constraints. We outline the method following (Goddard, 2004). Starting point is the maximization of the Shannon-Gibbs entropy functional for the PDF of microstates $P(\mathbf{q})$, where $\mathbf{q}$ describes the degrees of freedom of the system, e.g., positions or contact forces

$$S[P] = -\langle \log P \rangle = -\int_{\Omega} \mathrm{d}\Omega(\mathbf{q}) P(\mathbf{q}) \log P(\mathbf{q}), \tag{39}$$

subject to constraints in terms of averages over $P(\mathbf{q})$. For an average energy constraint $\langle E(\mathbf{q}) \rangle = \text{const}$, we recover immediately the Boltzmann distribution $P(\mathbf{q}) \propto$

$e^{-\beta E(\mathbf{q})}$, where β is the Lagrange multiplier associated with the constraint. In the case of a repulsive soft sphere system without friction, the potential energy depends on the contact force as $E(f) \propto f^\nu$, where $f \geq 0$ and ν is typically in the range $2 \leq \nu \leq 5/2$ (see Sec. III.A.2). Eq. (39) then already provides force statistics of the form

$$P(f) = \Omega(f) \exp(-\beta f^\nu)/\mathcal{Z}, \tag{40}$$

where $\mathcal{Z}$ is the normalization constant. The term $\Omega(f)$ arises mathematically from the probability measure $\mathrm{d}\Omega(f) = \Omega(f)\mathrm{d}f$, where $\Omega(f)$ is a density of states in physical terms, which needs to be provided from additional considerations. These a priori probabilities can, e.g., be related to the energy law $E(f)$, such that $\Omega(f) \propto f^{\nu-1}$ (Goddard, 2004; O'Hern *et al.*, 2001).

The formalism is able to incorporate friction and more general stress states by maximizing Eq. (39) subject to an average stress. With Eq. (17) the average stress tensor follows as (Bagi, 1997, 2003; Goddard, 2004; Kruyt and Rothenburg, 2002)

$$\bar{\hat{\sigma}} = \frac{1}{V}\sum_{i=1}^{N} \hat{\sigma}_i = \frac{1}{V}\sum_{i=1}^{N}\sum_{a\in\partial i} \mathbf{d}_a^i \otimes \mathbf{f}_a^i, \tag{41}$$

where $\mathbf{f}_a^i$ and $\mathbf{d}_a^i$ are defined in Fig. 2. The state space is now defined by $\mathbf{q} = \{\mathbf{d}_a^i \otimes \mathbf{f}_a^i\}$ and the entropy maximization under the constraint of a stationary Eq. (41) yields the distribution

$$P(\mathbf{q}) = \exp\left\{-\hat{\alpha} : \bar{\hat{\sigma}}\right\}/\mathcal{Z}. \tag{42}$$

The Lagrange multiplier $\hat{\alpha}$ is now also a tensor and corresponds formally to an inverse angoricity. In (Bagi, 1997, 2003) an exponential distribution of forces has been obtained. In (Kruyt and Rothenburg, 2002) both normal and tangential force components are discussed and marginal distributions obtained. In (Ngan, 2004, 2003) a related free energy has been minimized with similar results.

3. Maximum entropy of modified Edwards ensemble

A maximum entropy approach that takes into consideration Newton's laws in the formulation of the microscopic force density of states has been proposed in (Metzger, 2004; Metzger and Donahue, 2005). The exact program is somewhat involved, we refer to (Metzger, 2004) for a detailed treatment in 2d. The key ideas are: (1) To express the density of states in phase space using the contact force functional (Edwards and Grinev, 2001b) and Edwards assumption of a flat measure. The contact force functional constrains the density to the accessible regions of phase space that satisfy mechanical equilibrium. In addition, the density is related to the stress and fabric tensors. (2) Perform variable transformations to obtain uniform constraints at the cost of a non-flat measure. The reasoning is that although Edwards' measure is uniform across the regions of accessible phase space, the volume of those regions is not uniformly distributed across the coordinates. (3) Once only extensive and conserved quantities remain as constraints, the distribution of single grain states $\rho_\mathrm{g}(w_x, w_y, \theta_1, \ldots, \theta_4)$ is obtained from the standard Gibbs' method. Here, $w_{x,y}$ are the Cartesian loads

$$w_x = \frac{1}{2}\sum_{a=1}^{4} f_a |\cos\theta_a|, \quad w_y = \frac{1}{2}\sum_{a=1}^{4} f_a |\sin\theta_a|, \tag{43}$$

where f_a and θ_a are the contact force magnitudes and contact angles on the reference particle, respectively, with $a \in [1,4]$ (assuming frictionless isostatic spheres). In terms of the quantities defined in Fig. 2, the angle θ_a is determined as $\cos\theta_a = \mathbf{d}_a^i \cdot \hat{\mathbf{x}}/R$ and $f_a = f_a^i$.

The result of the entropy maximization is

$$\rho_\mathrm{g}(w_x, w_y, \theta_1, \ldots, \theta_4) = G(\theta_1, \ldots, \theta_4) e^{-\lambda_x w_x - \lambda_y w_y} \times \prod_{a=1}^{4} \left[P_{f\theta}\left(f_a, \theta_a\right)\right]^{1/2} \Theta\left(f_a\right), \tag{44}$$

where λ_x and λ_y are the Lagrange multipliers associated with the loads, and G derives from the array of Lagrange multipliers used to conserve the fabric distribution $P_{4\theta}(\theta_1, \ldots, \theta_4)$ (Metzger, 2004). The joint distribution of contact forces and angles, $P_{f\theta}(f, \theta)$ is itself related to ρ_g by

$$P_{f\theta}(f,\theta) = \int_0^\infty \mathrm{d}^2 w \int_0^{2\pi} \mathrm{d}^4\theta \; \rho_\mathrm{g} \frac{1}{4}\sum_{a=1}^{4} \delta(\theta - \theta_a) \times \delta\left[f - f_a(w_x, w_y, \theta_1, \ldots, \theta_4)\right]. \tag{45}$$

Eqs. (44) and (45) form a recursion relation in $P_{f\theta}$ and ρ_g, which can be solved numerically using $P_{4\theta}$ and the mechanical loading as inputs. As a simplifying assumption ρ_g can be factorized (Metzger and Donahue, 2005)

$$\rho_\mathrm{g}(w_x, w_y, \theta_\beta) \approx \rho_w(w_x, w_y)\rho_\theta(\theta_\beta) \times \Theta(f_a(w_x, w_y, \theta_\beta)), \tag{46}$$

which is equivalent to assuming no correlations between the load and fabric parts (apart from selecting only mechanically stable configurations). The resulting force distribution is in excellent agreement with results from a DEM simulation reproducing all the characteristic features (Metzger and Donahue, 2005). The simulations verify in particular the prediction of the theory that the variable $t = w_x + w_y$ follows a Gamma distribution $P_t(t) = t^{\alpha-1}e^{-\alpha t}$ with $\alpha = 5$. Since the Gamma distribution arises as a convolution of α exponential distributions, this result suggests that the hydrostatic load on a grain in a disordered packing is distributed as if it were composed of independent Gibbs-like distributions, even though the contact forces themselves are neither independent nor canonically distributed.

4. Force network ensemble

The force network ensemble (FNE) proposed in (Snoeijer *et al.*, 2004) and motivated by work of Bouchaud (Bouchaud, 2002) is based on a separation of scales relevant for the particle configurations and forces. In quantitative terms, one can introduce the parameter

$$\epsilon = \frac{\langle f_{ij}\rangle}{\langle r_{ij}\rangle}\left\langle \frac{\mathrm{d}f_{ij}}{\mathrm{d}r_{ij}}\right\rangle^{-1}, \tag{47}$$

where $\langle ...\rangle$ denotes an average over all particles in the packing and we introduce the notation f_{ij} for the normal force component f_a^i of contact a on particle i with particle j. For $\epsilon \ll 1$ variations of the forces of order $\langle f\rangle$ only result in vanishing changes in the particle positions $\mathbf{r}_{ij}$. If the forces are underdetermined, i.e., not uniquely fixed by the force and torque balance equations, the forces are thus uncoupled from the configurational degrees of freedom. The FNE considers a fixed contact network (a fixed set of $\{\mathbf{r}_{ij}\}$) and constructs an ensemble of contact forces $\{f_{ij}\}$ with the following properties: *(i)* The forces are a priori uniformly distributed as in the Edwards ensemble; *(ii)* Force and torque balance equations are imposed as constraints; *(iii)* Forces are repulsive $\forall f_{ij} \geq 0$ and satisfy the Coulomb condition Eq. (5); *(iv)* A fixed external pressure $\mathcal{P}$ sets an overall force scale. The resulting force distribution can be evaluated analytically for a small number of spheres. For larger packings, $P(f)$ can be obtained by sampling methods such as simulated annealing and umbrella sampling. The underlying assumptions imply that the FNE is in principle applicable to frictional hyperstatic systems, but is mathematically well defined also for frictionless particles.

The simplest system for which predictions can be obtained is a 2d contact network of disks on a triangular lattice with isotropic stress (hydrostatic pressure) (Snoeijer *et al.*, 2004). The resulting $P(f)$ exhibits the characteristic features of the force statistics in jammed packings: The FNE reproduces the peak and shoulder for small forces (see Sec. III.A.5). The decay for large forces is faster than exponential $P(f) \sim \exp(-f^b)$, where b depends on dimensionality. Umbrella sampling methods that can probe the tail have established $b = 2$ in 2d (Gaussian tails), $b \approx 1.6$ in 3d, and $b \approx 1.4$ in 4d. For induced anisotropic stresses the system looses the peak at $\langle f\rangle$ and the right tail approaches an exponential decay in the limit of maximal anisotropy, i.e., when all forces point in one direction. This highlights that the observed peak might not be an essential signature of jamming.

Since the external pressure is fixed, the grain scale pressures $p_i = \sum_{a=1}^{z_i} f_a^i$ satisfy the conservation law $\sum_{i=1}^{N} p_i = \mathcal{P}$. An additional conservation law is provided by the area conservation Eq. (38) under rearrangements of the bulk forces satisfying force balance. These rearrangements can be sampled effectively, e.g., by so called wheel moves on a triangular lattice (Tighe *et al.*, 2008). With the two conservation laws, the distribution $P(p)$ of grain scale pressures can be obtained by maximizing the entropy $-\int_0^\infty \mathrm{d}p(P(p)\log P(p))\omega(p)$, where $\omega(p)$ is the density of force states. Neglecting correlations between neighbouring particles suggests $\omega(p) \propto p^\nu$, with a constant ν depending on the properties of the contact network and the friction coefficient. Overall, one obtains

$$P(p) = \frac{p^\nu}{\mathcal{Z}} e^{-\alpha p - \gamma\langle a(p)\rangle}, \tag{48}$$

where $\mathcal{Z}$ is a normalization constant, α and γ are the Lagrange multipliers associated with the canonical pressure and area constraints. The function $\langle a(p)\rangle$ is the average area of a tile with perimeter p, which is quadratic in p in the thermodynamic limit. Eq. (48) highlights that entropy maximization with the pressure constraint only ($\gamma = 0$) leads to exponential tails of $P(p)$, while incorporating the area constraint predicts Gaussian tails. If we assume that the tails of $P(p)$ and $P(f)$ have the same form, which is indicated from empirical data, this result would thus confirm the Gaussian tails found in simulations from a simple theoretical argument. It also indicates that exponential tails are not generically obtained from entropy maximization of force ensembles.

Formally extending the area conservation to higher dimensions, where the Maxwell argument does not strictly apply, predicts a force exponent of $b = d/(d-1)$. In 3d thus $b = 3/2$ in agreement with simulation data. In fact, Eq. (48) has been shown to capture well the whole range of the distribution $P(p)$ in both frictionless and frictional packings of regular lattices (Tighe and Vlugt, 2010, 2011).

For an isostatic system at jamming the applicability of the force network ensemble is somewhat questionable, since the contact geometry uniquely defines the contact forces (Charbonneau *et al.*, 2015b; Gendelman *et al.*, 2016; Lerner *et al.*, 2013). In this case, $P(f)$ can be determined with the cavity method assuming a locally tree-like contact geometry (Bo *et al.*, 2014) (see Sec. V.A).

5. Stress ensemble

A statistical ensemble based on the stress-moment tensor is conveniently constructed by introducing auxiliary force variables based on the voids surrounded by contacting particles in 2d (Ball and Blumenfeld, 2002; Henkes and Chakraborty, 2005). If we choose the centre of an arbitrary void as the origin of a height field, we can construct the height vectors $\mathbf{h}_\nu$ iteratively as (Henkes and Chakraborty, 2005)

$$\mathbf{h}_\nu = \mathbf{f}_a^i + \mathbf{h}_\mu. \tag{49}$$

Here, μ, ν label voids and $\mathbf{f}_a^i$ is the force vector at the contact that is crossed when going from the centre of void μ to the centre of void ν (see Fig. 8). Since the contact

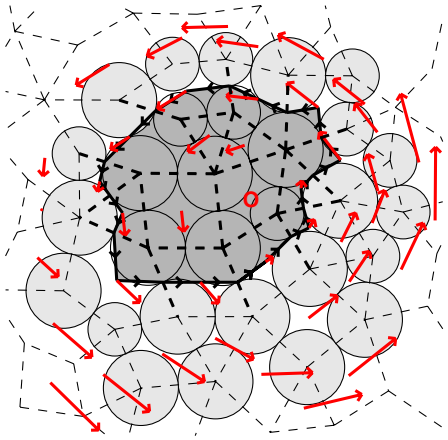

FIG. 8 (Colors online) Height vectors $\mathbf{h}_\mu$ (red arrows) with origin at O obtained from simulations (Henkes *et al.*, 2007). The boundary vectors $\mathbf{r}_{\mu 1}$ and $\mathbf{r}_{\mu 2}$ of the area A (shaded in grey) are indicated by black arrows. The dashed lines denote the intergrain contacts. Figure reprinted from (Henkes *et al.*, 2007).

forces on a particle sum to zero due to force balance, the height vectors are well defined and represent a one-to-one mapping of the contact forces. If we consider the microscopic stress tensor of a single grain, Eq. (17), we see that $\hat{\sigma}_i$ can likewise be expressed in terms of the height fields (Ball and Blumenfeld, 2002)

$$\hat{\sigma}_i = \sum_{a\in\partial i} (\mathbf{r}_{a1} + \mathbf{r}_{a2}) \otimes \mathbf{h}_\mu, \tag{50}$$

where $\mathbf{r}_{a1}$ and $\mathbf{r}_{a2}$ denote the vectors connecting void a with the contact points (see Fig. 8). The macroscopic force-moment tensor Eq. (18) of a macroscopic assembly of N particles occupying area A in the quadron convention is thus

$$\hat{\Phi} = \sum_{i=1}^{N} \hat{\sigma}_i = \sum_{\mu\in\partial A} (\mathbf{r}_{\mu 1} + \mathbf{r}_{\mu 2}) \otimes \mathbf{h}_\mu. \tag{51}$$

The sum in the last expressions runs only over all voids defining the boundary of the area A, since all contributions from particles in the bulk cancel. We see that $\hat{\Phi}$ is conserved under rearrangement of the contact forces in the bulk that preserve force balance, which is a manifestation of the area conservation Eq. (38). Therefore, packings with different values of $\hat{\Phi}$ can not be transformed into each other by rearranging the bulk forces. This allows us to define a granular entropy $S = \log \Omega(A, \hat{\Phi}, N)$ via the number of force configurations $\Omega(A, \hat{\Phi}, N)$ leading to a given $\hat{\Phi}$.

In order to obtain the canonical distribution, we divide the system into a small partition of size m and the remaining system $N - m$, which acts as a reservoir. The conditional probability to observe a stress $\hat{\Phi}_m$ in a system characterized by $\hat{\Phi}$ is (Henkes and Chakraborty, 2009)

$$P(\hat{\Phi}_m|\hat{\Phi}) = \frac{\Omega_m(\hat{\Phi}_m)\Omega_{N-m}(\hat{\Phi}_N - \Phi_m)}{\Omega_N(\hat{\Phi})}. \tag{52}$$

Taking the logarithm and expanding to first order in $\hat{\Phi}_m$ yields

$$\log P(\hat{\Phi}_m|\hat{\Phi}) = \log \Omega_m(\hat{\Phi}_m) - \sum_{i,j}^{d} \frac{\partial \log \Omega_N(\hat{\Phi})}{\partial \hat{\Phi}_{ij}}. \tag{53}$$

With the definition of the inverse angoricity $\alpha_{ij} = \partial \log \Omega_N(\hat{\Phi})/\partial \hat{\Phi}_{ij}$, we thus obtain

$$P(\hat{\Phi}_m) = \frac{\Omega_m(\hat{\Phi}_m)}{\mathcal{Z}(\hat{\alpha})} e^{-\hat{\alpha}:\hat{\Phi}_m}, \tag{54}$$

where the partition function $\mathcal{Z}(\hat{\alpha})$ provides the normalization.

For frictionless isotropic systems the only independent part of $\hat{\Phi}$ is the trace $\Gamma = \operatorname{tr} \hat{\Phi}$, which represents a simple hydrostatic pressure $p = \Gamma/A$. In this case, the formalism simplifies: $\alpha = \log \Omega_N(\Gamma)/\partial\Gamma$ and the canonical distribution is (Henkes and Chakraborty, 2009; Henkes *et al.*, 2007)

$$P(\Gamma_m) = \frac{\Omega_m(\Gamma_m)}{\mathcal{Z}(\alpha)} e^{-\alpha\Gamma_m}, \qquad \Gamma_m = \sum_{i,j} d_{ij} F_{ij}, \tag{55}$$

where the sum is taken over all contact vectors and forces in the m-particle cluster.

Eq. (55) leads to the following testable predictions:

- All subregions in an equilibrated packing k should have the same granular temperature α_k. Thus measuring $P(\Gamma_m)$ in two packings k and k' yields the ratio (Henkes *et al.*, 2007)

$$\log \left[\frac{P_k(\Gamma_m) P_{k'}(\Gamma'_m)}{P_k(\Gamma'_m) P_{k'}(\Gamma_m)} \right] = (\alpha_k - \alpha_{k'})(\Gamma_m - \Gamma'_m). \tag{56}$$

  Moreover, the distribution $P_k(\Gamma_m)$ satisfies the scaling (Henkes *et al.*, 2007)

$$P_k(\Gamma_m) = P_{k'}(\Gamma_m) e^{-(\alpha_k - \alpha_{k'})\Gamma_m}. \tag{57}$$

  Eqs. (56,56) require that packings k and k' are sufficiently close in density to neglect changes in Ω due to different volumes.

- At the isostatic point the partition sum $Z(\alpha)$ can be evaluated analytically by summing over all force degrees of freedom assuming a uniform distribution. In a monodisperse system of spheres, this yields the predictions (Henkes and Chakraborty, 2009): $\Omega(\Gamma_m) = \Gamma^{2m}$ for $m \gg 1$ and

$$\alpha = \frac{N z_{\mathrm{iso}}}{2\langle\Gamma\rangle}, \tag{58}$$

where $\langle\Gamma\rangle = -\partial \log Z/\partial\alpha$. We also obtain the exponential force distribution

$$P(F) \propto e^{-\alpha r_0 F}, \tag{59}$$

where r_0 is the sphere radius.

Simulations of soft sphere systems have confirmed predictions Eqs. (56,56) for different packing densities (Henkes *et al.*, 2007). Eq. (58) has also been shown close to the J-point, but deviations are observed for larger densities, where instead the relation $\alpha = Na\langle z\rangle/\Gamma_N$ is observed. Here, a increases monotonically from $a = 2$ for $\langle z\rangle > z_{\rm iso}$ (Henkes and Chakraborty, 2009).

III. PHENOMENOLOGY OF THE JAMMED STATES AND SCRUTINIZATION OF THE EDWARDS ENSEMBLE

In this section we first describe the phenomenological results characterizing the jammed states and then proceed to review work dedicated to test the Edwards assumption of equiprobability of jammed states.

A. Jamming in soft and hard sphere systems

Over the past two decades, considerable progress has been made in our understanding of jammed particles packings. Here we summarize the main results of this work needed for the remainder of this review. One can refer to several recent review articles for more details. (Bi *et al.*, 2015; van Hecke, 2010; Liu and Nagel, 2010; Torquato and Stillinger, 2010)

1. Isostaticity in jammed packings

The average coordination number in packings is easily estimated by naive Maxwell counting arguments (Alexander, 1998; Maxwell, 1870) which consider the force variables constrain only by force and torque balance Eqs. (2,3) and Newton's third law Eq. (7), but ignore the crucial constraints of Coulomb, Eqs. (5), and repulsive forces, Eq. (6). In particular, attractive forces are allowed, contradicting the fact that the forces are purely repulsive, Eq. (6). Thus one obtains an estimation on the average coordination number z. A packing is geometrically rigid if it can not be deformed under any translation or rotation of the particles without deforming the particles or breaking any of the contacts (Alexander, 1998). In d dimensions, there are d force balance equations Eq. (2) and $d(d-1)/2$ torque balance equations Eq. (3). The number of equations can in general be associated with the configurational degrees of freedom (dofs), so that per particle we have in total $d_{\rm f} = d(d+1)/2$ configurational dofs.

Geometrical rigidity requires that all $Nd_{\rm f}$ degrees of freedom in the packing are constrained by contacts (assuming periodic boundary conditions). For frictional particles there are d force components at contact and since all contacts are shared by two particles we thus require $Ndz/2 \geq Nd_{\rm f}$ or

$$z \geq 2d_{\rm f}/d = d+1. \tag{60}$$

For frictionless particles there is only a single force component at each contact due to Eq. (4): The normal unit vector is fixed by $\mathbf{d}_a^i$. The equivalent rigidity condition is thus $Nz/2 \geq Nd_{\rm f}$ or

$$z \geq 2d_{\rm f}. \tag{61}$$

For frictionless spheres the normal unit vector is parallel to $\mathbf{d}_a^i$ so that Eqs. (3) are always trivially satisfied. In this case $d_{\rm f} = d$, which corresponds to the translational dofs since rotations are irrelevant.

If Eqs. (60,61) are not satisfied there exist zero energy modes (so called floppy modes) that can deform the packing without any energy cost. If the equalities hold, i.e., $z = d+1$ for frictional particles and $z = 2d_{\rm f}$ for frictionless particles, the packing is *isostatic* under the naive Maxwell counting argument: The number of force and torque balance equations exactly equals the number of contact force components. Therefore, the configurational dofs fully determine the force dofs and vice versa, which allows to construct ensembles based on only configurational or force dofs. Since isostatic packings have the minimal number of contacts for a geometrically rigid packings they are also referred to as marginally stable. Packings with z smaller or larger than the isostatic value are referred to as hypostatic and hyperstatic, respectively.

On the other hand, we can obtain an upper bound on z by imposing that a generic disordered packing will have the minimal number of contacts. If any two particles precisely touch at a single point without deformation, we find that a single contact fixes one component of the vector connecting the two center of masses. Overall, there are then $Nz/2$ constraints on the configurational dofs from touching contacts. From the constraint $Nz/2 \leq Nd_{\rm f}$ we obtain

$$z \leq 2d_{\rm f} \tag{62}$$

for both frictional and frictionless particles. Note that for particles interacting with a soft potential the touching condition can only be satisfied at zero pressure. Likewise, realistic hard particles usually suffer slight deformations when jammed, complicating the analysis (Donev *et al.*, 2007; Roux, 2000)

Equations (61,62) imply that packings of frictionless particles should in general be isostatic with

$$z = 2d_{\rm f}. \tag{63}$$

Equation (63) predicts that packings of frictionless spheres have $z = 6$, while rotationally symmetric shapes such as spheroids and spherocylinders have $z = 10$ and fully asymmetric shapes have $z = 12$. The isostaticity for spheres is indeed widely observed to hold very closely in experiments and simulations for both soft and hard sphere systems. In fact it has been shown (Moukarzel, 1998) that non-cohesive sphere packings become exactly isostatic, when their stiffness goes to infinity. However, if we consider a small deformation from the spherical shape to, e.g., a spheroid, the isostatic condition would predict a discontinuous jump in the average coordination number from $z = 6$ to $z = 10$. Instead, one finds that packings of non-spherical shapes are in general hypostatic with a smooth increase from the spherical isostatic z value under deformation (Donev *et al.*, 2004, 2007; Schreck *et al.*, 2012; Williams and Philipse, 2003; Wouterse *et al.*, 2009). These hypostatic packings are indeed mechanically stable contrary to the argument leading to Eq. (60). The breakdown of Eq. (60) can be explained by taking into account the effect of the shape curvature at the contact point (Roux, 2000). As a consequence, one can construct configurations that are mechanically stable even though there are fewer contacts than configurational dofs per particle (see Sec. IV.G.3). Interestingly, also for larger aspect ratios the average coordination number generally stays below the isostatic value, which is just slightly lower for spheroids and fully asymmetric ellipsoids (Donev *et al.*, 2004), but exhibits a much stronger decrease for spherocylinders (Baule *et al.*, 2013; Williams and Philipse, 2003; Wouterse *et al.*, 2009; Zhao *et al.*, 2012).

For polyhedral particles with flat faces and edges the above counting arguments need to be modified, since, e.g., two touching faces constrain more than a single configurational dof. In (Jaoshvili *et al.*, 2010) it has been suggested to associate every contact with the number of configurational dofs that are constrained by it: Contact of two faces $\rightarrow$ 3 constraints; face and edge contact $\rightarrow$ 2 constraints; face and vertex, edge and edge contacts $\rightarrow$ 1 constraint. With these correspondences the isostaticity of disordered jammed packings of tetrahedra and other Platonic solids could indeed be demonstrated (Jaoshvili *et al.*, 2010; Jiao and Torquato, 2011; Smith *et al.*, 2011).

For frictional particles Eqs. (60,62) predict the range of coordination numbers $4 \leq z \leq 6$ for spheres and $4 \leq z \leq 12$ for general shapes. For spheres it is generally observed that $z \rightarrow 6$ for a friction coefficient $\mu \rightarrow 0$ (frictionless limit) and $z \rightarrow 4$ for $\mu \rightarrow \infty$ (infinitely rough spheres) (see Sec. III.A) For intermediate μ sphere packings are thus generally hyperstatic. Hyperstaticity is also found for frictional ellipsoids (Schaller *et al.*, 2015b) and frictional tetrahedra, when the different types of contact are translated into constraints on the configurational dofs (Neudecker *et al.*, 2013).

The Coulomb condition Eq. (5) restricts the possible force configurations compared with the infinitely rough limit: A stable force configuration with a certain $z(\mu)$ is also stable for all larger μ values. Any determined value $z(\mu)$ is thus in principle a lower bound on the possible combinations of z and μ, although it might not be possible to generate these combinations in practice. This highlights that $z(\mu)$ is not unique and depends strongly on the history of the packing generation. It should be stressed that the above isostatic conjectures are valid only under the naive Maxwell counting argument ignoring the repulsive nature of the interactions and the inequalities derived from Coulomb conditions. A model generalizing Maxwell arguments to this more realistic scenario was proposed in (Bo *et al.*, 2014) leading to a more complex constraint satisfaction problem (CSP). This recent work has suggested the existence of a well defined lower bound on $z(\mu)$ and will be discussed in Sec. V.A.

2. Packing of soft spheres

An idealized granular material is modeled as a packing of soft spheres with radius R interacting with a repulsive normal force: (Johnson, 1985; Landau *et al.*, 1986):

$$f^i_{a,n} = k_n \xi^\alpha, \tag{64}$$

where the normal overlap is $\xi = (1/2)[2R - |\mathbf{r}_1 - \mathbf{r}_2|] > 0$, and $\mathbf{r}_{1,2}$ are the positions of the grain centres. The normal force acts only in compression, $f^i_{a,n} = 0$ when $\xi < 0$. The effective stiffness $k_n = \frac{8}{3}\mu_g R^{1/2}/(1 - \pi_g)$ is defined in terms of the shear modulus of the grains μ_g and the Poisson ratio π_g of the material from which the grains are made (typically $\mu_g = 29$ GPa and $\pi_g = 0.2$, for spherical glass beads). The exponent α is typically chosen among two possibilities: (i) $\alpha = 1$ for simple harmonic springs, and (ii) $\alpha = 3/2$ for 3d spherical geometries at the contact (Hertz forces).

The situation in the presence of a tangential force, $\mathbf{f}^i_{a,\tau}$, is more complicated. In the case of spheres under oblique loading, the tangential contact force was calculated by Mindlin (Mindlin, 1949). For the special case where the partial increments do not involve microslip at the contact surface (i.e., $|\Delta f^i_{a,\tau}| < \mu \Delta f^i_{a,n}$, where μ is the static friction coefficient between the spheres, typically $\mu = 0.3$) Mindlin (Mindlin, 1949) showed that the incremental tangential force is

$$\Delta f^i_{a,\tau} = k_t \xi^{1/2} \Delta s, \tag{65}$$

where $k_t = 8\mu_g R^{1/2}/(2 - \pi_g)$, and the variable s is defined such that the relative shear displacement between the two grain centers is $2s$. This is called the Mindlin "no-slip" solution.

Typical packing preparation protocols employ Molecular Dynamics (called Discrete Element Method in the

engineering literature) compressing an initially loose dissipative gas (Makse *et al.*, 2004, 1999, 2000). In 2d it is necessary to use bidisperse mixtures in order to avoid crystallization. Other protocols start from a random configuration corresponding to a large "temperature" $T = \infty$ initial state. Jammed packings at $T = 0$ are generated by bringing the system to the closest energy minimum using conjugate-gradient techniques to minimize the energy of the system, which is well defined for frictionless systems (O'Hern *et al.*, 2002). Another simple protocol for numerically constructing jammed states consists in putting particles at random positions above the packing at a certain height and letting particles settle under a weak gravity (Herrmann, 1993). Also sophisticated experimental realizations of this procedure have been developed (Pouliquen *et al.*, 1997).

In the $T = 0$ limit or the mechanical equilibrium state assemblies of these particles exhibit a transition to the jammed state. There exists in particular a critical packing density ϕ_c characterizing the onset of jamming at which the static shear moduli G_∞ and the pressure p (and therefore, the static bulk modulus as well) become zero simultaneously (under decompression) and the coordination number attains the isostatic value (Makse *et al.*, 1999). For finite N the precise value of ϕ_c depends on the initial T state and the protocol employed, but scaling behaviour of G_∞ and p for each of the different α values is observed when using the distance to jamming $\phi - \phi_c$ as a control parameter for packings near isostaticity. The critical density ϕ_c in the $T = 0$ limit and zero shear stress is referred to as *J-point* (O'Hern *et al.*, 2002). For quenches starting at infinite temperature, in the thermodynamic limit $N \to \infty$ the distribution of ϕ_c values converges to a delta function at a value $\phi^* = 0.639 \pm 0.001$ for frictionless monodisperse spheres in 3d. The J-point becomes thus a well defined point in this limit, which is close to values typically found for random close packings (RCP) of hard spheres.

The following power-law scalings have been observed by many studies and are independent of polydispersity or dimensionality: (van Hecke, 2010; Liu and Nagel, 2010; Majmudar *et al.*, 2007; Makse *et al.*, 1999, 2000; O'Hern *et al.*, 2003, 2002; Zhang and Makse, 2005):

- Pressure:

$$p \sim (\phi - \phi_c)^\alpha \tag{66}$$

- Static bulk modulus:

$$B_\infty \sim (\phi - \phi_c)^{\alpha - 1} \tag{67}$$

- Static shear modulus:

$$G_\infty \sim (\phi - \phi_c)^{\alpha - 1/2} \tag{68}$$

- Average coordination number:

$$z - z_c \sim (\phi - \phi_c)^{1/2}, \tag{69}$$

  where z_c, the critical coordination number measured at ϕ_c, agrees in fact with the isostatic value $z = 2d_{\mathrm{f}}$ within error bars.

The square root scaling of $z - z_c$ is observed for all α values, which indicates that this scaling is only due to the packing geometry independent of the interaction potential. The scaling of the pressure can be interpreted as an affine response of the packing to deformations. This argument, which is usually referred as the Effective Medium Approximation in granular matter (Digby, 1981; Jenkins *et al.*, 2005; Makse *et al.*, 2004, 1999; Norris and Johnson, 1997; Walton, 1987), also predicts an exponent $\alpha - 1$ for the bulk modulus Eq. (67) (proportional to the second derivative of the energy) as observed (although the scaling law has a different prefactor as expected from affine deformations). However, the shear modulus should then also scale with an exponent $\alpha - 2$, which is not observed, highlighting the effects of non-affine motion under shear (Magnanimo *et al.*, 2008; Makse *et al.*, 2004, 1999). Equation (68) highlights the effect of non-affine deformations close to the jamming threshold, which is particularly pronounced for shear deformations. The observed scaling of the shear modulus has been reproduced in models of disordered solids by taking into account the non-affine response within an approximate analytical scheme (Zaccone and Scossa-Romano, 2011). Equation (69) has been shown to be a bound for stability in (Wyart *et al.*, 2005b) based on physical arguments and confirmed analytically in a replica calculation of the perceptron model of jamming (Franz *et al.*, 2015). Lattice models that exhibit critical behaviour related to Eqs. (67)–(69) capture the jamming transition in terms of a percolation transition (k-core or bootstrap percolation) (Schwarz *et al.*, 2006; Toninelli *et al.*, 2006).

Anomalous behaviour at point J is also indicated in the density of normal mode frequencies (Charbonneau *et al.*, 2015a; DeGiuli *et al.*, 2014; O'Hern *et al.*, 2003; Silbert *et al.*, 2005, 2009; Wyart *et al.*, 2005a,b). In a crystal the low frequency excitations are sound modes with a vibrational density of states $\sim \omega^{d-1}$ (Debye scaling). In a disordered packing theoretical arguments based on marginal stability predict instead (DeGiuli *et al.*, 2014)

$$D(\omega) \sim \begin{cases} \omega^{d-1} & \omega \ll \omega_0 \\ \omega^2/\omega^{*2} & \omega_0 \ll \omega \ll \omega^* \\ \text{constant} & \omega \gg \omega^* \end{cases}, \tag{70}$$

which is also exhibited by the perceptron model (Franz *et al.*, 2015) and found in simulations of jammed soft spheres in dimensions 3–7 (Charbonneau *et al.*, 2015a). In Eq. (70), ω^* is a characteristic frequency that vanishes

at jamming as

$$\omega^* \sim z - z_c \tag{71}$$

and ω_0 is a small threshold frequency.

At jamming the density of states thus stays non-zero for arbitrary small frequencies. This highlights that at point J there is an excess of low frequency modes compared with crystals. This anomaly is sometimes seen analogous to the Boson peak observed in glassy materials (Franz *et al.*, 2015). The vanishing crossover frequency ω^* allows to identify a length scale l^*, which diverges upon reaching point J as: $l^* \sim (z - z_c)^{-1}$ (Wyart *et al.*, 2005a). Such a diverging length scale has been observed numerically in the vibrational eigenmodes and in the response to point perturbations (Ellenbroek *et al.*, 2009, 2006; Silbert *et al.*, 2005). However, theoretical arguments predict for point responses $l^* \sim (z - z_c)^{-1/2}$ (Lerner *et al.*, 2014). The length scale l^* has been computed in Refs. (Lerner *et al.*, 2013; Wyart, 2010). Diverging length scales when approaching point J from below have also been identified related to velocity correlation functions (Olsson and Teitel, 2007) and clusters of moving particles (Drocco *et al.*, 2005). When approaching point J from above finite point correlation functions are not sufficient to detect such a length scale. Instead, point to set correlation functions are necessary, which can provide a quantitative description of the sensitivity of force propagation in granular materials to boundary conditions (Mailman and Chakraborty, 2011, 2012).

The concept of frequency dependent complex-valued effective mass $M_{\text{eff}}(\omega)$ (Hsu *et al.*, 2009) obtained as the packing is subjected to a vertical acceleration at a given frequency is directly related to the vibrational density of states (Hu *et al.*, 2014a). Indeed, the vibrational density of states can be accessed experimentally through the measurement of $M_{\text{eff}}(\omega)$ via a pole decomposition of the normal modes of the system (Hu *et al.*, 2014a). By measuring the stress dependence of the effective mass, it was shown that the scaling of the characteristic frequency ω^* deviates from the mean field prediction Eq. (71) (Hu *et al.*, 2014a) in real frictional packings. Furthermore, the presence of dissipative modes can be readily studied via the imaginary part of the complex valued effective mass (Hu *et al.*, 2014b; Johnson *et al.*, 2015). The isostatic limit, which is typically attained at the J-point has been shown to exhibit diverging force response functions (Moukarzel, 1998, 2005). The distribution of displacements induced by a perturbation is power-law with an exponentially large cutoff.

When friction is added, the observed packing densities and coordination numbers at point J are generally smaller than RCP (Kasahara and Nakanishi, 2004; Makse *et al.*, 2000; Papanikolaou *et al.*, 2013; Shen *et al.*, 2014; Shundyak *et al.*, 2007; Silbert, 2010; Silbert *et al.*, 2002a). As a function of the friction coefficient μ the densities decrease monotonically from $\phi \approx 0.64$ for frictionless spheres to $\phi \approx 0.55$ in the limit of infinitely rough spheres. Experiments find much lower packing fractions in the large friction limit (Farrell *et al.*, 2010). The densities are also dependent on the packing preparation for the same μ highlighting the history dependence of frictional packings. An open question is whether there is a well-defined lower bound on the packing density for a given μ, which could specify random loose packing (RLP) densities (Makse *et al.*, 2000; Onoda and Liniger, 1990): the lowest density packings that are mechanically stable. Extremely low density mechanically stable packings can be generated with additional attractive interactions, e.g., due to adhesion. Adhesive packings of spheres are discussed in Sec. IV.F.

Likewise, the coordination number decreases monotonically for $\mu \geq 0$ from the isostatic frictionless value $2d_{\text{f}}$, reaching the frictional isostatic value $z^{\mu}_{\text{iso}} = d + 1$ in the limit $\mu \to \infty$. Frictional packings are thus in general hyperstatic, so that particle configurations do not uniquely determine the contact forces. How this indeterminacy depends on the friction coefficient and affects the mechanical properties has been investigated in detail using contact dynamics by (Unger *et al.*, 2005). It was also found that the contacts with large indeterminacy are also those contacts that make up force chains (McNamara and Herrmann, 2004).

The following scaling results at point J have been obtained in simulations of frictional soft spheres with Hertz-Mindlin forces (Henkes *et al.*, 2010; Makse *et al.*, 2000; Shundyak *et al.*, 2007; Silbert, 2010; Somfai *et al.*, 2007; Zhang and Makse, 2005). For the coordination number one finds a scaling analogous to Eq. (69)

$$z - z_c \sim z_0(\mu)(\phi - \phi_c)^{1/2}, \tag{72}$$

where $z_c \approx 2d_{\text{f}}$ is the frictionless isostatic value at point J and $z_0(\mu)$ a weakly μ-dependent prefactor. However, other quantities like the critical frequency ω^* and the bulk/shear modulus do not scale with $\phi - \phi_c$ contrary to the frictionless case. One finds

$$\omega^* \sim z - z^{\mu}_{\text{iso}}, \qquad G_\infty/B_\infty \sim z - z^{\mu}_{\text{iso}}. \tag{73}$$

By comparison, Eqs. (67,68,69) predict the scaling $G_\infty/B_\infty \sim z - z_c$. Therefore, one can conclude that the critical observables generally scale with the distance to isostaticity (Wyart, 2005).

3. Packing of hard spheres

The structural properties of packings have been also investigated in considerable detail with computer simulations and experiments of hard spheres satisfying constraint Eq. (1). Hard sphere results should coincide with soft spheres at zero pressure. A widely used simulation algorithm for jammed hard particles is the Lubachevsky-Stillinger (LS) algorithm (Lubachevsky and Stillinger,

1990). Here, starting from a random initial configuration of spheres in the given volume with periodic boundary conditions generated, e.g., by random sequential addition of spheres, the sphere radii are expanded uniformly with a rate λ. Collisions occur due to the expansion and thermal motion of the particles, which are resolved in an event-driven manner. Eventually, a jammed state is reached with diverging collision rates at the contacts, apart from typically a small number of spheres that remain unjammed (of order 2-3%). The properties of the final state are then independent of the random initial state, but depend on the expansion rate. For $\lambda \to 0$ the system is in equilibrium leading to crystallization, while for small $\lambda > 0$ the system is able to reach a quasiequilibrium jammed state with a density $\phi(\lambda)$. These states have been characterized as long-lived metastable glass states which in infinite dimensions are described (Parisi and Zamponi, 2010) by the replica symmetry breaking theory adapted from the solution of the Sherrington-Kirkpatrick (SK) model of spin-glasses (Sherrington and Kirkpatrick, 1975) (see Secs. III.A.4 and V).

Event driven simulations bear the disadvantage that forces do not appear explicitly and can only be obtained making additional assumptions, e.g. on elasticity. The only known numerical technique that can deal with perfectly rigid and at the same time obtain the contact forces precisely is Contact Dynamics (CD), as reviewed for instance in (Radjai and Richefeu, 2009). In fact, granular structures turn out to be more stable under gravity when using CD than any other numerical method (McNamara and Herrmann, 2004). CD has been used extensively to explore force networks, their fluctuations and their indeterminacies in frictional packings, see e.g. (Unger *et al.*, 2005).

Experiments of hard sphere packings go back to the seminal work by Bernal and Scott (Bernal, 1960; Bernal and Mason, 1960; Scott, 1960, 1962). Indeed, in the old days Mason, a postgraduate student of Bernal, took on the task of shaking glass balls in a sack and 'freezing' the resulting configuration by pouring wax over the whole system. He would then carefully take the packing apart, ball by ball, noting the positions of contacts for each particle. Since this labor-intensive method patented half a century ago, yet still used in recent studies (Donev *et al.*, 2004), other groups have extracted data at the level of the constituent particles using x-ray tomography (Richard *et al.*, 2003). The most sophisticated experiment to date has resolved coordinates of up to 380000 spheres using X-ray tomography (Aste *et al.*, 2004, 2005). The packing densities achieved are in general sensitive to the packing protocol, friction, and polydispersity. The effect of boundary walls can be reduced by focusing the analysis on bulk particles or preparing the walls with randomly glued spheres. Mechanically stable disordered packings of spheres are typically found in the range $\phi \approx 0.55$ – 0.64. Empirical studies have shown that one can identify different density regions depending on variations in the protocol (Aste, 2005): *(i)* $\phi \approx 0.55 - 0.58$: packings are only created by reducing the effect of gravity (Onoda and Liniger, 1990); *(ii)* $\phi \approx 0.58 - 0.61$: packings are unstable under tapping; *(iii)* $\phi \approx 0.61 - 0.64$: packings are generated by tapping and compression (Knight *et al.*, 1995; Nowak *et al.*, 1998, 1997; Philippe and Bideau, 2002). Packings in the range $\phi \approx 0.64 - 0.74$, i.e., up to the FCC crystal density are usually only generated by introducing local crystalline order. This has been achieved experimentally by pouring spheres of equal size homogeneously over plate, that vibrates horizontally at a very low frequency (Pouliquen *et al.*, 1997). The attained density depends on the frequency.

Establishing the number of contacting spheres in experiments is somewhat challenging. The celebrated Bernal packings (Bernal and Mason, 1960) find a coordination number close to $z = 6$, while compressed jammed emulsions near the jamming transition studied by confocal microscopy (Brujić *et al.*, 2007) finds an average coordination $\langle z \rangle = 6.08$, both in agreement with the isostatic conjecture. One generally finds that larger densities coincide with larger values of z exhibiting a monotonic increase over the range $\phi \approx 0.55 - 0.64$ from $z \approx 4$ – 7 (Aste, 2005; Aste *et al.*, 2004, 2005, 2006) largely in agreement with simulation results on frictional soft-sphere systems at small pressure.

The following consensus on the structural properties of the pair correlation function $g_2(r)$ of hard-spheres at random close packing has been reached from simulations and experiments:

- A delta function peak at $r = \sigma$ due to contacting particles, where $\sigma = 2R$ is the contact radius. The area under the peak is the average coordination number, which has the isostatic value $z_{\rm iso} = 2d_{\rm f} = 6$ at jamming in frictionless systems.

- A power-law divergence due to a large number of near-contacting particles

$$g_2(r) \sim (r - \sigma)^{-\gamma}. \tag{74}$$

  The exponent γ has been measured as $\gamma \approx 0.4$ in simulations of hard spheres (Charbonneau *et al.*, 2012; Donev *et al.*, 2005b; Lerner *et al.*, 2013; Skoge *et al.*, 2006) and $\gamma \approx 0.5$ in simulations of stiff soft spheres (O'Hern *et al.*, 2003; Silbert *et al.*, 2002b, 2006). Theoretical arguments based on the marginal stability of jammed packings provide (Müller and Wyart, 2015)

$$\gamma = 1/(2 + \theta), \tag{75}$$

  where θ is the exponent of the force distribution: $P(f) \sim f^{\theta}$. Empirical studies find $\theta \approx 0.2 - 0.5$ (see Sec. III.A.5).

- A split-second peak at $r = \sqrt{3}\sigma$ and $r = 2\sigma$ away from contact. The precise shapes of the two peaks have not been clearly established yet. Simulations show a strong asymmetry of the $r = 2\sigma$ peak. The values 2σ and $\sqrt{3}\sigma$ have been related to the contact network: 2σ is the maximal distance between two particles sharing one neighbour, while $\sqrt{3}\sigma$ is the maximal distance between two particles sharing two (Clarke and Jónsson, 1993). The split-second peak is indicative of structural order between the first and second coordination shells. However, no signs of crystalline order using quantitative order metrics, e.g., the spherical harmonics Q_6 indicating icosahedral rotational symmetry as in FCC crystals, have been observed.

- Long-range order $g_2(r) - 1 \sim -r^{-4}$ for $r \to \infty$ (Donev *et al.*, 2005a). This is equivalent to a non-analytic behaviour of the structure factor $S(k) \sim |k|$ for $k \to 0$, which is typically only seen in systems with long-range interactions and is uncharacteristic for liquids. The fact that $S(0) = 0$ is characteristic of a hyperuniform system (Torquato and Stillinger, 2003). Recently (Xia *et al.*, 2015) proposed that the formation of local geometrically frustrated quasi-regular tetrahedra is the microscopic mechanism for the dynamic arrest in packings of glass beads. They define quasi-regular tetrahedra as Delaunay cells having a shape close to a regular tetrahedron, with the shape deviation less than some threshold value of a polytetrahedral order parameter $d = e_{\max} - 1$, where $e_{\max}$ is the length of the longest edge of the tetrahedron measured in units of mean particle diameters. Within the percolation context they identify polytetrahedral clusters and define a static correlation length of polytetrahedral order which increases rapidly with volume fraction. By showing that this polytetrahedral order is spatially correlated with the slow relaxation dynamics, they establish that the order associated with these quasi-regular tetrahedra corresponds to the glass order in hard-sphere glasses.

4. The nature of random close packing

The nature of RCP of frictionless hard spheres and whether it is indeed a well-defined concept has been a long-standing issue. In (Torquato *et al.*, 2000) it has been argued that "random" and "close-packed" are at odds with each other, since inducing partial order typically increases packing densities, such that both can not be maximized simultaneously. As an alternative it has been suggested to use a more quantitative approach based on an order metric (such as Q_6). RCP can then be replaced by the concept of a maximally random jammed (MRJ) packing: The packing with the minimal order among all jammed ones. Despite the apparent ill-definition, many different packing protocols and algorithms seem to robustly achieve disordered packings with maximal densities around $\phi \approx 0.64$. This value coincides with the densities of MRJ packings for many different order parameters, but the underlying physical mechanisms leading to this reproducibility are still debated.

When approaching jamming from the unjammed state it is possible to continue the equation of state of a hard sphere fluid beyond the freezing point at $\phi = 0.49$ using phenomenological approaches motivated by free volume theory (Aste and Coniglio, 2004; Kamien and Liu, 2007). RCP can then be identified as the packing density at which the pressure of such a metastable branch of the equation of state diverges. Although there are possibly different metastable branches depending on the way crystallization is suppressed (e.g., varying γ), it has been conjectured that $\phi_{\rm rcp}$ is a well-defined point of divergence for a whole set of metastable continuations (Kamien and Liu, 2007).

Such a picture agrees with the viewpoint that RCP represents a state of maximum entropy (O'Hern *et al.*, 2003, 2002). In numerical studies of soft sphere systems the density at point J (or $\phi_{\rm rcp}$) is obtained as the peak of the distribution of jamming thresholds, which becomes a delta peak in the infinite system size limit. The J-point/RCP is thus represented by the largest fraction of phase space, which is equivalent to a maximum entropy state. Although, the jamming density might in principle depend on the way the energy landscape is sampled, it has been shown for small system sizes that the effect of the protocol dependence can be neglected when $\phi_{\rm rcp}$ is defined as the packing density in the limit of an infinite quench (Xu *et al.*, 2005). It is also found that $\phi_{\rm rcp}$ is independent of the force exponent α, such that the hard sphere limit can be reached with the same ϕ.

A more formal definition of entropy is obtained in the Edwards ensemble approach as treated in Sec. II.C. Using this framework for a system of monodisperse spheres, RCP has been identified as the freezing point of disordered sphere packings of equal size, with a corresponding freezing point at $\phi_{\rm f} \approx 0.64$ and a melting point at $\phi_{\rm m} \approx 0.68$ (Jin and Makse, 2010). Between these two densities a coexistence of disordered and ordered states exists at the coordination number of isostaticity $z = 6$ (see Fig. 9). Two branches then exist: a disordered branch from the RLP at $\phi_{\rm rlp} = 0.55$ upto the freezing point $\phi_{\rm f} \approx 0.64$ and an ordered branch from the melting point $\phi_{\rm m} \approx 0.68$ to FCC at $\phi_{\rm fcc} = 0.74$. The signature of this disorder-order transition is a discontinuity in the entropy density of jammed configurations as a function of the compactivity. This highlights the fact that beyond RCP, denser packing fractions of spheres can only be reached by partial crystallization up to the homogeneous FCC crystal phase in agreement with the interpretation

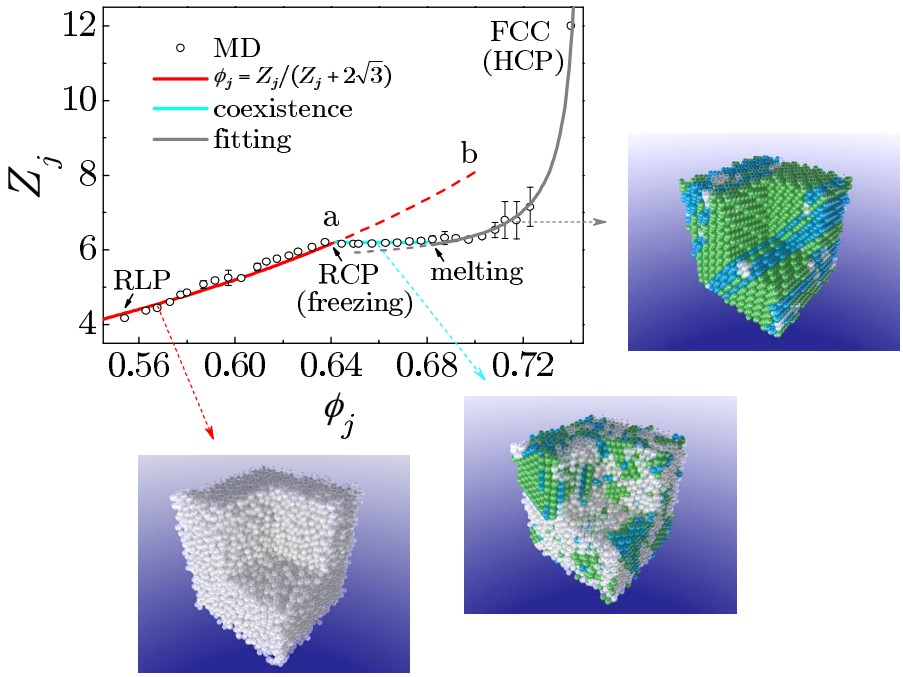

FIG. 9 (Colors online) Interpretation of RCP in a 3d system made of monodisperse spheres as a first order freezing transition between disordered and ordered phases. In low dimensional systems (3d and specially 2d) crystallization prevails around RCP and precludes the appearance of the J-line reminiscent of the glass transition as discussed in (Parisi and Zamponi, 2010). In infinite dimensions where the calculations of (Parisi and Zamponi, 2010) are performed, crystallization is avoided and the Jline appears around RCP. Avoiding crystallization by considering a polydisperse system is another way to study the J-line in 3d systems, see Choudhury et al. The coordination number z_j is plotted versus the volume fraction ϕ_j for each packing at jamming. One can identify: (i) a disordered branch which can be fitted by the equation of state (105) derived in Sec. IV.A; (ii) a coexistence region; and (iii) an ordered branch. Error bars are calculated over 523 packings obtained from initial LS configurations. The 3d plots visualize how the transition occurs in terms of arrangements of contacting particles. White particles are random clusters, light blue are HCP and green are FCC clusters. The dashed line from $a \to b$ denotes the states beyond crystallization. Figure reprinted from (Jin and Makse, 2010).

of RCP as a MRJ state (Torquato *et al.*, 2000). Indeed, RCPs are known to display sharp structural changes (Anikeenko and Medvedev, 2007; Anikeenko *et al.*, 2008; Aristoff and Radin, 2009; Kapfer *et al.*, 2012; Klumov *et al.*, 2014, 2011; Radin, 2008) signalling the onset of crystallization at a freezing point $\phi_{\rm f}$ (Torquato and Stillinger, 2010). Remarkably, the first-order transition scenario observed numerically in (Jin and Makse, 2010) has been verified in a set experiments of 3d hard sphere packings (Francois *et al.*, 2013; Hanifpour *et al.*, 2015, 2014). In (Francois *et al.*, 2013) the onset of crystallization at the freezing point $\phi_{\rm f} \approx 0.64$ has been identified from the variance of the Voronoi volume fluctuations (Jin and Makse, 2010), a "granular specific heat" (Aste and Di Matteo, 2008), and the frequency of polytetrahedral structures. The coexistence line at isostaticity between $\phi_{\rm f} \approx 0.64$ and $\phi_{\rm m} \approx 0.68$ has been observed not only for frictionless packings but also for frictional ones, where high densities have been achieved by applying intense vibrations (Hanifpour *et al.*, 2015, 2014).

The existence of the first-order crystallization transition at RCP is expected to be dominant in a finite dimensional 3d system of equal size spheres and therefore excludes the appearance of more interesting glassy-like phases. In the presence of polydispersity in the particle size or in higher dimensions, crystallization is strongly suppressed and the physics of the glass transition is expected to dominate the corresponding jamming transition. Indeed solutions of hard sphere glasses under the approximation of a fully connected system in infinite dimensions based on replica symmetry breaking (RSB) theory adapted from the solution of the Sherrington-Kirkpatrick model of spin-glasses (Charbonneau *et al.*, 2014a,b; Franz *et al.*, 2015; Parisi and Zamponi, 2010) and other mean-field models (Mari *et al.*, 2009) predict that there is J-line of metastable jammed states when crystallization is suppressed. We will review this approach in Section V. Briefly, a glass transition interrupts the continuation of the liquid equation of state considered in (Aste and Coniglio, 2004; Kamien and Liu, 2007) at densities $\phi \in [\phi_{\rm d}, \phi_{\rm K}]$, where $\phi_{\rm d}$ signals the dynamical glass transition at the density at which many metastable

states first appear in the liquid phase and $\phi_{\rm K}$ is the Kauzmann density of the ideal glass. Upon fast compression (avoiding the crystallization) of the metastable states the pressure diverges at jamming densities $\phi_j \in [\phi_{\rm th}, \phi_{\rm gcp}]$. Here the threshold density $\phi_{\rm th} \approx 0.64$ is the jamming density corresponding to an infinite pressure quench from $\phi_{\rm d}$ and corresponds to the most probable state to be found empirically. Although some simulations have found lower thresholds, see Fig. 1 in (Rainone and Urbani, 2015) and Fig. 2 in (Charbonneau *et al.*, 2014b). It might be possible also to obtain configurations that are locally metastable over a broad range of packing fractions rather than only at $\phi_{\rm th}$, although it might not have been carefully measured in previous studies. The maximal density is the glass close packing $\phi_{\rm gcp} \approx 0.68$ corresponding to the infinite pressure limit quench of the ideal glass $\phi_{\rm K}$. Therefore, jamming can be achieved in a whole range of densities along a J-line: $\phi_j \in [\phi_{\rm th}, \phi_{\rm gcp}]$ depending on the packing protocol.

The value of the densities have been calculated at the 1 step replica symmetry breaking 1RSB level (Parisi and Zamponi, 2010). However, it has been shown that the 1RSB solution is unstable and produces inconsistent predictions regarding the force distribution (e.g., it predicts $\theta = 0$, see Eq. (76) below) and does not agree with the isostatic conjecture at jamming. Indeed, a recent full-RSB calculation (Charbonneau *et al.*, 2014a,b) has explained this disagreement by the existence of a Gardner transition where the 1RSB solution becomes unstable near the isostatic jamming point. This indicates the fragmentation of the configuration space into an infinite fractal hierarchy of disconnected regions, which, in turn, brings about isostaticity and marginal stability.

This result highlights the fact that packing problems, and more generally CSPs, undergo a phase transition separating a satisfiable (SAT) (hypostatic or under-constrained) regime from an unsatisfiable (UNSAT) (hyperstatic or over-constrained) phase, as one varies the ratio of constraints over variables. The jamming transition is equivalent to this SAT-UNSAT phase transition in the broad class of continuous CSPs, which are conjectured to belong to the same "super-universality" class based on models displaying SAT/UNSAT like the celebrated perceptron model (Franz and Parisi, 2016; Franz *et al.*, 2015) which admits a much simpler solution at the full RSB level than the hard-sphere glass (Parisi and Zamponi, 2010).

Thus, this viewpoint indicates the existence of a J-line rather than a single J-point/RCP of jammed hard spheres. This picture has been tested in finite dimensional simulations of sphere glasses with polydispersivity with varying jamming protocols extending the quenches from $T = \infty$ to finite T (Charbonneau *et al.*, 2012; Chaudhuri *et al.*, 2010; Ciamarra *et al.*, 2010; Skoge *et al.*, 2006) obtaining values of packing densities as high as $\phi_j \approx 0.66$.

The Lubachevsky-Stillinger (LS) protocol (Skoge *et al.*, 2006) provides this range of packings for different compression rates. The densities $[\phi_{\rm th}, \phi_{\rm gcp}]$ are achieved by the corresponding compression rates (from large to small) $[\gamma_{\rm th}, \gamma_{\rm gcp} \to 0]$. Compression rates larger than $\gamma_{\rm th}$ all end at $\phi_{\rm th}$. The threshold value $\gamma_{\rm th}$ corresponds to the relaxation time $1/\gamma_{\rm th}$ of the least dense metastable glass states. The denser states at GCP are unreachable by experimental or numerically generated packings, and as a matter of fact, any state denser than $\phi_{\rm th}$, as it requires to equilibrate the supercooled liquid beyond the dynamical glass transition towards the ideal glass phase, a region where the relaxation time is infinite. In general, large compression rates lead to lower packing fractions. This picture is particularly valid for high dimensional systems where crystallization is avoided (Parisi and Zamponi, 2010).

Interestingly, the values of the limiting densities $\phi_j \in [\phi_{\rm th}, \phi_{\rm gcp}]$ coincide approximately with the densities of the melting and freezing points in the first-order transition obtained for monodisperse 3d systems (Jin and Makse, 2010). However, these states are unrelated. It should be noted that the analysis of structure and order parameters is generally supportive of the existence of a glass-crystal coexistence mixture in the density region $0.64 \leq \phi \leq 0.68$ in monodisperse sphere packings where crystallization dominates over the glass phase. All the (maximally random) jammed states along the segment $[\phi_{\rm th}, \phi_{\rm gcp}]$ can be made denser at the cost of introducing some partial crystalline order. Support for an order/disorder transition at $\phi_{\rm f}$ is also obtained from the increase of polytetrahedral substructures up to RCP and its consequent decrease upon crystallization (Anikeenko *et al.*, 2008). In terms of protocol preparation, like the LS algorithm, there exists a typical time scale t_c corresponding to crystallization. Crystallization appears in LS (Parisi and Zamponi, 2010; Torquato and Stillinger, 2010) if the compression rate is smaller than $\gamma_c = 1/t_c$, around the freezing packing fraction (Cavagna, 2009). A possible path to avoid crystallization and obtain RCP in the segment $[\phi_{\rm th}, \phi_{\rm gcp}]$ is to equilibrate with $\gamma > \gamma_c$ to pass the freezing point, and eventually setting the compression rate in the range $[\gamma_{\rm th}, \gamma_{\rm gcp} \to 0]$ to achieve higher volume fraction.

The connection of the replica approach with the Edwards ensemble for jammed disordered states is summarized in Table I and will be discussed in detail in Sec. V. The hierarchy of metastable jammed states k-PD with $k \in [1, \infty)$ is analogous to k-SF with $k \in [1, \infty)$ metastable states in spin-glasses which in turn are related to the continuity of jammed states along the J-line $\phi_j \in [\phi_{\rm th}, \phi_{\rm gcp}]$ predicted by the mean-field theory of hard-sphere glasses. This is the picture emerging in any RSB solution, at the mean-field level of fully connected systems, like the SK model of spin-glasses (Sherrington and Kirkpatrick, 1975). Thus, we expect that a con-

tinuous jamming line of states should emerge from the Edwards ensemble solution of the JSP, since it is another realization of a typical NP-hard CSP.

On the other hand, the mean field solution of the Edwards volume ensemble (Song *et al.*, 2008) reviewed in Section IV predicts a single jamming point at RCP Eq. (114) $\phi_{\rm rcp} = \frac{1}{1+1/\sqrt{3}} = 0.634$ at $z = 6$. This prediction corresponds to the ensemble average over a coarse-grained Voronoi volume for a fixed coordination number. Since an ensemble average over all packings at a fixed coordination number is performed in the coarse-graining of the volume function, the obtained volume fractions $\phi_{\rm rcp}$ are in fact averaged over the J-line predicted by the replica method. Thus, $\phi_{\rm rcp}$ can be associated to the state with the largest entropy (largest complexity) along $[\phi_{\rm th}, \phi_{\rm gcp}]$, expected to be near the highest entropic state $\phi_{\rm th}$ in the replica theory picture. Indeed, high-dimensional calculations performed in Sec. IV.C confirm this conjecture: the scaling obtained with dimension d of the Edwards prediction for RCP and $\phi_{\rm th}$ agree within a prefactor, see Eqs. (129) and (134) below.

5. Force statistics

It has been realized early on that jammed granular aggregates exhibit non-uniform stress fields due to arching effects (Cates *et al.*, 1998; Jaeger *et al.*, 1996). More recent work has focused on the interparticle contact force network. The key quantity is the force distribution $P(f)$, which exhibits characteristic features at jamming as observed in both experiments (Brujić *et al.*, 2003a,b; Corwin *et al.*, 2005; Erikson *et al.*, 2002; Liu *et al.*, 1995; Løvoll *et al.*, 1999; Makse *et al.*, 2000; Mueth *et al.*, 1998; Zhou *et al.*, 2006) and simulations (Makse *et al.*, 2000; O'Hern *et al.*, 2001; Radjai *et al.*, 1996; Tkachenko and Witten, 2000):

- $P(f)$ has a peak at small forces (approximately at the mean force $\langle f \rangle$). This peak has been argued to represent a characteristic signature of jamming (O'Hern *et al.*, 2001).
- For large forces, the decay of $P(f)$ has been generally measured as exponential. Although a faster than exponential decay has also been observed in experiments (Majmudar and Behringer, 2005) and simulations (van Eerd *et al.*, 2007).

These properties are observed in both hard and soft sphere systems, largely independent of the force law.

For $f \to 0^+$, $P(f)$ converges to a power-law

$$P(f) \sim f^{\theta}, \quad f \to 0^+, \tag{76}$$

with some uncertainty regarding the value of the exponent: $\theta \approx 0.2 - 0.5$. The existence of this power-law has been explained by the marginal stability of the packing which is controlled by small forces (Wyart, 2012). As a consequence, θ is related to the exponent γ of near contacting neighbours by Eq. (75). A more detailed investigation of the excitation modes related to the opening and closing of contacts suggests that there are in fact two relevant exponents $\theta_{\rm e}$ and $\theta_{\rm l}$ (Lerner *et al.*, 2013): $\theta_{\rm e}$ corresponding to motions of particles extending through the entire systems; and $\theta_{\rm l}$ corresponding to a local buckling of particles. A marginal stability analysis provides $\gamma = (2 + \theta_{\rm e})^{-1} = (1 - \theta_{\rm l})/2$ (Müller and Wyart, 2015), which has also been demonstrated numerically (Lerner *et al.*, 2013). Asymptotically $\theta = \min(\theta_{\rm l}, \theta_{\rm e})$ and thus $\theta = \theta_l \approx 0.2$ for $\gamma \approx 0.4$.

Theoretically, one step replica symmetry 1RSB theory for fully connected hard sphere packings in infinite dimensions predicts $\theta = 0$ (Parisi and Zamponi, 2010), while a full RSB calculation provides a non-zero $\theta = 0.42..$ and $\gamma = 0.41..$ (Charbonneau *et al.*, 2014a,b), a result corroborated theoretically with a simpler jamming model, the Perceptron model from machine learning, which exhibits a jamming transition as well (Franz and Parisi, 2016; Franz *et al.*, 2015). This result further indicates the importance of the jamming transition to general CSPs. The full-RSB values are seemingly in disagreement with the scaling relations from marginal stability in the presence of localized modes, since they predict $\theta_{\rm l} = 0.17...$ However, based on simulation results it has been shown that the probability of localized modes decreases exponentially with dimension and thus they do not contribute to the full RSB solution for $d \to \infty$ (Charbonneau *et al.*, 2015b). As a consequence, $\theta = \theta_{\rm e}$ in agreement with the scaling relations.

On the other limit of sparse graphs, replica symmetry calculations predict $\theta = 0$ in the thermodynamic limit using population dynamics (Bo *et al.*, 2014) (see Sec. V.A).

B. Test of ergodicity and the flat assumption in Edwards ensemble

Assuming ergodicity for a jammed system of grains as proposed by Edwards (see Sec. II.C) seems contradictory at first, but has become meaningful in the first place in light of certain compaction experiments developed over the years starting from the work of Nowak *et at.* in the 90's (Brujić *et al.*, 2005; Chakravarty *et al.*, 2003; Knight *et al.*, 1995; Makse *et al.*, 2005; Nowak *et al.*, 1998, 1997; Philippe and Bideau, 2002; Richard *et al.*, 2005).

Nowak, *et al.* (Nowak *et al.*, 1998, 1997) performed a set of experiments of the compaction of spherical glass beads as a function of increasing and decreasing vertical tapping intensity. Figure 10 shows their results for the packing fraction ρ versus the tapping intensity Γ (normalized by the acceleration due to gravity). The key observation is that the system, after initial transient behavior on the 'irreversible branch', reaches a 'reversible branch'

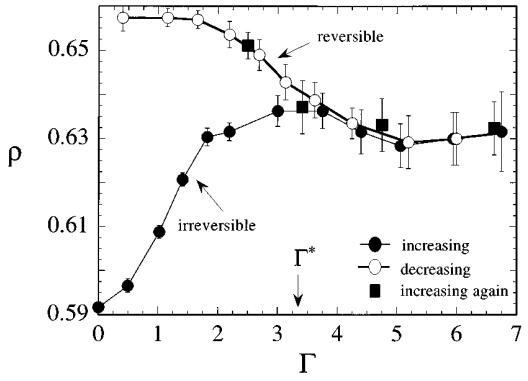

FIG. 10 The packing fraction ρ plotted as a function of the shaking intensity Γ from experiments of granular packings undergoing vertical tapping (Nowak *et al.*, 1998). The intensity is defined as the ratio of the peak acceleration during a single tap to the gravitational acceleration. The system is prepared initially at low packing fraction and subjected to taps of increasing intensity. The tapping intensity is then successively reduced, and the system falls on a reversible branch, where the system retraces the density versus intensity behavior upon subsequent increases and decreases of the intensity. Figure reprinted with permission from (Nowak *et al.*, 1998).

on which it retraces the variation of the packing fraction upon increasing and decreasing the intensity. The initial tapping breaks the frictional contacts that support loose packed configurations and store information about the system preparation. On the reversible branch, small tapping intensities induce denser packings with packing fractions slightly above random close packing for equal-sized spheres.

In principle, we can interpret the reversible packings as equilibrium-like states, in which the details of the microscopic configurations and the compaction protocol are irrelevant, as demonstrated by the reversible nature of the states evidenced by the unique branch traveled by the system as the external intensity is increased and decreased. These are the states for which we expect, in principle, a statistical mechanical formalism to hold. The existence of such a reversible branch has been corroborated in a number of experimental systems with different compaction techniques, e.g., under mechanical oscillations and vibrations, shearing, or pressure waves (Brujić *et al.*, 2005; Chakravarty *et al.*, 2003; Philippe and Bideau, 2002) and studied with theory and modelling (Caglioti *et al.*, 1997; Krapivsky and BenNaim, 1994; Nicodemi, 1999; Nicodemi *et al.*, 1997a,b,c, 1999; Prados *et al.*, 2000). However, this interpretation has been challenged in a number of studies of ergodicity in jammed matter.

Systems that are subjected to a constant drive such as infinitesimal tapping or also small shear are able to explore their phase space dynamically, such that ergodicity can be tested directly by comparing time averages and averages with respect to the constant volume ensemble. We stress here, that only infinitesimal driving forces should be applied to test equiprobable states (see discussion in Sec. VI). An agreement of the two averages has indeed been observed in simple models (Berg *et al.*, 2002; Gradenigo *et al.*, 2015), as well as soft sphere systems with a small number of particles $N = 30$ (Wang *et al.*, 2010a, 2012).

Some recent systematic results are more controversial though, motivating a continued investigation of this fascinating concept. A very detailed and rigorous numerical analysis confirms that at low tapping intensities, the system can not be considered to be ergodic: Two different realizations of the same preparation protocol do not correspond to the same stationary distribution, indicated by a statistical test of data for both the packing density (Paillusson, 2015; Paillusson and Frenkel, 2012) using volume histograms sample over time (McNamara *et al.*, 2009a,b), and the trace of the force-moment tensor (Gago *et al.*, 2016). When considering the fraction of persistent contacts as a function of tapping intensity, one observes that the non-ergodic regime coincides with a larger percentage of persistent contacts, while such contacts are almost absent in the ergodic regime (Gago *et al.*, 2016). The picture that emerges is that the breakdown of ergodicity is connected to the presence of contacts that do not break under the effect of the tapping. In accordance with physical intuition, the system can then not sample its whole phase space, but is stuck in specific regions with the consequent breaking of ergodicity. An additional reason to doubt the validity of ergodicity is the violation of the time reversal symmetry due to dissipation (Dauchot, 2007).

Ergodicity is also intimately related to the existence of non-equilibrium fluctuation-dissipation relations (FDR) characterized by an effective temperature (Cugliandolo, 2011). For equilibrium systems, the FDR is a very general result relating time correlations and responses through the temperature of the thermal environment. Non-equilibrium FDRs have been shown to hold in a wide range of systems starting with the work of Ref. (Cugliandolo *et al.*, 1997), e.g., for glassy systems (Bellon and Ciliberto, 2002; Crisanti and Ritort, 2003; Leuzzi, 2009) and models of driven matter (Berthier *et al.*, 2000; Loi *et al.*, 2008) (see also the review (Marconi *et al.*, 2008)). It has recently also been demonstrated in single molecule DNA driven out of equilibrium by an optical tweezer (Dieterich *et al.*, 2015). Non-equilibrium FDRs and effective temperatures are often linked to the slow modes of the relaxation in a glassy phase (Cugliandolo *et al.*, 1997). In granular compaction, the relaxation to the final density is similarly slow, following, e.g., an inverse logarithmic law under tapping (Krapivsky and BenNaim, 1994; Nowak *et al.*, 1998, 1997) and a Kohlrausch-Williams-Watts law

under shear (Lu *et al.*, 2008a). The fluctuations induced by the continuous driving allow for the definition of an effective temperature, which, in an ergodic system, should agree with the granular temperature associated with the canonical volume ensemble (Cugliandolo, 2011). This allows for an indirect test of ergodicity, which has been established in a number of systems, both toy models (Barrat *et al.*, 2000; Brey *et al.*, 2000; Coniglio *et al.*, 2004; Dean and Lefèvre, 2001; Fierro *et al.*, 2002a, 2003; Lefevre, 2002; Lefèvre and Dean, 2002; Nicodemi, 1999; Nicodemi *et al.*, 2004; Prados and Brey, 2002; Tarjus and Viot, 2004) and more realistic ones using MD simulation of slowly sheared granular materials (Makse and Kurchan, 2002), as well as experiments measuring effective temperatures in colloidal jammed systems (Song *et al.*, 2005) and slowly sheared granular materials in a vertical Couette cell (Potiguar and Makse, 2006; Wang *et al.*, 2008, 2006) and vibrating cell (Ribiere *et al.*, 2007). The observation of ratcheting in packings of polygonal particles under cyclic load (Alonso-Marroquín and Herrmann, 2004) sheds however some doubts about the exploration of configuration space due to systematic irreversible displacements on the grain scale: not only is time reversal violated, but a steady state does not seem to be reached.

Apart from ergodicity, the second controversial concept underlying Edwards statistical mechanics is the assumption of equiprobability of jammed microstates. One strategy to test this assumption of a flat microstate distribution is to evaluate all possible jammed configurations and counting the occurrence of distinct microstates. In realistic systems, a conclusive study of the microstate statistics is restricted to a small number of particles, for which an exhaustive search of all jammed configurations is feasible. In simulations the jammed states have been enumerated by determining the minima in the potential energy landscape of frictionless soft disks (Gao *et al.*, 2006; Wang *et al.*, 2012, 2006). Here, one can consider two packings to be identical (i.e., belonging to the same microstate) if they have the same network of contacts. In principle, this would require to test if their networks can be mapped onto each other by translation, rotation, or by permutation of particles of the same size. For practical purposes, it is sufficient to test whether the eigenvalues of their dynamical matrix are equal (within a noise threshold) (Gao *et al.*, 2006). A highly non-uniform distribution has been found for $N = 10-30$, as confirmed also in ingenious experiments mimicking the simulation results where small vibrations are used to simulate a frictionless system (Gao *et al.*, 2009). In fact, key features of the frequency distribution do not change when the packing-generation algorithm is changed: frequent packings remain frequent and rare ones remain rare. These results indicate that the frequency distribution of jammed packings is strongly influenced by geometrical properties of the multidimensional configuration space. The conclusion is that (for a very small number of particles) the structural and mechanical properties of dense granular media are not dominated equally by all possible configurations as Edwards assumed, but by the most frequent ones. A simplification in the counting of configurations can be achieved if a 2d system is confined between two parallel plates less than two particle diameters apart. For this case it was found by complete enumeration of all possible jammed structures (Bowles and Ashwin, 2011) that all states of equal density are equivalent, thus confirming Edwards' flatness assumption for this simple system. They also find that all configurations are isostatic and that at the spontaneous equilibration of two subsystems in contact the entropy increases.

In (Asenjo *et al.*, 2014; Xu *et al.*, 2011) the number of distinct jammed microstates of systems of up to 128 polydisperse soft disks have been evaluated by computing the volume of basins of attraction of individual minima on the potential energy landscape. Here, the observation that different basins have different volumes already implies that they will not be equally populated and thus equiprobability breaks down. An important consequence of this breakdown is that the granular entropy is then strictly no longer given by $S = \log \Omega(V)$. However, as shown in (Asenjo *et al.*, 2014) it is possible to identify the more general expression

$$S^* = -\sum_i p_i \ln p_i - \ln N!, \tag{77}$$

as entropy, where p_i is the probability to generate the ith packing. The subtracted term $-\ln N!$ ensures that two systems in identical macrostates are in equilibrium under an exchange of particles. Equation (77) is indeed physically meaningful satisfying both additivity and extensivity. One important consequence is that a system-size independent equilibrium between different packings is indeed well defined. One can conclude that, even though S^* is not strictly Edwards granular entropy, entropic concepts are still significant for jammed granular matter and might elucidate in particular why these athermal systems are successfully described by an equilibrium-like thermodynamics. In fact, the equilibration of the temperature-like parameters in Edwards statistical mechanics has been demonstrated in experiments (Jorjadze *et al.*, 2011; Puckett and Daniels, 2013; Schröter *et al.*, 2005), although only the angoricity and not the compactivity has been shown to equilibrate (Puckett and Daniels, 2013). An upper bound on the Edwards entropy in frictional hard-sphere packings has recently been suggested (Baranau *et al.*, 2016).

C. Are there alternatives to Edwards' approach?

As stated above, there are currently several observations that are used to either justify or reject a thermodynamic description of granular media. For example the reversibility of the packing fraction ϕ during increasing and

decreasing of the vertical tapping amplitude Γ in compaction experiments in Fig. 10 seems to be an indication in favor of the existence of equilibrium states. The interesting aspect of this experiment is that it suggests that ϕ and Γ might represent state variables of the system since $\phi(\Gamma)$ seems independent on how it is reached. However, this is only suggestive of a state variable; these experiments do not prove that these variables indeed uniquely define a state of the system. In fact other state variables have been proposed, including topological descriptors of the contact network (Arevalo *et al.*, 2013)

On the other side, there are many observations that assert the invalidity of the Edwards' statistical description as discussed above. Reference is usually made to the fact that different protocols for generating packings may access different states of the system, and thus the ensemble and dynamical averages do not yield the same results. Consequently, the right state variables for a thermodynamic description of granular media have not yet been identified. This view, encountered in the literature, asserts that Edwards' thermodynamics is ill-founded (as regards to its basic principles) (see e.g. (Dauchot, 2007)).

A perusal of the current literature would find that the community of scientists interested in the foundation of Edwards thermodynamics is practically divided between these two camps. In a Hegelian dialectical debate, Edwards ensemble has been first proposed in its entire glory (the thesis), then discredited with equal strength in a series of experiments and simulations (the antithesis). We believe that both, praises and criticisms (thesis and antithesis) have their merits, although they are produced somehow artificially, because the foundation of Edwards ensemble has not yet been formulated in a rigorous way. It seems obvious that the stage is set now for a Hegelian synthesis that will resolve this tension reinterpreting the two opposing views in light of current state-of-the-art understanding of disordered systems.

Encouraging examples abound: Firstly because the statistical laws emerging as a result of a large number of grains become debatable when applied to granular media with few degrees of freedom. Is the presence of a large number of grains that gives rise to regularities (e.g. statistical uniformity) which are absent in systems with few degrees of freedom? Secondly, the statistical properties of a large number of grains may never be explained in purely mechanical terms, and hence a thermodynamic approach may become unavoidable. And thirdly, because if one starts from the very beginning by defining the metastable jammed states and not the protocols, then one avoids the whole question of the ergodic hypothesis or protocol dependence or similar issues, which are not really essential for Edwards' statistics. We will discuss in detail this line of reasoning in Section V by exploiting an inspired analogy between metastable jammed states with the metastable states of spin-glass systems.

IV. EDWARDS VOLUME ENSEMBLE

In this chapter we focus on the Voronoi convention to define the microscopic volume function of an assembly of jammed particles. As we discuss in detail, Edwards statistical mechanics of a restricted volume ensemble can then be cast into a predictive framework to determine packing densities for both spherical and non-spherical particles. Even though other conventions like the quadrons discussed in Sec. II.D.1 also tessellate space and satisfy the additivity condition Eq. (20), the Voronoi convention has the added advantage that the resulting cell volumes can be identified with the available volume per particle, giving it a clear physical interpretation. In the next sections we outline the mean-field statistical mechanical approach based on a coarse-graining of the Voronoi volume function Eq. (27). In Secs. IV.C–IV.F, we discuss different aspects of packings of spheres, such as the effects of dimensionality, bidispersity, and adhesion. In Sec. IV.G we focus on packings of non-spherical shapes. A comprehensive phase diagram classifying packings of frictional/frictionless/adhesive spheres and non-spherical shapes is presented in Sec. IV.H.

A. Mean-field calculation of the microscopic volume function

The key question is how analytical progress can be made with the volume function Eq. (27). The global minimization in the definition of $l_i(\hat{\mathbf{c}})$, Eq. (28), implies that the volume function is a complicated non-local function. This global character indicates the existence of strong correlations and greatly complicates the calculation of, e.g., the partition function in the Edwards ensemble approach. In order to circumvent these difficulties, we review here a mean-field geometrical viewpoint developed in a series of papers (Baule and Makse, 2014; Baule *et al.*, 2013; Bo *et al.*, 2014; Briscoe *et al.*, 2008, 2010; Liu *et al.*, 2015; Meyer *et al.*, 2010; Portal *et al.*, 2013; Song *et al.*, 2010, 2008; Wang *et al.*, 2010a,b, 2011, 2010c), where the central quantity is not the exact microscopic volume function, but rather the average or coarse-grained volume of an individual cell in the Voronoi tessellation. The packing density ϕ of a system of monodisperse particle of volume V_0 is given by

$$\phi = \frac{NV_0}{\sum_{i=1}^{N} \mathcal{W}_i} = \frac{V_0}{\frac{1}{N}\sum_{i=1}^{N} \mathcal{W}_i}. \tag{78}$$

In the limit $N \to \infty$ we replace the denominator by the ensemble averaged volume of an individual cell $\overline{W} = \langle \mathcal{W}_i \rangle_i$:

$$\frac{1}{N}\sum_{i=1}^{N} \mathcal{W}_i \longrightarrow \overline{W}, \qquad N \to \infty. \tag{79}$$

As a result the volume fraction is simply

$$\phi = V_0/\overline{W}. \tag{80}$$

Considering Eq. (27), we can perform an ensemble average to obtain:

$$\begin{aligned}\overline{W} &= \left\langle \frac{1}{d}\oint \mathrm{d}\hat{\mathbf{c}}\, l_i(\hat{\mathbf{c}})^d \right\rangle_i = \frac{1}{d}\oint \mathrm{d}\hat{\mathbf{c}}\, \left\langle l_i(\hat{\mathbf{c}})^d \right\rangle_i \\ &= \frac{1}{d}\oint \mathrm{d}\hat{\mathbf{c}} \int_{c^*(\hat{\mathbf{c}})}^{\infty} \mathrm{d}c\, c^d p(\mathbf{c}, z).\end{aligned} \tag{81}$$

In the last step we have introduced the pdf $p(\mathbf{c}, z)$ which is the probability density to find the Voronoi boundary VB at a value c in the direction $\hat{\mathbf{c}}$. This involves a lower cut-off c^* in the direction $\hat{\mathbf{c}}$ due to the hard-core boundary of the particles. Crucially, we assume that the pdf is a function of $\mathbf{c}$ and the coordination number z only rather than a function of the exact particle configurations in the packing. This is the key step in the coarse-graining procedure, which replaces the exact microscopic information contained in $l_i(\hat{\mathbf{c}})$ by a probabilistic quantity. In the following, we focus on spheres, where $p(\mathbf{c}, z) = p(c, z)$ and $c^*(\hat{\mathbf{c}}) = R$ due to the statistical isotropy of the packing and the isotropy of the reference particle itself. More complicated shapes will be treated in subsequent sections.

We now introduce the cumulative distribution function (CDF) $P_>(c, z)$ via the usual definition $p(c, z) = -\frac{\mathrm{d}}{\mathrm{d}c}P_>(c, z)$. Eq. (81) becomes then in 3d

$$\begin{aligned}\overline{W}(z) &= \frac{4\pi}{3}\int_R^{\infty} \mathrm{d}c\, c^3 p(c, z) \\ &= V_0 + 4\pi \int_R^{\infty} \mathrm{d}c\, c^2\, P_>(c, z),\end{aligned} \tag{82}$$

where $V_0 = \frac{4\pi}{3}R^3$. The advantage of using the CDF $P_>$ rather than the pdf, is that the CDF has a simple geometrical interpretation. We notice first that $P_>$ contains the probability to find the VB in a given direction $\hat{\mathbf{c}}$ at a value larger than c, given z contacting particles. But this probability equals the probability that $N-1$ particles are outside a volume Ω centered at $\mathbf{c}$ relative to the reference particle (Fig. 11). Otherwise, if they were inside that volume, they would contribute a VB smaller than c. The volume Ω is thus defined as

$$\Omega(\mathbf{c}) = \int \mathrm{d}\mathbf{r}\, \Theta(c - s(\mathbf{r}, \hat{\mathbf{c}}))\Theta(s(\mathbf{r}, \hat{\mathbf{c}})), \tag{83}$$

where $s(\mathbf{r}, \hat{\mathbf{c}})$ parametrizes the VB in the direction $\hat{\mathbf{c}}$ for two spheres of relative position $\mathbf{r}$. $\Theta(x)$ denotes the usual Heavyside step function. Due to the isotropy of spheres, the direction $\hat{\mathbf{c}}$ can be chosen arbitrarily. We refer to Ω as the *Voronoi excluded volume*, which extends the standard concept of the hard-core excluded volume V_{ex} that dominates the phase behaviour of interacting particle systems at thermal equilibrium (Onsager, 1949).

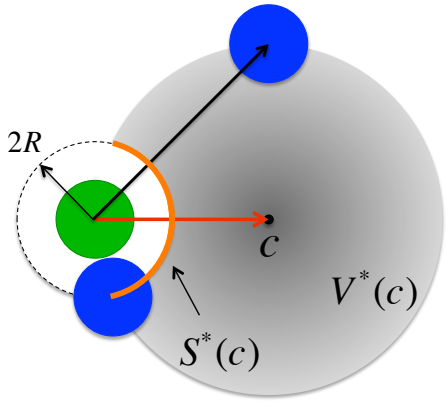

FIG. 11 (Colors online) The condition to have the VB in the direction $\hat{s}$ from the reference particle (green sphere) at the value c is geometrically related to the exclusion volume Ω for all other particles (blue spheres). Taking into account the conventional hard-core excluded volume leads to the Voronoi excluded volume Eq. (86) (the Moon phase - grey volume V^*) and Voronoi excluded surface Eq. (86) (orange line).

This geometrical interpretation allows us to connect $P_>(c, z)$ with the N-particle pdf $P_N(\{\mathbf{r}_1, \mathbf{r}_2, ..., \mathbf{r}_N\})$ in an exact way. Without loss of generality we denote the reference particle i as particle 1. Then, $P_>(c, z) = P_>(\mathbf{r}_1; \Omega)$, i.e., the probability that the $N-1$ particles apart from particle 1 are outside the volume Ω. Since $P_N(\{\mathbf{r}_1, \mathbf{r}_2, ..., \mathbf{r}_N\})$ expresses the probability to find particle 1 at $\mathbf{r}_1$, particle 2 at $\mathbf{r}_2$, etc., we have (Jin *et al.*, 2010)

$$\begin{aligned}P_>(\mathbf{r}_1; \Omega) = \mathcal{C} \int \mathrm{d}\mathbf{r}^{N-1} P_N(\{\mathbf{r}_1, \mathbf{r}_2, ..., \mathbf{r}_N\}) \\ \times \prod_{i=2}^{N} \left[1 - m(\mathbf{r}_i - \mathbf{r}_1; \Omega\right],\end{aligned} \tag{84}$$

where $\mathcal{C}$ ensures proper normalization. The indicator function $m(\mathbf{r}; \Omega)$ is given by

$$m(\mathbf{r}; \Omega) = \begin{cases} 1, & \mathbf{r} \in \Omega \\ \\ 0, & \mathbf{r} \notin \Omega \end{cases} \tag{85}$$

Equation (84) is the starting point for the calculation of $P_>(c, z)$ from a systematic treatment of the particle correlations as discussed in Sec. IV.D for 2d packings (Jin *et al.*, 2014) and in Sec. IV.C for high-dimensional packings (Jin *et al.*, 2010). Here, we proceed with a more intuitive approach based on an exact treatment in 1d which is used as an approximation to the 3d case, as originally developed in (Song *et al.*, 2008).

We can first separate contributions to $P_>$ stemming from bulk and contacting particles. We introduce two CDFs, the bulk contribution P_B and the contact contribution P_C:

- $P_{\rm B}$ denotes the probability that spheres in the bulk are located outside the Moon-phase grey volume V^* in Fig. 11. The volume V^* is the volume excluded by Ω for bulk particles and takes into account the overlap between Ω and the hard-core excluded volume $V_{\rm ex}$:

$$V^* = \Omega - \Omega \cap V_{\rm ex} = \int {\rm d}\mathbf{r}\, \Theta(r-2R)\Theta(c-s(\mathbf{r},\hat{\mathbf{c}}))\Theta(s(\mathbf{r},\hat{\mathbf{c}})). \quad (86)$$

  We call V^* the Voronoi excluded volume.

- $P_{\rm C}$ denotes the probability that contacting spheres are located outside the boundary of the grey area indicated in orange in Fig. 11 and denoted S^*. The surface S^* is the surface excluded by Ω for contacting particles:

$$S^* = \partial V_{\rm ex} \cap \Omega = \oint {\rm d}\hat{\mathbf{r}}\, \Theta(c-s(\mathbf{r},\hat{\mathbf{c}}))\Theta(s(\mathbf{r},\hat{\mathbf{c}}))\Big|_{r=2R}, \quad (87)$$

  where $\partial V_{\rm ex}$ denotes the boundary of $V_{\rm ex}$.

A key assumption to make analytical progress is to assume $P_{\rm B}$ and $P_{\rm C}$ to be statistically independent, thus $P_> = P_{\rm B}P_{\rm C}$. There is no a priori reason why this should be the case, so the independence should be checked a posteriori from simulation data. For spheres and non-spherical particles close to the spherical aspect ratio, it has been verified that independence is a reasonable assumption (Baule *et al.*, 2013; Song *et al.*, 2008). It is then natural to consider only $P_{\rm C}$ to be a function of z. Therefore,

$$P_>(c,z) = P_{\rm B}(c) \times P_{\rm C}(c,z). \quad (88)$$

We now derive a functional form of the $P_{\rm B}$ term. In 1d, the distribution of possible arrangements of N hard rods in a volume V can be mapped to the distribution of ideal gas particles by removing the occupied volume NV_0 (Krapivsky and BenNaim, 1994; Palásti, 1960; Rényi, 1958; Tarjus and Viot, 2004). The probability to locate one particle at random outside the volume V^* in a system of volume $V - NV_0$ is then $P_>(1) = 1 - V^*/(V - NV_0)$. For N ideal particles, we obtain

$$P_>(N) = \left(1 - \frac{V^*}{V - NV_0}\right)^N. \quad (89)$$

The particle density is $\tilde{\rho} = N/(V - NV_0)$. Therefore

$$\lim_{N\to\infty} P_>(N) = \lim_{N\to\infty} \left(1 - \frac{\tilde{\rho}V^*}{N}\right)^N = e^{-\tilde{\rho}V^*}. \quad (90)$$

In the thermodynamic limit the probability to observe N particles outside the volume V^* is given by a Boltzmann-like exponential distribution. In this limit, the particle density becomes

$$\tilde{\rho} = \lim_{N\to\infty} \frac{1}{\frac{1}{N}\sum_{i=1}^N \mathcal{W}_i - V_0} = \frac{1}{\overline{W} - V_0}, \quad (91)$$

using the tessellation of the total volume and Eq. (79). While the above derivation is exact in 1d, the extension to higher dimensions is an approximation: Even if there is a void with a large enough volume, it might not be possible to insert a particle due to the constraint imposed by the geometrical shape of the particles (which does not exist in 1d). Nevertheless, in what follows, we assume the exponential distribution of Eq. (90) to be valid in 3d as well and write

$$P_{\rm B}(c) = e^{-\tilde{\rho}V^*(c)}, \quad (92)$$

where the Voronoi excluded volume can be calculated explicitly from Eq. (86):

$$V^*(c) = V_0\left(\left(\frac{c}{R}\right)^3 - 4 + 3\frac{R}{c}\right). \quad (93)$$

Furthermore, we also assume $P_{\rm C}$ to have the same exponential form as Eq. (92), despite not having the large number approximation leading to it [the maximum coordination is the kissing number 12]. Introducing a surface density $\sigma(z)$, we write

$$P_{\rm C}(c) = e^{-\sigma(z)S^*(c)}, \quad (94)$$

where the Voronoi excluded surface follows from Eq. (87):

$$S^*(c) = 2S_0\left(1 - \frac{R}{c}\right), \quad (95)$$

where $S_0 = 4\pi R^2$. To obtain an expression for $\sigma(z)$ we calculate the average $\langle S^*\rangle$ with respect to the pdf $-\frac{\rm d}{{\rm d}c}P_{\rm C}(c)$, which yields a simple result (Song *et al.*, 2010, 2008; Wang *et al.*, 2011)

$$\langle S^*\rangle \approx 1/\sigma(z). \quad (96)$$

In turn, $\langle S^*\rangle$ is defined as the average of the solid angles of the gaps left between z contacting spheres around the reference sphere. An alternative operational definition assuming an isotropic distribution of contact particles is:

(i) Generate z contacting particles at random.

(ii) For a given direction $\hat{\mathbf{c}}$, determine the minimal value of the VB, denoted by c_m.

(iii) The average $\langle S^*\rangle$ follows as a Monte-Carlo average in the limit.

$$\langle S^*\rangle = \lim_{n\to\infty} \frac{1}{n}\sum_{i=1}^n S^*(c_{m,i}), \quad (97)$$

where $c_{m,i}$ is the c_m value of the ith sample. Simulations following this procedure and considering $z = 1$ up to the kissing number $z = 12$ suggest that

$$\sigma(z) \approx \frac{z}{4\pi}\sqrt{3}, \qquad z > 1, \tag{98}$$

for a chosen radius $R = 1/2$. The exact constants appearing in this expression are motivated from an exact treatment of the single particle case plus corrections due to the occupied surface of contact particles (Song *et al.*, 2010; Wang *et al.*, 2011).

Due to the dependence of $\tilde{\rho}$ on $\overline{W}$, the CDF $P_>$ is thus

$$P_>(c, z) = \exp\left[-\frac{V^*(c)}{\overline{W} - V_0} - \sigma(z)S^*(c)\right], \tag{99}$$

where V^*, S^*, and σ are given by Eqs. (93,95,98). Overall, Eq. (99) with Eq. (82) leads to a self-consistent equation to determine $\overline{W}$ as a function of z:

$$\overline{W}(z) = V_0 + 4\pi \int_R^\infty \mathrm{d}c\, c^2 \exp\left[-\frac{V_0}{\overline{W}(z) - V_0} \times \right.$$
$$\left. \times \left(\frac{c^3}{R^3} - 4 + 3\frac{R}{c}\right) - \sigma(z) 2S_0 \left(1 - \frac{R}{c}\right)\right] \tag{100}$$

for which, remarkably, an analytical solution can be found. By using Eqs. (93,95,98), Eq. (100) is satisfied when (Song *et al.*, 2008):

$$\frac{\mathrm{d}}{\mathrm{d}c}\left(\frac{1}{w}\left(3\frac{R}{c}\right) + \sigma(z)S^*(c)\right) = 0, \tag{101}$$

where the free volume is

$$w \equiv (\overline{W} - V_0)/V_0. \tag{102}$$

Then, with Eq. (95) we obtain the solution for w

$$w(z) = \frac{3}{2S_0\sigma(z)} = \frac{2\sqrt{3}}{z}, \tag{103}$$

using Eq. (98) and setting $R = 1/2$ for consistency.

As the final result of this section, we arrive at the coarse-grained mesoscopic volume function

$$\overline{W}(z) = V_0 + \frac{2\sqrt{3}}{z}V_0, \tag{104}$$

which is a function of the observable coordination number z rather than the microscopic configurations of all the particles in the packing. With Eq. (78), we also obtain the packing density as a function of z

$$\phi(z) = \frac{V_0}{\overline{W}} = \frac{z}{z + 2\sqrt{3}}. \tag{105}$$

Equation (105) can be interpreted as an equation of state of disordered sphere packings. In the next section we will show that it corresponds to the equation of state in z–ϕ space in the limit of infinite compactivity.

B. Packing of jammed spheres

In the hard sphere limit angoricity can be neglected, such that the statistical mechanics of the packing is described by the volume function alone. The partition function is then given by Edwards' canonical one, Eq. (15). With the result on the coarse-grained volume function it is possible to go over from the fully microscopic partition function Eq. (15) to a mesoscopic one (Song *et al.*, 2008; Wang *et al.*, 2011). To this end we change the integration variables in Eq. (15) from the set of microscopic configurations $\mathbf{q} = \{\mathbf{q}_1, ..., \mathbf{q}_N\}$ (positions and orientations of the N particles) to the volumes $\mathcal{W}_i(\mathbf{q})$, Eq. 27, of each cell in the Voronoi tessellation. Since the microscopic volume function is given as a superposition of the individual cells, Eq. (20), the partition function Eq. (15) can be expressed as

$$\mathcal{Z} = \prod_{i=1}^{N} \int \mathrm{d}\mathcal{W}_i\, g(\boldsymbol{\mathcal{W}}) e^{-\sum_{i=1}^{N} \mathcal{W}_i/X} \Theta_{\mathrm{jam}}. \tag{106}$$

Here, the function $g(\boldsymbol{\mathcal{W}})$ for $\boldsymbol{\mathcal{W}} = \{\mathcal{W}_1, ..., \mathcal{W}_N\}$ denotes the density of states. In the coarse-grained picture all the volume cells are non-interacting and effectively replaced by the volume function Eq. (104). The partition function thus factorizes $\mathcal{Z} = \mathcal{Z}_i^N$, where

$$\mathcal{Z}_i(X) = \left(\int \mathrm{d}W\, g(W) e^{-W/X} \Theta_{\mathrm{jam}}\right)^N \tag{107}$$

Averages over the volume ensemble as well as all thermodynamic information is thus accessible via Eq. (107). The crucial step to go from the full microscopic partition function Eq. (15) to Eq. (107) is to introduce the density of states $g(W)$ for a given volume W. Although this step formally simplifies the integral, the complexity of the problem is now transferred to determining $g(W)$, which is as difficult to solve as the model itself. We discuss below suitable approximations to model $g(W)$ motivated by the uncertainty principle from quantum mechanics characterizing the discreteness of the phase space. In Eq. (107), X is the compactivity measured in units of the particle volume V_0, and Θ_{jam} imposes the condition of jamming.

In the mean-field view developed in the previous section, W is directly related to the geometrical coordination number z via Eq. (104). Therefore, we map $g(W)$ to $g(z)$, the density of states for a given z via a change of variables

$$g(W) = \int P(W|z) g(z) \mathrm{d}z, \tag{108}$$

where $P(W|z)$ is the conditional probability of a volume W for a given z, which, with Eq. (104), is given by

$$P(W|z) = \delta(W - \overline{W}(z)), \tag{109}$$

where we have neglected fluctuations in z, see (Wang *et al.*, 2010c). Substituting Eq. (108) with Eq. (109)

into Eq. (107) effectively changes the integration variable from W to z leading to the single particle (isostatic) partition function

$$\mathcal{Z}_{\rm iso}(X, Z_{\rm m}) = \int_{Z_{\rm m}}^{6} g(z)\, \exp\left[-\frac{2\sqrt{3}}{zX}\right] {\rm d}z. \quad (110)$$

The jamming condition is now absorbed into the integration range, which constrains the coordination number to isostatic packings (therefore the name isostatic partition function). Notice that in this mesoscopic mean-field approach the force and torque balance jamming conditions from $\Theta_{\rm jam}$ Eq. (10) are incorporated when we set the coordination number to the isostatic value. Thus, in this way, we circumvent the most difficult problem of implementing the force jamming condition Eq. (10).

More precisely, the geometric and force/torque constraints from Eq. (10) imply that there are two types of coordination numbers:

(i) The geometrical coordination number z, parametrizing the free volume function Eq. (103) as a function of all contacting particles, constraining the position of the particle via the hard-core geometrical interaction Eq. (1).

(ii) The mechanical coordination number $Z_{\rm m}$, counting only the geometrical contacts z that at the same time carry non-zero force (Oron and Herrmann, 1999, 1998) and therefore takes into account the force and torque balance conditions Eqs. (2)-(7) via the isostatic condition.

From the definition we have $z \geq Z_m$ since there could be a geometric contact that constraints the motion of the particle but carries no force. This distinction makes sense when there is friction in the packing. For instance, imagine a frictionless particle at the isostatic point $z = Z_m = 6$ (although isostatic is a global property). Now add friction to the interactions. The mechanical coordination number can be as low as $Z_m = 4$, but still $z = 6$; the geometrical constraints are the same, only two forces have been set to zero, allowing for tangential forces to appear in the remaining 4 contacts.

For frictionless packings, we have $z = Z_m$. Furthermore, in the limit of infinite compactivity, where the entropy of the packings is maximum and therefore, the packings are the most probable to find in experiments, we will see that again $z = Z_m$ and the distinction between mechanical and geometrical coordination number disapears. In what follows, we will consider the consequences of considering the two coordination numbers only for the following 3d monodisperse system of spheres. The distinction between z and Z_m will allow us to describe the phase diagram for all compactivities as in Fig. 12a, below. In the remaining sections where we treat non-spherical particles and others, either we will assume frictionless particles or packings at infinite compactivity for which we simply set $z = Z_m$ and get a single equation of state rather than the yellow area in Fig. 12a.

The mechanical coordination $Z_{\rm m}$ defines isostatic packings, which, strictly applies only to the two limits $Z_{\rm m} = 2d = 6$ for frictionless particles with friction $\mu \to 0$ and $Z_{\rm m} = d+1 = 4$ for infinitely rough particles $\mu \to \infty$. An important assumption is that $Z_{\rm m}$ varies continuously as a function of μ

$$4 \leq Z_{\rm m}(\mu) \leq z \leq 6. \quad (111)$$

In fact, a universal $Z_{\rm m}(\mu)$ curve has been observed for a range of different packing protocols (Song *et al.*, 2008) and calculated analytically in (Bo *et al.*, 2014). The upper bound of z is the frictionless isostatic limit. This effectively excludes from the ensemble the partially crystalline packings, which are characterized by larger z.

The next step in the derivation is the calculation of the density of states $g(z)$ which is developed in three steps (we notice that this is not needed if only the equation of state at $z = Z_m$ is sought).

(i) First, we consider that the packing of hard spheres is jammed in a $\infty-$PD configuration where there can be no collective motion of any contacting subset of particles leading to unjamming when including the normal and tangential forces between the particles. As discussed in the introduction, this jammed state is the ground state and corresponds to the collectively jammed category proposed in Ref. (Torquato and Stillinger, 2001). While the degrees of freedom are continuous, the fact that the packing is collectively jammed implies that the jammed configurations in the volume space are not continuous. Otherwise there would be a continuous transformation in the position space that would unjam the system contradicting the fact that the packing is collectively jammed. Thus, we consider that the configuration space of jammed matter is discrete, since we cannot change one configuration to another in a continuous way. A similar consideration of discreteness has been studied in (Torquato and Stillinger, 2001).

(ii) Second, we refer to the dimension per particle of the configuration space as $\mathcal{D}$ and consider that the distance between two jammed configurations is not broadly distributed (meaning that the average distance is well-defined). We call the typical (average) distance between configurations in the volume space as h_z, and therefore the number of configurations per particle is proportional to $(h_z)^{-\mathcal{D}}$. The constant h_z plays the role of Planck's constant in quantum mechanics which sets the discreteness of the phase space via the uncertainty principle.

(iii) Third, we add z constraints per particle due to the fact that the particle is jammed by z contacts. Thus, there are Nz position constraints ($|r_{ij}| = 2R$) for a jammed state of hard spheres as compared to the unjammed "gas" state. Therefore, the number of degrees of freedom is reduced to $\mathcal{D} - z$, and the number of configurations is then $1/(h_z)^{\mathcal{D}-z}$ leading to

$$g(z) = (h_z)^{z-\mathcal{D}}. \quad (112)$$

Note that the factor $(h_z)^{-\mathcal{D}}$ will drop out when performing ensemble averages. Physically, we expect $h_z \ll 1$. The exact value of h_z can be determined by a fitting of the theoretical values to the simulation data, but it is not important as long as we take the limit at the end: $h_z \to 0$.

Having defined the jammed ensemble via the partition function $\mathcal{Z}_{\rm iso}$, we can calculate the ensemble averaged packing density $\phi(X, Z_{\rm m}) = \langle \phi(z) \rangle$ as

$$\phi(X, Z_{\rm m}) = \frac{1}{\mathcal{Z}_{\rm iso}} \int_{Z_{\rm m}}^{6} \frac{z}{z + 2\sqrt{3}} e^{-\frac{2\sqrt{3}}{zX} + z \log h_z} {\rm d}z, \quad (113)$$

Equation (113) gives predictions on the packing densities as a function of X over the whole range of friction values $\mu \in [0, \infty)$ since $Z_m(\mu)$ is determined by friction (Song *et al.*, 2008). We can identify three distinct regimes (see Fig. 12):

1. In the limit of vanishing compactivity ($X \to 0$), only the minimum volume at $z = 6$ contributes. The density is the RCP limit $\phi_{\rm rcp} = \phi(X = 0, Z)$:

$$\phi_{\rm rcp} = \frac{1}{1 + 1/\sqrt{3}} = 0.634.., \qquad Z_{\rm m}(\mu) \in [4, 6], \quad (114)$$

and the corresponding RCP free volume is

$$w_{\rm rcp} = \frac{1}{\sqrt{3}}. \quad (115)$$

$\phi_{\rm rcp}$ defines a vertical line in the phase diagram ending at the J-point: (0.634, 6). Here, RCP is identified as the ground state of the jammed ensemble with maximal density and coordination number. Notice that this result is also obtained from Eq. (105) at $z = 6$.

2. In the limit of infinite compactivity ($X \to \infty$), the Boltzmann factor $\exp[-2\sqrt{3}/(zX)] \to 1$, and the average in Eq. (113) is taken over all states with equal probability. The $X \to \infty$ limit defines the random loose packing equation of state $\phi_{\rm rlp}(Z) = \phi(X \to \infty, Z_{\rm m})$ as a function of $Z_{\rm m}$:

$$\phi_{\rm rlp}(Z_{\rm m}) = \frac{1}{\mathcal{Z}_{\rm iso}(\infty, Z_{\rm m})} \int_{Z_{\rm m}}^{6} \frac{z}{z + 2\sqrt{3}} e^{z \ln h_z} {\rm d}z$$
$$\approx \frac{Z_{\rm m}}{Z_{\rm m} + 2\sqrt{3}}, \qquad Z_{\rm m}(\mu) \in [4, 6]. \quad (116)$$

The approximation comes from $h_z \to 0$. For small but finite $h_z \ll 1$, an interesting regime appears of negative compactivity (Briscoe *et al.*, 2010), yet unstable, leading to the limit of RLP when $X \to 0^-$ which has been termed as the random very loose packing (Ciamarra and Coniglio, 2008). Thus, $\phi_{\rm rlp}$ spans a whole line in the phase diagram between the frictionless value $\phi_{\rm rcp}$ upto the limit $\mu \to \infty$ at:

$$\phi_{\rm rlp}^{\rm min} = \frac{1}{1 + \sqrt{3}/2} = 0.536.., \qquad \text{for } Z_m = 4. \quad (117)$$

The corresponding RLP free-volume is

$$w_{\rm rlp}^{\rm min} = \frac{\sqrt{3}}{2}. \quad (118)$$

These values are interpreted as the minimal density of mechanically stable sphere packings appearing at $Z_m = 4$. We notice that Eq. (116) can be obtained from the single particle Eq. (105), by setting $z = Z_m$. Indeed, in the limit of infinite compactivity the mechanical coordination takes the value of the geometrical one.

3. Finite compactivity X defines the packings inside the triangle bounded by the RCP and RLP lines and the limit for isostaticity $Z_{\rm m} = 4$ as $\mu \to \infty$ (granular line) are characterized. In this case, Eq. (113) can be solved numerically. Figure 12a shows the lines of constant compactivity plotted parametrically as a function of $Z_{\rm m}$.

Further thermodynamic characterisation is obtained by considering the entropy of the jammed configurations, which can be identified by analogy with the equilibrium framework. In equilibrium statistical mechanics we have $F = E - TS$, such that $S = E/T + \ln \mathcal{Z}$ using the free energy expression $F = -T \ln \mathcal{Z}$ (setting $k_{\rm B}$ to unity). By analogy we obtain the entropy density of the jammed configuration $s(X, Z_{\rm m})$ (entropy per particle) (Briscoe *et al.*, 2008, 2010; Brujić *et al.*, 2007):

$$s(X, Z_{\rm m}) = \langle W \rangle / X + \ln \mathcal{Z}_{\rm iso} \quad (119)$$

substituting the partition function Eq. (110) in the last step. In Fig. 12b each curve corresponds to a packing with a different Z_m value determined by Eq. (119). The projections $s(\phi)$ and $s(X)$ characterize the nature of randomness in the packings. When comparing all the packings, the maximum entropy is at $\phi_{\rm rlp}$ for $X \to \infty$, while the entropy is minimum at $\phi_{\rm rcp}$ for $X \to 0$. Following the granular line in the phase diagram we obtain the entropy for infinitely rough spheres showing a larger entropy for the RLP than the RCP. The same conclusion is obtained for the other packings at finite friction ($4 < Z_{\rm m} < 6$). We conclude that the RLP states are more disordered than the RCP states.

Approaching the frictionless J-point at $Z_m = 6$ the entropy vanishes. The interpretation of the RCP as the ground state, $X \to 0$, with vanishing entropy and therefore a unique state is surprising and somewhat at odds with the concept of MRJ (Torquato *et al.*, 2000) (see Sec. III.A.4). We notice that there exist packings above

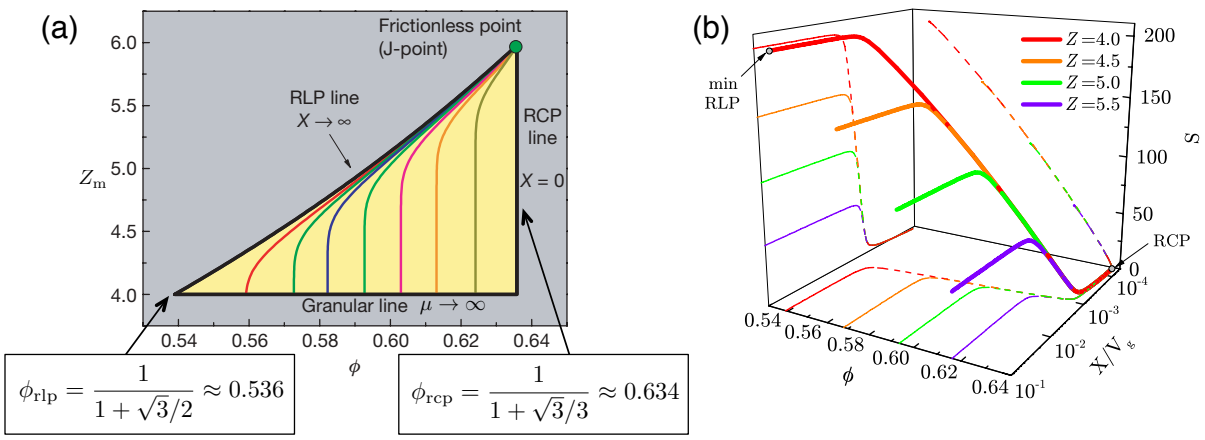

FIG. 12 (Colors online) (a) Theoretical prediction of the statistical theory Eq. (113). All disordered packings of spheres lie within the yellow triangle demarcated by the RCP line at $\phi_{rcp} = 0.634..$, the RLP line parametrized by Eq. (116) and the lower limit for stable packings at $Z = 4$ (granular line) for $\mu \to \infty$. Lines of constant finite compactivity X are in colour. Packings are forbidden in the grey area. (b) Predictions of the equation of state of jammed matter in the (X, ϕ, s)–space determined with Eq. (119). Each line corresponds to a different system with $Z_m(\mu)$ as indicated. The projections in the (ϕ, s) and (X, s) planes show that RCP ($X = 0$) is less disordered than RLP ($X \to \infty$).

RCP all the way to the FCC density (Jin and Makse, 2010; Pouliquen *et al.*, 1997), but these packings have some degree of order and are excluded from the ensemble by requiring isostaticity. This interprets the RCP in the context of a third-law of thermodynamics.

As stated, in the following results we will focus always on the $X \to \infty$ regime, where the volume function that is obtained from the solution of the self-consistent equation is also the equation of state, since we simply have $z \to Z_m$ for $X \to \infty$ when calculating the ensemble averaged packing density (compare Eqs. (105) and (116)). Therefore, we can drop the distinction between Z_m and z (for simplicity we consider z), while keeping in mind that there exist further packing states for finite X that are implied but not explicitly discussed in the next sections (e.g., in the full phase diagram Fig. 22).

C. Packing of high-dimensional spheres

According to Eq. (82), the key quantity to calculate exactly the average volume $\overline{W}$ is the CDF $P_>(\mathbf{r}_1; \Omega)$ as defined in Eq. (84). This CDF has been approximated in the work of (Song *et al.*, 2008) reviewed in previous Section IV.A by using a simple one dimensional gas-like model which is analogous in 1d to a parking lot model (Krapivsky and BenNaim, 1994; Palásti, 1960; Rényi, 1958; Tarjus and Viot, 2004), leading to the exponential form (99). It turns out that in the opposite limit of infinite dimensions (mean-field), a closed form of $P_>$ can be obtained as well, based on general considerations of correlations in liquid state theory. In this mean-field high d-limit, the form obtained in (Song *et al.*, 2008) can be obtained as a limiting case, with the added possibility to develop a systematic expansion of $P_>$ in terms of pair distribution functions allowing to include higher order correlations which were neglected in (Song *et al.*, 2008). Furthermore, the high-d limit is important to compare the predictions of the Edwards ensemble to other mean-field theories such as the RSB solution of hard-sphere packings (Parisi and Zamponi, 2010). The high-dimensional limit is treated next (Jin *et al.*, 2010).

In large dimensions, the effect of metastability between amorphous and crystalline phases is strongly reduced, because nucleation is increasingly suppressed for large d (van Meel *et al.*, 2009a,b; Skoge *et al.*, 2006). Moreover, mean-field theory becomes exact for $d \to \infty$, because each degree of freedom interacts with a large number of neighbours (Parisi, 1988) opening up the possibility for exact solutions.

In the following, we discuss the mean-field high-dimensional limit of the coarse-grained Voronoi volume theory starting from liquid state theory. We only sketch the main steps in the calculation, for full details we refer to (Jin *et al.*, 2010). Assuming translational invariance of the system, Eq. (84) can be rewritten as

$$P_>(\mathbf{r}_1; \Omega) = 1 + \sum_{k=1}^{N-1} (-1)^k \frac{\rho^k}{k!} \times \int_\Omega g_{k+1}(\mathbf{r}_{12}, \ldots, \mathbf{r}_{1(k+1)}) d\mathbf{r}_{1i} \cdots d\mathbf{r}_{1(k+1)}, \quad (120)$$

where g_n denotes the n-particle correlation function

$$g_n(\mathbf{r}_{12}, \mathbf{r}_{13}, ..., \mathbf{r}_{1n}) = \frac{N!}{\rho^n (N-n)!} \int P_N(\mathbf{r}^n, \mathbf{r}^{N-n}) \mathrm{d}\mathbf{r}^{N-n}, \quad (121)$$

with $\rho = N/V$ the particle density. The integrals in Eq. (120) express the probabilities of finding a pair, triplet, etc., of spheres within the volume Ω. For an exact calculation of $P_>$, we thus need the exact form of $g_n(\mathbf{r}_{12}, \mathbf{r}_{13} \ldots \mathbf{r}_{1n})$ to all orders, which is not available. However, assuming the generalized Kirkwood superposition approximation from liquid theory (Kirkwood, 1935), we can approximate g_n in high dimensions by a simple factorized form (Jin *et al.*, 2010):

$$g_n(\mathbf{r}_{12}, \mathbf{r}_{13}, \ldots, \mathbf{r}_{1n}) \approx \prod_{i=2}^{n} g_2(\mathbf{r}_{1i}), \tag{122}$$

where g_2 is the pair correlation function.

Equation (122) indicates that spheres $2, ..., n$ are correlated with the central sphere 1 but not with each other, which is reasonable for large d since the sphere surface is then large compared with the occupied surface. The term S_{d-1} in Eq. (124) denotes the surface of a d-dimensional sphere with radius $2R$. Substituting Eq. (122) in Eq. (120) yields

$$\begin{aligned} P_>(\mathbf{r}_1; \Omega) &= \sum_{k=0}^{N-1} (-1)^k \frac{\rho^k}{k!} \left(\int_\Omega g_2(\mathbf{r}) d\mathbf{r} \right)^k \\ &= \exp\left[-\rho \int_\Omega g_2(\mathbf{r}) d\mathbf{r} \right], \end{aligned} \tag{123}$$

in the limit $N \to \infty$ ($\rho \to 1/\overline{W}$).

Thus, we see that calculating the CDF $P_>$ reduces to know the form of the pair correlation function. Indeed, the exponential form calculated in Section IV.A using a 1d model, Eq. (99), is obtained from Eq. (123) by assuming the following simplified pair correlation function (which has been considered also in (Torquato and Stillinger, 2006)):

$$g_2(r) = \frac{z}{\rho S_{d-1}} \delta(r - 2R) + \Theta(r - 2R). \tag{124}$$

This form corresponds to assuming a set of z contacting particles contributing to the delta-peak at $2R$ plus a set of uncorrelated bulk particles contributing to a flat (gas-like) distribution characterized by the Θ-function. This form, depicted in Fig. 13, further assumes the factorization of the contact and bulk distribution and represents the simplest form of the pair correlation function, yet, it gives rise to accurate results for the predicted packing densities. The important point is that the high-d result Eq. (123) allows to express more accurate pair correlation functions than Eq. (124) into the formalism to systematically capture higher order features in the correlations, thus allowing for an improvement of the theoretical results. Such improvements are treated in Sections IV.D and IV.F.

Using Eq. (124) and the definition of Ω, Eq. (83), we see that the volume integral $\int_\Omega g_2(\mathbf{r}) d\mathbf{r}$ becomes

$$\int_\Omega g_2(\mathbf{r}) d\mathbf{r} = \frac{z S^*(c)}{\rho S_{d-1}} + V^*(c), \tag{125}$$

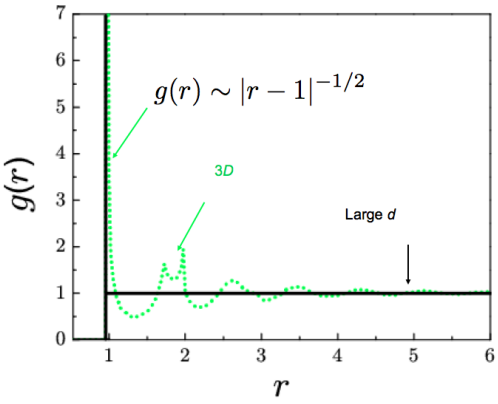

FIG. 13 (Colors online) At the core of the mean-field approach developed in (Song *et al.*, 2008) to calculate the volume fraction of 3d packings is the approximation of the real pair correlation function (green curve) with its characteristic peaks indicating short-range correlations in the packing and the power-law decay of the near contacting particles, Eq. (74), by a simple delta-function (black curve) at the contacting point plus a flat distribution charactering a gas-like bulk of uncorrelated particles. Surprisingly, such an approximation, which is expected to work better at high dimensions than at low dimensions, gives accurate results for the volume fraction in 3d, as shown in Section IV.A. High-dimensional analyses allow to treat higher-order correlations neglected in (Song *et al.*, 2008) to improve the theoretical predictions in a systematic way as shown in Secs. IV.C, IV.D and IV.F.

where V^* and S^* are the Voronoi excluded volume and surface, Eqs. (86,87), for general d. We thus recover the same factorized form of the CDF as in 3d, Eq. (99), but now generalized to any dimension d, separating bulk and contact contributions

$$P_>(c, z) = \exp\left[-\rho V^*(c) - \frac{z S^*(c)}{S_{d-1}} \right], \tag{126}$$

whose validity should increase with increasing dimension (see Fig. 14). The Voronoi excluded volume and surface, V^* and S^*, can be calculated with Eqs. (86,87) for general d. The term z/S_{d-1} can be interpreted as the surface density $\sigma(z)$ in the 3d theory.

The d-dimensional generalization of Eq. (82) is

$$\overline{W} = V_0^{(d)} + \frac{V_0^{(d)} d}{R^d} \int_R^\infty \mathrm{d}c\, c^{d-1} P_>(c, z). \tag{127}$$

For large d an analytical solution of Eq. (127) can be obtained. In terms of $w = (\overline{W} - V_0^{(d)})/V_0^{(d)}$ one obtains the following asymptotic predictions of the Edwards ensemble in high-d (Jin *et al.*, 2010) for the free volume:

$$w_{\mathrm{Edw}} = \frac{3}{4d} 2^d, \tag{128}$$

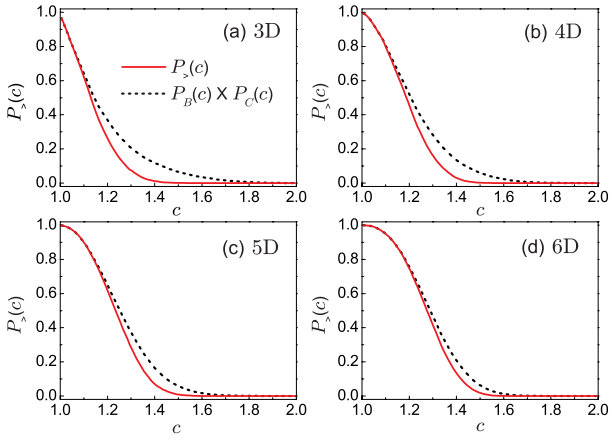

FIG. 14 (Colors online) Evaluation of the factorization approximation of $P_>$ with increased dimensionality. The CDFs $P_>$, $P_{\rm B}$, and $P_{\rm C}$ are all evaluated from simulation data. The factorized CDF approximates the true CDF increasingly well for larger dimensions and is assumed to become exact as $d \to \infty$. Figure reprinted with permission from (Jin *et al.*, 2010).

and the volume fraction in the Edwards ensemble

$$\phi_{\rm Edw} = \frac{4}{3} d\, 2^{-d}. \tag{129}$$

The scaling:

$$\phi \sim d\, 2^{-d} \tag{130}$$

is also found in other approaches for jammed spheres in high dimensions. In principle, it satisfies the Minkowski lower bound (Torquato and Stillinger, 2010):

$$\phi_{\rm Mink} = \frac{\zeta(d)}{2^{d-1}}, \tag{131}$$

where $\zeta(d)$ is the Riemann zeta function, $\zeta(d) = \sum_{k=1}^{\infty} \frac{1}{k^d}$, although this can be regarded as a minimal requirement. Density functional theory predicts (Kirkpatrick and Wolynes, 1987):

$$\phi_{\rm dft} \sim 4.13\, d\, 2^{-d}. \tag{132}$$

Mode-coupling theory with a Gaussian correction predicts (Ikeda and Miyazaki, 2010; Kirkpatrick and Wolynes, 1987):

$$\phi_{\rm mct} \sim 8.26\, d\, 2^{-d}. \tag{133}$$

Replica symmetry breaking theory at the 1 step predicts (Parisi and Zamponi, 2010)

$$\phi_{\rm th}^{\rm 1RSB} \sim 6.26\, d\, 2^{-d}, \tag{134}$$

and the full RSB solution predicts (Charbonneau *et al.*, 2014b)

$$\phi_{\rm th}^{\rm fullRSB} \sim 6.85\, d\, 2^{-d} \tag{135}$$

as the lower limit of jamming in the J-line ($\phi_j \in [\phi_{\rm th}, \phi_{\rm gcp}$).

In general, we see that the Edwards prediction has the same asymptotic dependence on d, Eq. (130), as the competing theories. However the prefactors are in disagreement, specially with the 1RSB calculation. While Edwards ensemble predicts a prefactor 4/3, the 1RSB prediction is 6.26. A comparison of the large d results for $P_{\rm B}$ and $P_{\rm C}$ with those in 3d (Fig. 14) indicates that the low d corrections are primarily manifest in the expressions for particle density ρ and the surface density $\sigma(z) = z/S_{d-1}$. In 3d, the density exhibits van der Waals like corrections due to the particle volume: $\rho \to \tilde{\rho} = 1/(\overline{W} - V_0)$. Likewise, there are small corrections to the surface density $z/4\pi \to \langle S^* \rangle^{-1} \approx (z/4\pi)\sqrt{3}$. The origin of the additional $\sqrt{3}$ factor is not clear. In 2d, further corrections are needed to obtain agreement of the theory with simulation data, a case that is treated next.

D. Packing of discs

The high-dimensional treatment discussed in the previous section shows that improvements on the mean field approach of (Song *et al.*, 2008) can be achieved through better approximations to the pair distribution function by including neglected correlations between neighboring particles. These correlations become crucial in low-dimensional systems, in particular in 2d systems of disc packings. Interestingly, below we show that the 2d case allows for a systematic improvement of the predictions based on a systematic layer expansion of the pair distribution function through a dimensional reduction of the problem to a one-dimensional one, as treated next.

In principle, disordered packings of monodisperse discs are difficult to investigate in 2d, since crystallization typically prevents the formation of an amorphous jammed state. In (Berryman, 1983) the density of jammed discs has been estimated as $\phi_{\rm rcp} = 0.82 \pm 0.02$ by extrapolating from the liquid phase. Only recently, MRJ states of discs have been generated in simulations using a linear programming algorithm (Torquato and Jiao, 2010). These packings achieve a packing fraction of $\phi_{\rm mrj} = 0.826$ including rattlers and exhibit an isostatic jammed backbone (Atkinson *et al.*, 2014). By comparison, the densest crystalline arrangement of discs is a triangular lattice with $\phi = \frac{\pi}{\sqrt{12}} \approx 0.9069$, which has already been proven by Thue (Thue, 1892). For disordered packings, replica theory predicts the J-line in 2d from $\phi_{\rm th} = 0.8165$ to the maximum density of glass close packing at $\phi_{\rm gcp} = 0.8745$ (Parisi and Zamponi, 2010). A recent theory based on the geometric structure approach estimates $\phi_{\rm mrj} = 0.834$ (Tian *et al.*, 2015).

In order to elucidate the 2d problem from the viewpoint of the Edwards ensemble, one can adapt as a first approach the same statistical theory developed for 3d

spheres in Sec. IV.A to the 2d case. This would lead to a self-consistent equation for the average Voronoi volume as in Eq. (82) (Meyer *et al.*, 2010):

$$\overline{W}(z) = V_0 + 2\pi \int_R^\infty \mathrm{d}c\, c\, P_>(c,z), \qquad (136)$$

where $P_>(c,z)$ has the form of Eq. (99) with $V_0 = \pi R^2$ and the 2d analogues of V^* and S^* are easily calculated. The surface density $\sigma(z)$ follows from simulations of local configurations via Eq. (96). In the relevant z range between the isostatic frictionless value $z = 2d = 4$ and the lower limit $z = d + 1 = 3$ for frictional discs, $\sigma(z)$ is found to be approximately linear: $\sigma(z) = (z - 0.5)/\pi$ for $R = 1/2$ (Meyer *et al.*, 2010).

Overall, such an implementation would predict a RCP density of 2d frictionless discs of $\phi_{\rm rcp} \approx 0.89$ greatly exceeding the empirical values. The reason for the discrepancy are much stronger correlations between the contact and bulk particles in low dimensions, such that the assumed independence of the CDFs $P_{\rm B}$ and $P_{\rm C}$ in Eq. (88) is no longer valid. A phenomenological way to quantify the correlations has been discussed in (Meyer *et al.*, 2010). Here, the excluded volume V^* is replaced by $V^* - \Delta V$, where ΔV is the part of V^* that is excluded due to the hard-core exclusion volume of the closest disc in contact. The reasoning is that the actual V^* that is available for bulk particles is strongly reduced due to overlap by the contacting particles even if they are in contact outside of S^*. If we denote by s_c the Voronoi boundary contributed by this contacting disc along the direction $\hat{\mathbf{c}}$, we can express ΔV as a function $\Delta V = \Delta V(c, s_c)$, where $s_c \geq c$. A coupling between surface and bulk particles is then introduced in Eq. (136) by setting

$$P_>(c) = \int_c^\infty \mathrm{d}s_c P_{\rm C}(s_c) P_{\rm B}(c|s_c), \qquad (137)$$

where $P_{\rm C}$ has the usual form of Eq. (94) and $P_{\rm B}$ is now given by

$$P_{\rm B}(c|s_c) = e^{-\frac{1}{\overline{W}-V_0}[V^*(c)-\Delta V(c,s_c)]}. \qquad (138)$$

The numerical solution of Eq. (136) with Eq. (137) yields for $\phi = V_0/\overline{W}$

$$\phi(z) = \frac{1}{1.437 - 0.049z}, \qquad (139)$$

which predicts $\phi^{2d}_{\rm rcp} = 0.806...$ for $z = 4$ in the frictionless limit, and $\phi^{2d}_{\rm rlp} = 0.775...$ for $z = 3$ in the limit of infinite friction. While these results are closer to the results found in simulations, they still need improvement. A more general theory of correlations is developed next that allows for a systematic improvement over the above mean-field approach.

A more systematic way of dealing with the correlations can be developed by focusing only on particles close to the direction $\hat{\mathbf{c}}$, i.e., particles that could contribute a VB,

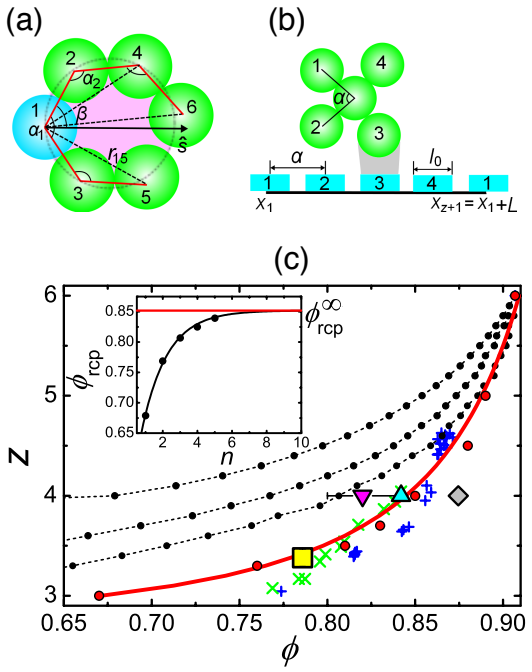

FIG. 15 (Colors online) (a) An illustration of the geometrical quantities used in the calculation of $P_>$, Eq. (140). The α_j are the angles between any two Voronoi particles for a given $\hat{s}$. (b) Mapping monodisperse contact discs to 1d rods. The 2d exclusive angle α corresponds to the 1d gap. (c) Phase diagram of 2d packings. Theoretical results for $n = 1, 2, 3$ (line points, from left to right) and $\phi^\infty_{\rm rcp}$ (red) are compared to (i) values in the literature: (Berryman, 1983) (down triangle), (Parisi and Zamponi, 2010) (diamond), and (O'Hern *et al.*, 2002) (up triangle), (ii) simulations of 10^4 monodisperse disks (crosses), and polydisperse disks (pluses), and (iii) experimental data of frictional disks (square). (Inset) The theoretical RCP volume fraction $\phi_{\rm rcp}(n)$ as a function of n. The points are fitted to a function $\phi(n) = \phi^\infty_{\rm rcp} - k_1 e^{-k_2 n}$, where $k_1 = 0.34 \pm 0.02$, $k_2 = 0.67 \pm 0.06$ and $\phi^\infty_{\rm rcp} = 0.85 \pm 0.01$.

and then constructing a layer expansion into coordination shells (Jin *et al.*, 2014). We denote these particles as Voronoi particles. In the exact Eq. (84), one can then consider the exclusion condition $\prod_{i=2}^{\tilde{n}} [1 - m(\mathbf{r}_i - \mathbf{r}_1; \Omega]$ over $\tilde{n}$ Voronoi particles (including the reference particle) rather than all N particles in the packing. In 2d, the Voronoi particles are located on the two closest branches to the direction $\hat{\mathbf{c}}$ and can be described by a correlation function of angles $G_{\tilde{n}}(\alpha_1, \alpha_2, ..., \alpha_n)$. Using angles instead of the position coordinates is a suitable parametrization of the Voronoi particles provided the underlying contact network is assumed fixed only allowing fluctuations in the angles without destroying contacts. For such a fixed contact network the degree of freedom per particle is thus reduced by one and allows to map the $\tilde{n} - 1$ position vectors $\mathbf{r}_{12}, \mathbf{r}_{13}, ..., \mathbf{r}_{1\tilde{n}}$ onto the angles $\alpha_1, \alpha_2, ..., \alpha_n$ of contacting Voronoi particles plus the angle β describing the direction $\hat{\mathbf{c}}$ (see Fig. 15).

This requires $\tilde{n}-1=n+1$. Transforming variables from $(\mathbf{r}_{12},\mathbf{r}_{13},...,\mathbf{r}_{1\tilde{n}})$ to $(\beta,\alpha_1,\alpha_2,...,\alpha_n)$ in Eq. (84) leads to (Jin *et al.*, 2014)

$$P_>(c)=\lim_{n\to\infty}\mathcal{C}'\int\cdots\int\Theta(\alpha_1-\beta)G_n(\alpha_1,...,\alpha_n)\times\prod_{j=2}^{n+2}\Theta\left(\frac{r_{1j}}{2\hat{\mathbf{c}}\cdot\hat{\mathbf{r}}_{1j}}-c\right)\mathrm{d}\beta\mathrm{d}\alpha_1\cdots\mathrm{d}\alpha_n, \quad (140)$$

where the constant $\mathcal{C}'=z/L$ with $L=2\pi$ ensures the normalization $P_>(R)=1$. Equation (140) becomes exact as $n\to\infty$ and provides a systematic approximation for finite n. In particular, n can be related to the coordination layers above and below $\hat{\mathbf{c}}$.

One can then make two key assumptions to make this approach tractable (Jin *et al.*, 2014). Firstly, one applies the Kirkwood superposition approximation as in the high-dimensional case for G_n:

$$G_n(\alpha_1,...,\alpha_n)\approx\prod_{j=1}^{n}G(\alpha_j). \quad (141)$$

Secondly, the system of contacting Voronoi particles is mapped onto a system of 1d interacting hard rods with an effective potential $V(x)$ (see Fig. 15). Considering the particles in the first coordination shell (Fig. 15b) leads to a set of z rods at positions x_i, $i=1,...,z$, where the rods are of length $l_0=\pi/3$ and the system size is $L=6l_0$ with periodic boundary conditions. In addition, the local jamming condition requires that each particle has at least $d+1$ contacting neighbours, which can not all be in the same "hemisphere". In 2d, this implies that $z\geq 3$ and $\alpha_j\leq\pi$. In the rod system, this constraint induces an upper limit $3l_0$ on possible rod separations. Thus, the jamming condition is equivalent to introducing an infinite square-well potential between two hard rods:

$$V(x)=\begin{cases}\infty, & \text{if } x/l_0<1 \text{ or } x/l_0>a\\ 0, & \text{if } 1<x/l_0<a,\end{cases} \quad (142)$$

with potential parameter $a=3$. The total potential is a sum of the pairwise potentials,

$$V(x_1,\cdots,x_z)=V(L-x_z)+V(x_z-x_{z-1})+\cdots+V(x_2-x_1). \quad (143)$$

Crucially, the partition function $Q(L,z)$ can be calculated exactly in 1d:

$$Q(L,z)=\int\cdots\int\exp[-V(x_1,\cdots,x_z)\prod_{i=2}^{z}dx_i=\sum_{k=0}^{\lfloor\frac{L/l_0-z}{2}\rfloor}(-1)^k\binom{z}{k}\frac{[L/l_0-z-2k]^{z-1}}{(z-1)!}\times\Theta(L/l_0-z)\Theta(3z-L/l_0), \quad (144)$$

where $\lfloor x\rfloor$ is the integer part of x and the inverse temperature has been set to unity since it is irrelevant. This allows to determine the distribution of angles (gaps) $G(\alpha)=\langle\delta(x_2-x_1-\alpha)\rangle$

$$G(\alpha)=\frac{1}{Q(L,z)}\int\cdots\int_{0=x_1<x_2<\cdots<x_z<L}\prod_{i=2}^{z}dx_i\times\exp[-\beta V(x_1,\cdots,x_z)]\delta(x_2-\alpha)=\frac{Q(\alpha,1)Q(L-\alpha,z-1)}{Q(L,z)}. \quad (145)$$

In the limit $a\to\infty$ the system becomes the classical Tonks gas of 1d hard rods (Tonks, 1936). In the thermodynamic limit ($L\to\infty$ and $z\to\infty$), the gap distribution is $G_{\mathrm{HR}}(\alpha)=\rho_f e^{-\rho_f(\alpha/l_0-1)}$, where $\rho_f=z/(L/l_0-z)$ is the free density.

The density of 2d disc packings follows by solving Eq. (136) with Eqs. (140,141,145) numerically using Monte-Carlo (Fig. 15c). The formalism reproduces the highest density of 2d spheres in a triangular lattice at $\phi\approx 0.91$ for $z=6$. For disordered packings one obtains the RCP volume fraction:

$$\phi^{2d}_{\mathrm{rcp}}=0.85\pm0.01, \qquad \text{for } z=4, \quad (146)$$

and the RLP volume fraction as:

$$\phi^{2d}_{\mathrm{rlp}}=0.67\pm0.01, \qquad \text{for } z=3. \quad (147)$$

We see that the prediction of the frictionless RCP point is close to the numerical results and the result of the 1RSB theory $\phi_{\mathrm{th}}=0.8165$, while a new prediction of RLP at the infinite friction limit is obtained.

E. Packing of bidisperse spheres

Polydispersity with a smooth distribution of sizes typically occurs in industrial particle synthesis and thus affects packings in many applications. Qualitatively, one expects an increase in packing densities due to size variations: The smaller particles can fill those voids that are not accessible by the larger particles leading to more efficient packing arrangements, which is indeed observed empirically (Brouwers, 2006; Desmond and Weeks, 2014; Sohn and Moreland, 1968). Simulations have shown that the jamming density in polydisperse systems depends also on the compression rate without crystallization (Hermes and Dijkstra, 2010) and the skewness of the size distribution (Desmond and Weeks, 2014). Since these issues are important in technological applications, as for instance the proportioning of concrete, very efficient phenomenological models have been developed to predict volume fractions of mixtures of various types of grains (de Larrard, 1999). For size distributions following a power-law, space-filling packings can be constructed (Herrmann *et al.*, 1990). On the theoretical side, a 'granocentric' model has been shown to reproduce the

packing characteristics of polydisperse emulsion droplets (Clusel *et al.*, 2009; Corwin *et al.*, 2010; Jorjadze *et al.*, 2011; Newhall *et al.*, 2011; Puckett *et al.*, 2011). Here, the packing generation is modelled as a random walk in the first coordination shell with only two parameters, the available solid angle around each particle and the ratio of contacts to neighbors, which can both be calibrated to experimental data.

Treating the full polydisperse case from a first-principle approach is highly challenging. The simpler case of two spheres with different radii has been treated in (Danisch *et al.*, 2010) with the volume ensemble. The key idea is to treat the spheres of radii $R_1 < R_2$ as different species 1 and 2 with independent statistical properties. If we denote by x_1 the fraction of small spheres 1, then $x_1 = N_1/(N_1+N_2)$, with N_i the number of spheres i in the packing. Likewise, $x_2 = 1 - x_1$. The overall packing density is

$$\phi = \frac{\overline{V}_g}{\overline{W}}, \qquad \overline{V}_g = \sum_{i=1}^{2} x_i V_g^{(i)} \tag{148}$$

where $V_g^{(i)} = \frac{4\pi}{3} R_i^3$ and $\overline{W}$ is the average volume of a Voronoi cell as before. The average now includes averaging over the different species, so that

$$\overline{W} = \sum_{i=1}^{2} x_i \overline{W}_i, \tag{149}$$

$$\overline{W}_i = V_g^{(i)} + 4\pi \int_{R_i}^{\infty} \mathrm{d}c\, c^2\, P_{>}^{(i)}(c,z), \qquad i = 1,2 \tag{150}$$

as a straightforward extension of Eq. (82). The CDF $P_{>}^{(i)}(c,z)$ contains the probability that, for a Voronoi cell of species i, the boundary is found at a value larger than c. This probability depends, of course, on both species. Assuming statistical independence we can introduce a factorization into bulk and contact particles of both species (Danisch *et al.*, 2010) analogously to the monodisperse case Eq. (88):

$$P_{>}^{(i)}(c,z) = P_{\mathrm{B}}^{(i1)}(c) P_{\mathrm{C}}^{(i1)}(c,z) P_{\mathrm{B}}^{(i2)}(c) P_{\mathrm{C}}^{(i2)}(c,z) \tag{151}$$

Here, $P_{\mathrm{B}}^{(ij)}$ denotes the CDF due to contributions of bulk particles of species j to a Voronoi cell of species i. Likewise $P_{\mathrm{C}}^{(ij)}$ refers to the contact particles. We express each of these terms in analogy to the monodisperse case, i.e., Eqs. (92,94),

$$P_{\mathrm{B}}^{(ij)} = \exp\left[-\tilde{\rho}_j V_{ij}^*(c)\right], \tag{152}$$

$$P_{\mathrm{C}}^{(ij)} = \exp\left[-\sigma_{ij}(z) S_{ij}^*(c)\right]. \tag{153}$$

The Voronoi excluded volume and surface, V_{ij}^* and S_{ij}^*, are defined by Eqs. (86,87), where now $s(\mathbf{r}, \hat{\mathbf{c}})$ denotes the VB between spheres of radii R_i and R_j, as parametrized by Eq. (26). The particle densities $\tilde{\rho}_j$ are given by

$$\tilde{\rho}_j = \frac{x_j}{\overline{W} - \overline{V}_g}, \qquad j = 1,2. \tag{154}$$

The main challenge is to obtain an expression for the surface density $\sigma_{ij}(z)$. For this, it is first necessary to distinguish different average contact numbers: z_{ij} is the average number of spheres j in contact with a sphere i. It follows that the average number of contacts of sphere i, denoted by z_i, is

$$z_i = z_{i1} + z_{i2}, \qquad z = \sum_{i=1}^{2} x_i z_i. \tag{155}$$

By relating the contact numbers z_i to the average occupied surface on sphere i, $\langle S_i^{\mathrm{occ}} \rangle$, one can obtain the following equations to relate z_{ij} with z

$$z_1 = \frac{z}{x_1 + x_2 \frac{\langle S_1^{\mathrm{occ}} \rangle}{\langle S_2^{\mathrm{occ}} \rangle}}, \quad z_2 = \frac{z}{x_1 \frac{\langle S_2^{\mathrm{occ}} \rangle}{\langle S_1^{\mathrm{occ}} \rangle} + x_2}. \tag{156}$$

and

$$z_{11} = \frac{z_1^2 x_1}{z}, \qquad z_{12} = \frac{z_1 z_2 x_2}{z}, \tag{157}$$

$$z_{21} = \frac{z_1 z_2 x_1}{z}, \qquad z_{22} = \frac{z_2^2 x_2}{z}. \tag{158}$$

where $\langle S_i^{\mathrm{occ}} \rangle$ is approximated as $\langle S_i^{\mathrm{occ}} \rangle = \sum_{j=1}^{2} x_j S_{ij}^{\mathrm{occ}}$ with the exact expression for the occupied surface (see Fig. 16a)

$$S_{ij}^{\mathrm{occ}} = 2\pi \left(1 - \sqrt{1 - \left(\frac{R_j}{R_i + R_j}\right)^2}\right). \tag{159}$$

Eqs. (156,158,158) imply that we can express z_{ij} as a function of z: $z_{ij} = z_{ij}(z)$. As before, σ_{ij} can in principle be obtained from simulations using Eq. (96). However, a direct simulation of $\langle S_{ij}^* \rangle$ as a function of z contacting particles ignores the dependence of the different species that is not resolved in z. Therefore, $\tilde{\sigma}_{ij}$ is introduced via

$$\sigma_{ij}(z) = \tilde{\sigma}_{ij}(z_{ij}(z)). \tag{160}$$

In turn, we obtain $\tilde{\sigma}_{ij} = \langle S_{ij}^* \rangle^{-1}$ as a function of z_{ij} by generating configurations around sphere i with the proportions z_{i1}/z_i of spheres 1 and z_{i2}/z_i of spheres 2. $\langle S_{ij}^* \rangle$ follows operationally again as the Monte-Carlo average Eq. (97).

Overall, the packing density of the bi-disperse packing of spheres can be calculated by solving the following self-consistent equation for the free volume $w = \overline{W} - \overline{V}_g$

$$w = 4\pi \sum_{i=1}^{2} x_i \int_{R_i}^{\infty} \mathrm{d}c\, c^2 \times \exp\left\{-\sum_{j=1}^{2}\left[\frac{x_j}{w} V_{ij}^*(c) + \sigma_{ij}(z) S_{ij}^*(c)\right]\right\} \tag{161}$$

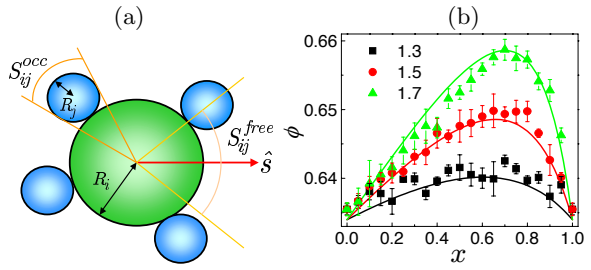

FIG. 16 (Colors online) (a) The occupied surface Eq. (159) and the Voronoi excluded surface S_{ij}^{*}. (b) Comparison between theory and numerical simulations of Hertzian packings at RCP vs the concentration x. Different symbols denote different ratios R_1/R_2.

We notice that Eq. (161) is the generalization of Eq. (100) from monodisperse to bidisperse packings. While the monodisperse self-consistent Eq. (100) admits a closed analytical solution, the bidisperse Eq. (161) does not. Thus, we resort to a numerical solution of this equation, and therefore the equation of state $w(z)$ is obtained numerically in these cases rather than in closed form as obtained for monodisperse spheres Eq. (103).

Calculations for all systems (from spheres to non-spheres, monodisperse or polydisperse and beyond) that use the present mean-field theory in the Edwards ensemble will end up with a self-consistent equation for the free volume of the form Eq. (100) or Eq. (161). However, so far, the only self-consistent equation that admits a closed analytical solution is the 3d monodisperse case leading to Eq. (103). The remaining equations of state for all systems studied so far are too involved and need to be solved numerically.

Results of numerical solutions of Eq. (161) are shown in Fig. 16b demonstrating good agreement with simulation data as well as the predictions of the 1RSB hard-sphere glasses calculations (Biazzo *et al.*, 2009). We observe the pronounced peak as a function of the species concentration $x = x_1 \in [0, 1]$. The extension of the theory to higher-order mixtures is straightforward in principle. The main challenge is to obtain the generalizations of Eqs. (156,158,158). Determining $\tilde{\sigma}_{ij}(z_{ij})$ from simulations of local packing configurations becomes also an increasingly complex task.

Using Edwards volume statistics based on Voronoi cells together with a simple mechanical model and mean-field type geometrical calculations (Srebro and Levine, 2003) considered the role of friction in 2d and 3d granular systems in order to study investigate segregation of binary mixtures of spheres having different friction coefficients. Unlike mixtures of grains differing in size, which can be mapped to the Ising model, frictional differences between grains result in larger entropy for the rougher grains; therefore, these systems can not be mapped anymore onto the Ising model. They find a critical compactivity above which segregation occurs and construct a phase diagram for segregation versus the two friction coefficients. By eliminating the compactivity they also provided a relation between the volume fraction and the nature of mixing or segregation, that allows identifying mixtures which are expected to segregate.

F. Packing of attractive colloids

Packings of particles with diameters of around $10\mu m$ or smaller enter the domain of colloids and are often dominated by adhesive van der Waals forces in addition to friction and hard-core interactions. In fact, packings of adhesive colloidal particles appear in many areas of engineering as well biological systems (Jorjadze *et al.*, 2011; Marshall and Li, 2014) and exhibit different macroscopic structural properties compared with non-adhesive packings of large grains treated so far, where attractive van der Waals forces are negligible in comparison with gravity.

In (Lois *et al.*, 2008) the mechanical response at the jamming transition has been studied in an attractive frictionless soft-sphere system. The system consists of N particles interacting via a pairwise, spherically symmetric potential, with a finite repulsive core and finite-range attraction. Instead of a single first-order transition as in purely repulsive systems, two second-order transitions are found in the attractive systems (Lois *et al.*, 2008): a connectivity percolation transition and a rigidity percolation transition, where a rigid backbone forms without floppy modes.

In repulsive systems, only non-percolated or jammed packing states can occur and they are separated by the first-order jamming transition at point J. However, in the attractive systems three different mechanical states can occur: percolated, percolated but unjammed, and jammed. A second-order connectivity percolation transition is found to separate the first two, and a second-order rigidity percolation transition the last two. The packing densities at the two transitions are $\phi_{\rm P} = 0.558 \pm 0.008$ (connectivity percolation) and $\phi_{\rm R} = 0.689 \pm 0.009$ (rigidity percolation) in 2d, and $\phi_{\rm P} = 0.214 \pm 0.003$ and $\phi_{\rm R} = 0.524 \pm 0.007$ in 3d.

Numerical studies of adhesive granular systems have found a range of packing fractions as a function of particle sizes $\phi \approx 0.1 - 0.6$ (Blum *et al.*, 2006; Kadau and Herrmann, 2011; Martin and Bordia, 2008; Parteli *et al.*, 2014; Valverde *et al.*, 2004; Yang *et al.*, 2000). The effect of varying the force of adhesion has been systematically investigated in (Liu *et al.*, 2015) using a DEM framework specifically developed for the ballistic deposition of adhesive Brownian soft spheres with sliding twisting and rolling friction (Marshall and Li, 2014). A dimensionless adhesion parameter Ad, defined as the ratio between interparticle adhesion work and particle inertia (Li and

Marshall, 2007), can be used to quantify the combined effect of size and deposition velocity. In the case of $Ad < 1$, particle inertia dominates the adhesion and frictions exhibiting a broad range of densities and coordination numbers. At $Ad \approx 1$ the isostatic value $z = 4$ for infinitely rough spheres is observed, indicating that weak adhesion has a similar effect on the packing as strong friction. However, when $Ad > 1$, an adhesion-controlled regime is observed with a unique curve in the z–ϕ diagram. The lowest packing density achieved numerically is $\phi = 0.154$ with $z = 2.25$ for $Ad \approx 48$. The lowest density agrees well with the data from a random ballistic deposition experiment (Blum *et al.*, 2006) and other DEM simulations (Parteli *et al.*, 2014; Yang *et al.*, 2000).

An analytical representation of the adhesive equation of state can be derived within the framework of the mean-field Edwards volume function Eq. (82), where the CDF $P_>$ is defined by Eq. (84). Assuming the same factorization of the n-point correlation function as in high dimensions leads to the approximation Eq. (123), which allows us to relate $P_>$ with the structural properties of the packing expressed in the pair distribution function g_2. We then model g_2 by extending the simple form considered so far for 3d hard-spheres in Eq. (124) in terms of four distinct contributions following the results of available simulations of hard-sphere packings and metastable hard-sphere glasses. We consider:

(i) A delta-peak due to contacting particles (Donev *et al.*, 2005b; Song *et al.*, 2008; Torquato and Stillinger, 2006);

(ii) A power-law peak as given by Eq. (74) over a range ϵ due to near contacting particles (Donev *et al.*, 2005b; Wyart, 2012);

(iii) A step function due to bulk particles (Song *et al.*, 2008; Torquato and Stillinger, 2006) mimicking a uniform density of bulk particles;

(iv) A gap of width b separating bulk and (near) contacting particles. This gap captures the effect of correlations due to adhesion and is assumed to depend on z: $b = b(z)$. In this way we model the increased porosity at a given z compared with adhesion-less packings. Overall, we obtain

$$g_2(\mathbf{r}, z) = \frac{z}{\rho\lambda}\delta(r - 2R) + \sigma(r - 2R)^{-\nu}\Theta(2R + \epsilon - r) + \Theta(r - (2R + b(z))). \quad (162)$$

For the power law term we assume $\nu = 0.38$ from (Lerner *et al.*, 2013) and a width of $\epsilon = 0.1R$, which is approximately the range over which the peak decreases to the bulk value unity as observed in (Donev *et al.*, 2005b). The value σ is then fixed by continuity with the step function term in the absence of a gap.

Next, we have to determine the gap of width function $b(z)$ which is the crucial assumption of the theory. $b(z)$ needs to satisfy a set of constraints that we impose purely on physical grounds:

(i) $b(z)$ is a smooth monotonically decreasing function of z. Here, the physical picture is that for small z (corresponding to looser packings), the gap width is larger due to the increased porosity of the packing.

(ii) At the isostatic limit $z = 6$, the gap disappears, $b(6) = \epsilon$, and we expect to recover the frictionless RCP value, since this value of z represents a maximally dense disordered packing of spheres. We obtain from Eq. (162) indeed the prediction for ϕ_{Edw}, Eq. (114), by choosing an appropriate value of λ and accounting for low dimensional corrections due to the hard-core excluded volume of the reference sphere, such that $\rho \to \overline{\rho} = 1/(\overline{W} - V_0)$. This constraint thus fixes ρ and λ, as well as one of the parameters in $b(Z)$.

(iii) In addition, we conjecture the existence of an asymptotic *adhesive loose packing* (ALP) at $z = 2$ and $\phi = 1/2^3$ which yields $b(2) = 1.47$ and fixes a second parameter in $b(z)$. This is motivated by the fact that $\phi = 1/2^d$ is the lower bound density of saturated sphere packings of congruent spheres in d dimensions for all d (Torquato and Stillinger, 2006). A saturated packing of congruent spheres of unit diameter satisfies that each point in space lies within a unit distance from the center of some sphere. Moreover, $z = 2$ is the lowest possible value for a physical packing: If $z < 2$ there are more spheres with a single contact (i.e., dimers) than with three or more contacts, which identifies that the ALP point is only asymptotic.

Clearly, $b(z)$ is a smoothly decreasing function, so that we can assume, e.g., the simple parametric form

$$b(z) = c_1 + c_2 e^{-c_3 z}, \quad (163)$$

such that one fitting parameter is left after the two constraints $b(6) = \epsilon$ and $b(2) = 1.47$ are imposed. Figure 17 highlights that the exponential decay of $b(z)$ provides an excellent fit to the simulation data providing the equation of state $\phi(z)$ for adhesive packings. Moreover, the resulting $P(c, z)$ also agrees well with the empirically measured CDF over a large range of Ad values (Liu *et al.*, 2015). This means that including $b(z)$ captures well the essential structural features of the packing. It is quite intriguing that such a simple modification of the non-adhesive theory, motivated on physical grounds, leads to such good agreement not only in the low density regime, but also for mid to high densities.

These results highlight that attraction in (spherical) particles leads to a lower density limit for percolation at the ALP with $\phi_c = 1/2^3$. The equivalent ϕ_c in attractive colloids is observed empirically over a range of densities $\phi_c \approx 0.1 - 0.2$ depending on the mechanism for the suppression of phase-separation (Zaccarelli, 2007), e.g., due to an interrupted liquid-gas phase separation (Lu *et al.*,

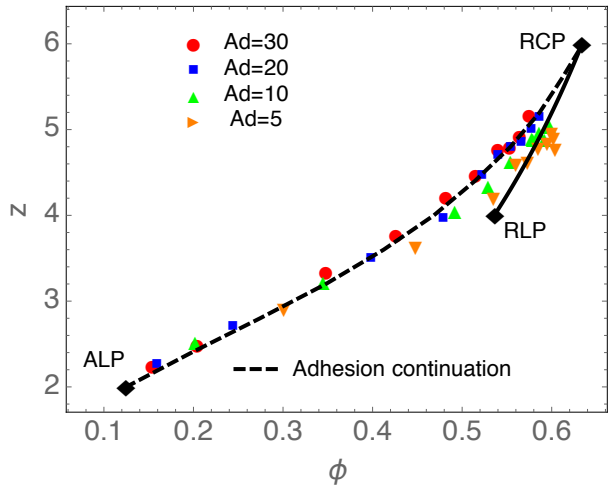

FIG. 17 (Colors online) Plot of high *Ad* simulation data in the z–ϕ plane (Liu *et al.*, 2015). The adhesive continuation with an exponential $b(z)$ connects the RCP at $\phi_{\rm Edw}$ and $z = 6$ with the conjectured adhesive loose packing point (ALP) at $\phi = 2^{-3}$ and $z = 2$. The black solid line is the RLP line of Fig. 12(b).

2008b; Trappe *et al.*, 2001). The situation is thus reminiscent of the adhesion-less and frictionless range of densities $\phi \in [\phi_{\rm th}, \phi_{\rm gcp}]$ of the J-line (see Sec. V).

G. Packing of non-spherical particles

The question of optimizing the density of packings made of particles of a particular shape is probably one of the most ancient scientific problems occupying scientists since the time of Apollonious of Perga (Andrade *et al.*, 2005; Herrmann *et al.*, 1990) and Kepler (Kepler, 1611; Weaire and Aste, 2008), and still of great practical importance for all industries involved in granular processing. Such packings are fundamental to industries involved in granular media and appear in a broad range of fields such as self-assembly of nano-particles, liquid crystals, glassy and bio-materials. Thus, understanding the structural and mechanical behaviour of packings from the properties of its individual constituents is a central problem in materials science (Glotzer and Solomon, 2007; Jaeger, 2015).

A deeper understanding of the packing optimization problem would lead to immediate benefits in many industrial sectors, especially pharmaceutical and chemical industries which rely on storage and transport of large amounts of granular material, as well as in the oil industry and materials science. New synthesis methods like emulsion drying, lithography, 3d printing, and droplet microfluidic allow for the efficient large-scale fabrication of nanoparticles with a large variety of anisotropies, ranging from cubes, tetrahedra, icosahedra to tripods, stars, and other exotic shapes (Shum *et al.*, 2010; Yi *et al.*, 2013). The complex structures that result from their assembly become increasingly important for the design of new functional materials (Baule and Makse, 2014; Damasceno *et al.*, 2012; Glotzer and Solomon, 2007; Jaeger, 2015). A general theory of packings of arbitrary shapes will, thus, allow us to address the problem of optimizing packing fractions in industry relevant scenarios and to explore novel states of matter due to particle shape.

Due to these practical applications, a lavish amount of activity has been dedicated to the problem of finding the optimal packing over the space of particle shape. Since the time of Bernal (Bernal and Mason, 1960), the densest random packing of spheres has been extensively studied in experiments and simulations. However, much less is known about anisotropic shapes, despite the fact that all shapes in nature deviate from the ideal sphere. Even though the increase in packing fraction by introducing particle anisotropy has been known for over a decade (Donev *et al.*, 2004; Williams and Philipse, 2003), no systematic theoretical investigation could be performed so far.

A theoretical investigation of the best packing for arbitrary shapes has proven notoriously difficult due to the strong positional and orientational correlations of dense packings. For instance, no theoretical prediction for the best packing density exists for arbitrary shapes. In the absence of theory, searches for the optimal random packing of non-spherical shapes have focused on empirical studies on a case-by-case basis. For elongated shapes such as ellipsoids, spherocylinders, and dimers, a peak in ϕ is typically observed for aspect ratios (length divided by width) of $\alpha \approx 1.4 - 1.5$ (Abreu *et al.*, 2003; Bargiel, 2008; Ciesla *et al.*, 2015; Delaney and Cleary, 2010; Donev *et al.*, 2004; Faure *et al.*, 2009; Jia *et al.*, 2007; Kyrylyuk *et al.*, 2011; Lu *et al.*, 2010; Man *et al.*, 2005; Williams and Philipse, 2003; Wouterse *et al.*, 2009; Zhao *et al.*, 2012). This suggests that optimally dense packings can be found within a given shape category.

Table II presents an overview of the maximal packing densities for a variety of shapes obtained in simulations, experiments and theory. Recent simulations, for instance, have found the densest random packing fraction of prolate ellipsoids at $\phi \approx 0.735$ for aspect ratios $\alpha \approx 1.5$ (Donev *et al.*, 2004), spherocylinders: $\phi \approx 0.772$ for $\alpha \approx 1.5$ (Zhao *et al.*, 2012) and two dimensional dimers: $\phi \approx 0.885$ (Schreck *et al.*, 2010). The densest random tetrahedra packing has been found in simulations with $\phi = 0.7858$ (Haji-Akbari *et al.*, 2009). More systematic investigations of the self-assembly of hard truncated polyhedra families has been done in (Chen *et al.*, 2014; Damasceno *et al.*, 2012). The organizing principles of ordered packings of Platonic and Archimedean solids and other convex and non-convex shapes have been investigated in (Torquato and Jiao, 2009, 2012). Interesting shapes have been considered also in a systematic way: su-

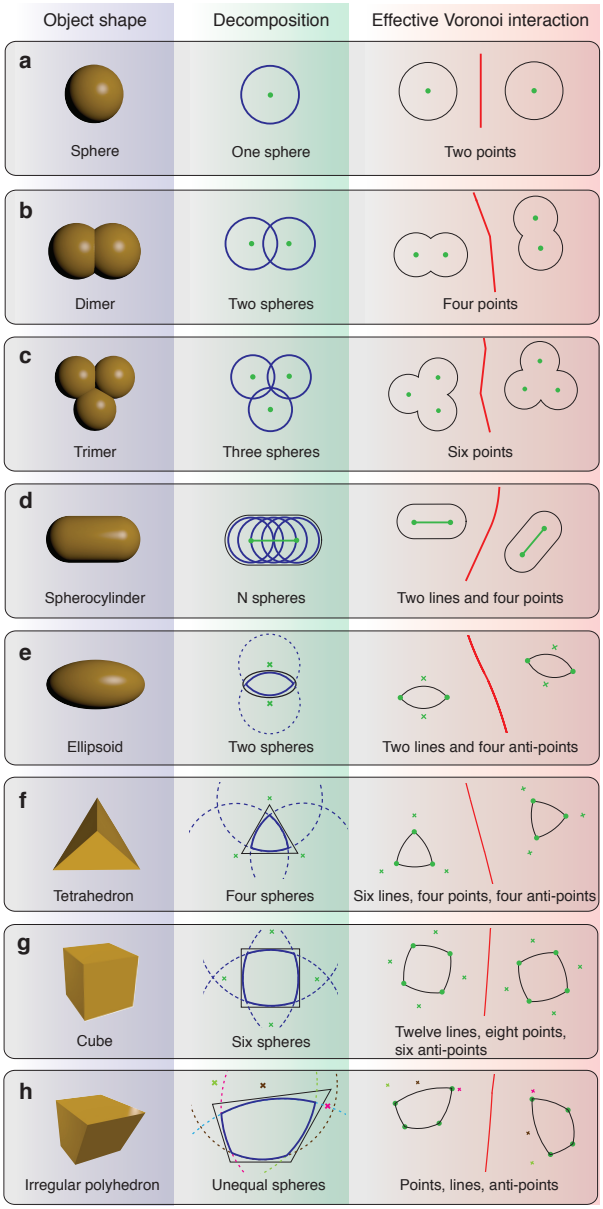

FIG. 18 (Colors online) Table of different shapes and their VBs (Baule *et al.*, 2013). (a–d) For shapes composed of spheres, the VB arises due to the effective interaction of the pints at the centres of the spheres. Since spherocylinders are represented by a dense overlap of spheres, the effective interaction is that of two lines and four points. (e–h) For more complicated shapes that would in principle be modelled by a dense overlap of sphere with different radii, we propose approximations in terms of intersections of spheres leading to effective interactions between 'anti-points'. For both classes of shapes, the VB follows an exact algorithm leading to analytical expressions (see Fig. 19).

perballs (Jiao *et al.*, 2010), puffy tetrahedra (Kallus and Elser, 2011), polygons (Wang *et al.*, 2015) and truncated vertices (Damasceno *et al.*, 2012; Gantapara *et al.*, 2013). A caveat of some empirical studies is the strong protocol dependence of the final close packed state even for the same shape: recent studies of spherocylinder packings, e.g., exhibit a large variance depending on the algorithm used (Abreu *et al.*, 2003; Bargiel, 2008; Jia *et al.*, 2007; Jiao and Torquato, 2011; Kyrylyuk *et al.*, 2011; Lu *et al.*, 2010; Williams and Philipse, 2003; Wouterse *et al.*, 2009; Zhao *et al.*, 2012). A generic theoretical insight is needed if one wants to search over more extended regions of parameter space of object shapes.

It is empirically clear that non-spherical shapes can generally achieve denser maximal packing densities than spheres. In fact, a conjecture attributed to Ulam (recorded in the book (Gardner, 2001)) in the context of regular packings, recently also formulated for random packings (Jiao and Torquato, 2011) and locally (Kallus, 2016), states that the sphere is, indeed, the worst packing object among all convex shapes. However, one should notice the local character of such a conjecture for random packings: Onsager already proved that elongated spaghetti-like thin rods pack randomly much worse than spheres (Onsager, 1949).

On the theoretical side, the main difficulty arises from the impossibility to exhaustively search the high-dimensional parameter space of shapes that renders the problem very hard to solve. Nevertheless, there are successful theories of high density liquids that have been extended to encompass non-spherical particles, such as mode-coupling theory (Götze, 2009) and density functional theory (Onsager, 1949). However, they do not apply to the jamming regime.

On the other hand, successful approaches to jamming based on replica theory so far only apply to spherical particles (Parisi and Zamponi, 2010) (see Sec. V). The difficulty to extend replica theory calculations from spheres to non-spherical particles might stem from the fact that metastable hard-particle glasses in replica theory are analytical extensions of supercooled liquid equations of state to infinite pressure glasses. Since equations of state for general non-spherical hard particles are not abundant, the broad applicability of replica theory to non-spherical particles might be compromised.

On the contrary, the mean-field Edwards approach is based entirely on the geometry of the particles; its building block is directly the shape of the constitutive particle. Therefore, Edwards ensemble allows for straightforward generalizations from spherical to non-spherical particles allowing for studying the large space of shapes in a simple way. Edwards ensemble provides further theoretical insight to search over extended regions of parameter space of object shapes that are not available to other theories of the jammed state.

From a numerical point of view, a promising approach to find the best shape has been put forward by Jaeger and collaborators (Jaeger, 2015; Miskin and Jaeger, 2013, 2014; Roth and Jaeger, 2016) who used genetic algorithms (GA) to map the possible space of the constitutive

particle shapes. They consider non-spherical composite particles formed by gluing spherical particles of different sizes rigidly connected into a polymer-like non-branched shape. A genetic algorithm starts with a given shape and perform 'mutations' to the constitutive particles until a desired property, for instance, maximal strength or maximal packing fraction is achieved. This reverse engineering approach can generate novel materials with desired properties but of limited shapes: within this framework, the limits to granular materials design are the limits to computation (Jaeger, 2015), since GA relies heavily on dynamically simulating (e.g., with MD or MC) the packings to be optimized. Thus, computational limitations are expected in more complicated shapes such as tetrahedra or irregular polyhedra, in general.

A theoretical framework to tackle this optimization problem is clearly desirable. Edwards statistical mechanics can provide the foundations for such an approach at the mean-field level, which has recently been solved for non-spherical particles (Baule *et al.*, 2013). A drawback of employing a general theoretical approach rather than direct simulations using, e.g., artificial evolution (Jaeger, 2015), is that current theories are at the mean-field level and thus only approximate. However, both approaches can be complementing: A mean-field theory could identify a reduced region in the space of optimal parameters, which can then be tackled with more detail using more focused reverse engineering techniques.

As discussed in the previous sections, the central quantity to calculate is the average Voronoi volume $\overline{W}$ as a function of z. In the case of frictionless spheres, z is fixed by isostaticity providing the prediction Eq. (114) for RCP. The situation is somewhat more complicated for frictionless non-spherical particles: Here, both z and $\overline{W}$ depend independently on the particle shape. For simplicity, we assume rotationally symmetric particles in the following, where deviations from the sphere can be parametrized by a single parameter, e.g., the aspect ration α measuring length over width. As a consequence, if we are interested in obtaining the function $\phi(\alpha)$ at RCP, we need to combine the dependencies $\overline{W}_\alpha(z)$ and $z(\alpha)$:

$$\phi(\alpha) = \frac{V_0}{\overline{W}_\alpha(z(\alpha))}. \tag{164}$$

We discuss next how to obtain $\overline{W}_\alpha(z)$ by extending the framework of the coarse-grained Voronoi volume to non-spherical particles. A quantitative approach to describe $z(\alpha)$ is discussed in Sec. IV.G.3, which requires a quantitative evaluation of the occurrence of degenerate configurations.

1. Coarse-grained Voronoi volume of non-spherical shapes

The key for the mean-field approach to the statistical mechanical ensemble based on the coarse-grained volume function is Eq. (81), which replaces the exact global minimization to obtain the Voronoi boundary $l_i(\hat{\mathbf{c}})$ in the direction $\hat{\mathbf{c}}$ by the pdf $p(\mathbf{c}, z)$. For a general particle-shape the cut-off c^* describes just the particle surface parametrized by $\hat{\mathbf{c}}$. Transforming Eq. (81) to the CDF $P_>$ using $p(\mathbf{c}, z) = -\frac{\mathrm{d}}{\mathrm{d}c} P_>(\mathbf{c}, z)$ leads to the volume integral (Baule *et al.*, 2013)

$$\overline{W}(z) = \int \mathrm{d}\mathbf{c}\, P_>(\mathbf{c}, z), \tag{165}$$

where $P_>$ is again interpreted as the probability that $N-1$ particles are outside a volume Ω centered at $\mathbf{c}$, since otherwise they would contribute a shorter VB. Ω is in principle defined as in Eq. (83), but is no longer a spherical volume due to the non-spherical interactions manifest in the parametrization of the VB. The VB now also depends on the relative orientation $\hat{\mathbf{t}}$ of the two particles suggesting the definition:

$$\Omega(\mathbf{c}, \hat{\mathbf{t}}) = \int \mathrm{d}\mathbf{r}\, \Theta(c - s(\mathbf{r}, \hat{\mathbf{t}}, \hat{c}))\Theta(s(\mathbf{r}, \hat{\mathbf{t}}, \hat{\mathbf{c}})), \tag{166}$$

for a fixed relative orientation $\hat{\mathbf{t}}$.

So far, the description of $\overline{W}$ is exact within the statistical mechanical approach. In order to solve the formalism, we introduce the following mean-field minimal model of the translational and orientational correlations in the packing (Baule *et al.*, 2013):

1. Following Onsager (Onsager, 1949), we treat particles of different orientations as belonging to different species. This is the key assumption to treat orientational correlations within a mean-field approach. Thus, the problem for non-spherical particles can be mapped to that of polydisperse spheres for which $P_>$ factorizes into the contributions of the different radii (see Sec. IV.E).

2. Translational correlations are treated as in the spherical case for high dimensions (see Sec. IV.C). Here, the Kirkwood superposition approximation leads to a factorization of the n-point correlation function into a product of pair-correlation functions, Eq. (122). Including also the factorization of orientations provides the form

$$P_>(\mathbf{c}, z) = \exp\left\{-\rho \int \mathrm{d}\hat{\mathbf{t}} \int_{\Omega(\mathbf{c},\hat{\mathbf{t}})} \mathrm{d}\mathbf{r}\, g_2(\mathbf{r}, \hat{\mathbf{t}})\right\}. \tag{167}$$

3. The pair correlation function is modelled by a delta function plus step function as for spheres, Eq. (124). This form captures the contacting particles and treats the remaining particles as an ideal gas-like background:

$$g_2(\mathbf{r}, \hat{\mathbf{t}}) = \frac{1}{4\pi}\left[\frac{\sigma(z)}{\rho}\delta\left(r - r^*(\hat{\mathbf{r}}, \hat{\mathbf{t}})\right) + \Theta(r - r^*(\hat{\mathbf{r}}, \hat{\mathbf{t}}))\right]. \tag{168}$$

Shape	$\phi_{\max}$ simulation	$\phi_{\max}$ experiment	$\phi_{\max}$ theory
discs (2d)	0.826 (Atkinson *et al.*, 2014)		0.85 (Jin *et al.*, 2014)
			0.874 (Parisi and Zamponi, 2010)
			0.834 (Tian *et al.*, 2015)
sphere	0.645 (Skoge *et al.*, 2006)	0.64 (Bernal and Mason, 1960)	0.634 (Song *et al.*, 2008)
			0.68 (Parisi and Zamponi, 2010)
M&M candy		0.665 (Donev *et al.*, 2004)	
dimer	0.703 (Faure *et al.*, 2009)		0.707 (Baule *et al.*, 2013)
ellipse (2d)	0.895 (Delaney *et al.*, 2005)		
oblate ellipsoid	0.707 (Donev *et al.*, 2004)		
prolate ellipsoid	0.716 (Donev *et al.*, 2004)		
spherocylinder	0.722 (Zhao *et al.*, 2012)		0.731 (Baule *et al.*, 2013)
lens-shaped particle			0.736 (Baule *et al.*, 2013)
tetrahedron	0.7858 (Haji-Akbari *et al.*, 2009)	0.76 (Jaoshvili *et al.*, 2010)	
cube		0.59 (Athanassiadis *et al.*, 2014)	
octahedron	0.697 (Jiao and Torquato, 2011)	0.57 (Athanassiadis *et al.*, 2014)	
dodecahedron	0.716 (Jiao and Torquato, 2011)	0.56 (Athanassiadis *et al.*, 2014)	
icosahedron	0.707 (Jiao and Torquato, 2011)	0.55 (Athanassiadis *et al.*, 2014)	
general ellipsoid	0.735 (Donev *et al.*, 2004)	0.74 (Man *et al.*, 2005)	
superellipsoid	0.758 (Delaney *et al.*, 2010)		
superball	0.674 (Jiao *et al.*, 2010)		
trimer	0.729 (Roth and Jaeger, 2016)		

TABLE II **Overview of maximal packing fractions $\phi_{\max}$ for a selection of regular shapes in disordered packings. Note that the $\phi_{\max}$ value is achieved for the aspect ratio, where ϕ is maximal, so every value is at a different aspect ratio.**

Here, the prefactor $1/4\pi$ describes the density of orientations, which we assume isotropic. The contact radius r^* denotes the value of r in a direction $\hat{\mathbf{r}}$ for which two particles are in contact without overlap. In the case of equal spheres the contact radius is simply $r^*(\hat{\mathbf{r}},\hat{\mathbf{t}}) = 2R$. For non-spherical objects, r^* depends on the object shape and the relative orientation.

Combining Eq. (168) with Eq. (167) recovers the product form of the CDF $P_>$:

$$P_>(\mathbf{c},z) = \exp\left\{-\rho\,\overline{V}^*(\mathbf{c}) - \sigma(z)\,\overline{S}^*(\mathbf{c})\right\}, \quad (169)$$

where $\overline{V}^*$ and $\overline{S}^*$ are now orientationally averaged excluded volume and surface: $\overline{V}^* = \langle \Omega - \Omega \cap V_{\text{ex}} \rangle_{\hat{\mathbf{t}}}$ and $\overline{S}^* = \langle \partial V_{\text{ex}} \cap \Omega \rangle_{\hat{\mathbf{t}}}$ (compare with Eqs. (86,87)). The orientational average is defined as $\langle ... \rangle_{\hat{\mathbf{t}}} = \frac{1}{4\pi} \oint ... \mathrm{d}\hat{\mathbf{t}}$. Substituting Eq. (169) into Eq. (165) leads to a self-consistent equation for $\overline{W}$ due to the dependence of ρ on $\overline{W}$. In order to be consistent with the spherical limit, we use $\rho \to \rho_f = 1/(\overline{W} - V_0)$ due to the low dimensional corrections discussed in Sec. IV.A.

In accordance with the treatment of the surface density term $\sigma(z)$ for 3d spheres, we obtain $\sigma(z)$ by simulating random local configurations of z contacting particles around a reference particle and determining the average available free surface. This surface is given by $\overline{S}^*(\mathbf{c}_{\text{m}})$, where c_{m} is the minimal contributed VB among the z contacts in the direction $\hat{\mathbf{c}}$. Averaging over many realizations with a uniform distribution of orientations and averaging also over all directions $\hat{\mathbf{c}}$ provides the surface density in the form of a Monte-Carlo average

$$\sigma(z) = \frac{1}{\left\langle \left\langle \overline{S}^*(\mathbf{c}_{\text{m}}) \right\rangle \right\rangle_{\hat{\mathbf{c}}}}. \quad (170)$$

In this way we can only calculate $\sigma(z)$ for integer values of z. For fractional z that are predicted from the evaluation of degenerate configurations in the next section, we use a linear interpolation to obtain $\overline{W}(z)$.

The theory developed so far captures the effect of particle shape on the average Voronoi volume as a function of a given z. The particle shape is taken into account in three quantities: *(i)* $c^*(\hat{\mathbf{c}})$, parametrizing the surface of the shape; *(ii)* $s(\mathbf{r},\hat{\mathbf{t}},\hat{\mathbf{c}})$, parametrizing the VB between two particles of relative position $\mathbf{r}$ and orientation $\hat{\mathbf{t}}$; and *(iii)* the contact radius $r^*(\hat{\mathbf{r}},\hat{\mathbf{t}})$. In the spherical limit, all these quantities simplify considerably and the spherical theory is recovered, which is analytically solvable as discussed in Sec. IV.A. For non-spherical shapes, the VB Point *(ii)* above is in general not known in closed form. In the next section, we discuss a class of shapes for which the VB can be expressed in exact analytical form. For

these shapes, the theory can be applied in a relatively straightforward way, solving $\overline{V}^*$ and $\overline{S}^*$ numerically and providing also $\overline{W}(z)$ in numerical form. In Sec. IV.G.3 we then discuss the missing part in the theory so far, the dependence of z itself on the particle shape.

2. Parametrization of non-spherical shapes

In Sec. II.D.1 the precise definition of the VB between two particles has been given. We have seen that the VB between two equal spheres is identical to the VB between two points and is a flat plane perpendicular to the separation vector. Finding the VB for more complicated shapes is a challenging problem in computational geometry, which is typically only solved numerically (Boissonat *et al.*, 2006). Already for ellipsoids, one of the simplest non-spherical shape, there is no exact expression for the VB. We nevertheless approach this problem analytically by considering a decomposition of the shape into overlapping spheres (see Fig. 18a–d). Such a decomposition is trivial for dimers, trimers, and n–mers, where the VB arises effectively due to the interaction of four, six and $2n$ points. It also applies exactly, e.g., to spherocylinders, which can be represented as dense overlaps of spheres. In this case, the VB arises due to the effective interaction of two lines and four points.

The Voronoi decomposition used for n–mers and spherocylinders can be generalized to arbitrary shapes by using a dense filling of spheres with unequal radii (Phillips *et al.*, 2012). However, even though this approach is algorithmically well defined, it may become practically tedious for dense unions of polydisperse spheres. An alternative approach that is analytically tractable has been proposed in (Baule *et al.*, 2013): Convex shapes are approximated by intersections of a finite number of spheres. An oblate ellipsoid, e.g., is approximated by a lens-shaped particle, which consists of the intersection of two spheres (Cinacchi and Torquato, 2015). Likewise, an intersection of four spheres can be considered an approximation to a tetrahedra, and six spheres that of a cube (see Fig. 18e–h).

The main insight is that the effective Voronoi interaction of these shapes is governed by a symmetry: Points map to 'anti-points' (since the interactions between spheres is inverted). The VB of ellipsoid-like objects arises from the interaction between four anti-points and four points in two dimensions or lines in three dimensions, and thus falls into the same class as spherocylinders. The VB between two tetrahedra is then due to the interaction between the vertices (leading to four point interactions), the edges (leading to six line interactions), and the faces (leading to four anti-point interactions). For cubes the effective interaction is that of twelve lines, eight points and six anti-points. This approach can be generalized to arbitrary polyhedra.

With such a decomposition into overlapping and intersecting spheres, we can study a large space of particle shapes using Edwards ensemble. The resulting VBs can be parametrized analytically following an exact algorithm (Baule *et al.*, 2013): Every segment of the VB arises due to the Voronoi interaction between a particular sphere on each of the two particles, reducing the problem to identifying the correct spheres that interact (see Fig. 19). The spheres that interact are determined by separation lines given as the VBs between the spheres in the filling. For dimers, there is one separation line for each object, tesselating space into four areas, in which only one interaction is correct (Fig. 19a). The dense overlap of spheres in spherocylinders leads to a line as effective Voronoi interaction at the centre of the cylindrical part. This line interaction has to be separated from the point interactions due to the centres of the spherical caps as indicated. Overall, the two separation lines for each object lead to a tessellation of space into nine different areas, where only one of the possible line-line, line-point, point-line, and point-point interactions is possible (Fig. 19b).

The spherical decomposition of ellipsoid-like lens-shaped particles is analogous to dimers, only that now the opposite sphere centres interact ("anti-points"). In addition, the positive curvature at the intersection point leads to an additional line interaction, which is a circle in 3d (a point in 2d) and indicated here by two points. The separation lines are then given by radial vectors through the intersection point/line. The Voronoi interaction between two ellipsoids is thus given by two pairs of two anti-points and a line, which is the same class of interactions as spherocylinders. The different point and line interactions are separated analogously to spherocylinders, as shown in Fig. 19c.

3. Dependence of coordination number on particle shape

As discussed in Sec. II.A the physical conditions of mechanical stability and assuming minimal correlations motivate the isostatic conjecture Eq. (63) $z = 2d_\mathrm{f}$ in the frictionless case. While isostaticity is well-satisfied for spheres, packings of non-spherical objects are in general hypoconstrained with $z < 2d_\mathrm{f}$, where $z(\alpha)$ increases smoothly from the spherical value for $\alpha > 1$ (Baule *et al.*, 2013; Donev *et al.*, 2004, 2007; Wouterse *et al.*, 2009). The fact that these packings are still in a mechanically stable state can be understood in terms of the occurrence of stable degenerate configurations, which have so far shown to occur in packings of ellipses, ellipsoids, dimers, spherocylinders, and lens-shaped particles (Baule *et al.*, 2013; Chaikin *et al.*, 2006; Donev *et al.*, 2007). In the case of ellipses, one needs in general four contacts to fix (jam) the ellipse locally such that no displacement is possible (Alexander, 1998). However, it is possible to construct

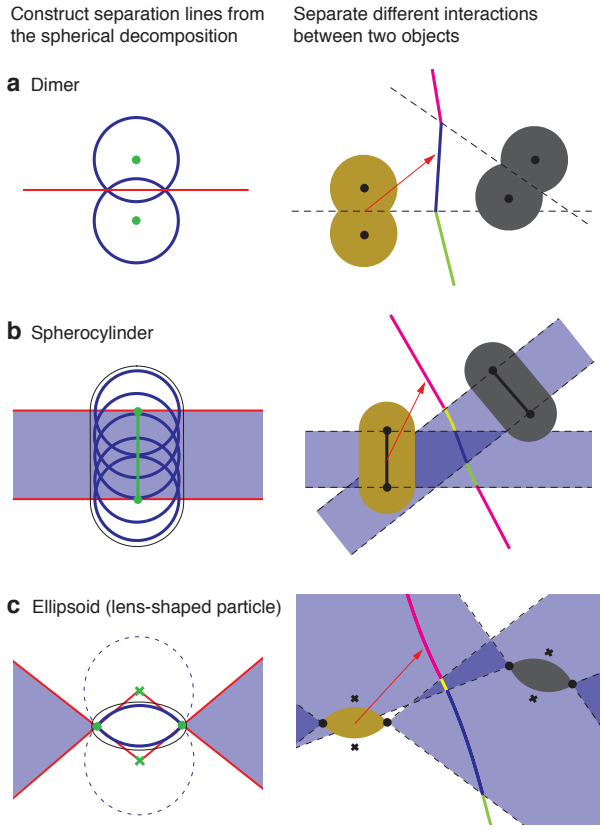
Construct separation lines from the spherical decomposition
Separate different interactions between two objects
a Dimer
b Spherocylinder
c Ellipsoid (lens-shaped particle)

FIG. 19 (Colors online) Exact algorithm to obtain analytical expressions for the VB from the construction of separation lines (Baule *et al.*, 2013). (a) For dimers, the two separation lines identify the correct surface out of four possible ones. The pink part of the VB, e.g., is the VB between the two upper spheres. (b) For spherocylinders, the line-line, line-point, point-line, and point-point interactions lead to nine different surfaces that are separated by four lines. The yellow part of the VB, e.g., is due to the upper point on spherocylinder 1 and the line of 2. Regions of line interactions are indicated by blue shades. (c) For lens-shaped particles the separation lines are given by radial vectors through the intersection line of the sphere segments (shown as points in 2d). The different point and line interactions are separated analogously to spherocylinders, as shown.

configurations, where only three contacts are sufficient, namely when the normal vectors from the points of contact meet at the same point and the curvature on at least one of the contacts is flat enough to prevent rotations (Chaikin *et al.*, 2006). Such a configuration is degenerate since force balance automatically implies torque balance such that the force and torque balance equations (2–3) are no longer linearly independent. Despite the fact that these configurations should have measure zero in the space of all possible configurations, they are believed to appear more frequently in simulation algorithms such as the LS algorithm (Donev *et al.*, 2007).

For spherocylinders, the degeneracy appears due to the

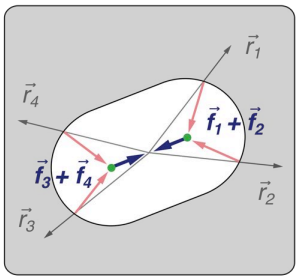

FIG. 20 (Colors online) Illustration of a degenerate configuration of a spherocylinder. Vectors $\mathbf{r}_1, ..., \mathbf{r}_4$ indicate contacts on the spherical caps. The normal vector projects the contact forces $\mathbf{f}_1, ..., \mathbf{f}_4$ onto the centres of the spherical caps. Due to the symmetry of the two centres, the respective force arms are equal and force balance automatically implies torque balance. The force and torque balance equations (2,3) are thus degenerate.

spherical caps, which project the normal forces onto the end points of the central line of the cylindrical part. If all of the contacts are on the spherical caps, which will frequently occur for small aspect ratios, force balance will then always imply torque balance, since the force arms of the two points are identical (see Fig. 20). A similar argument applies to dimers and lens-shaped particles, and can possibly be extended to other smooth shapes. In the case of spherocylinders, a degeneracy also appears for very large aspect ratios, because then all contacts will predominantly be on the cylindrical part. As a consequence, the normal vectors are all coplanar and the number of linear independent force and torque balance equations is reduced by one predicting the contact number $z \to 8$ as $\alpha \to \infty$, which is indeed observed in simulations (Wouterse *et al.*, 2009; Zhao *et al.*, 2012).

A quantitative method to estimate the probability of these degenerate configurations is based on the assumption that a particle is always found in an orientation such that the redundancy in the mechanical equilibrium conditions is maximal (Baule *et al.*, 2013). This condition allows us to associate the number of linearly independent equations involved in mechanical equilibrium with the set of contact directions. Averaging over the possible sets of contact directions then yields the average effective number of degrees of freedom $\tilde{d}_\mathrm{f}(\alpha)$, from which the coordination number follows as $z(\alpha) = 2\tilde{d}_\mathrm{f}(\alpha)$ (Baule *et al.*, 2013). This approach recovers the continuous transition of $z(\alpha)$ from the isostatic spherical value $z = 6$ at $\alpha = 1$, to the isostatic value $z = 10$, for aspect ratios above ≈ 1.5 observed in ellipsoids of revolution, spherocylinders, dimers, and lens-shaped particles, Fig. 21a. The trend compares well to known data for ellipsoids (Donev *et al.*, 2004) and spherocylinders (Wouterse *et al.*, 2009; Zhao *et al.*, 2012).

Combining these results on $z(\alpha)$ with the results of Sec. IV.G.1 on the average Voronoi volume $\overline{W}_\alpha$ leads

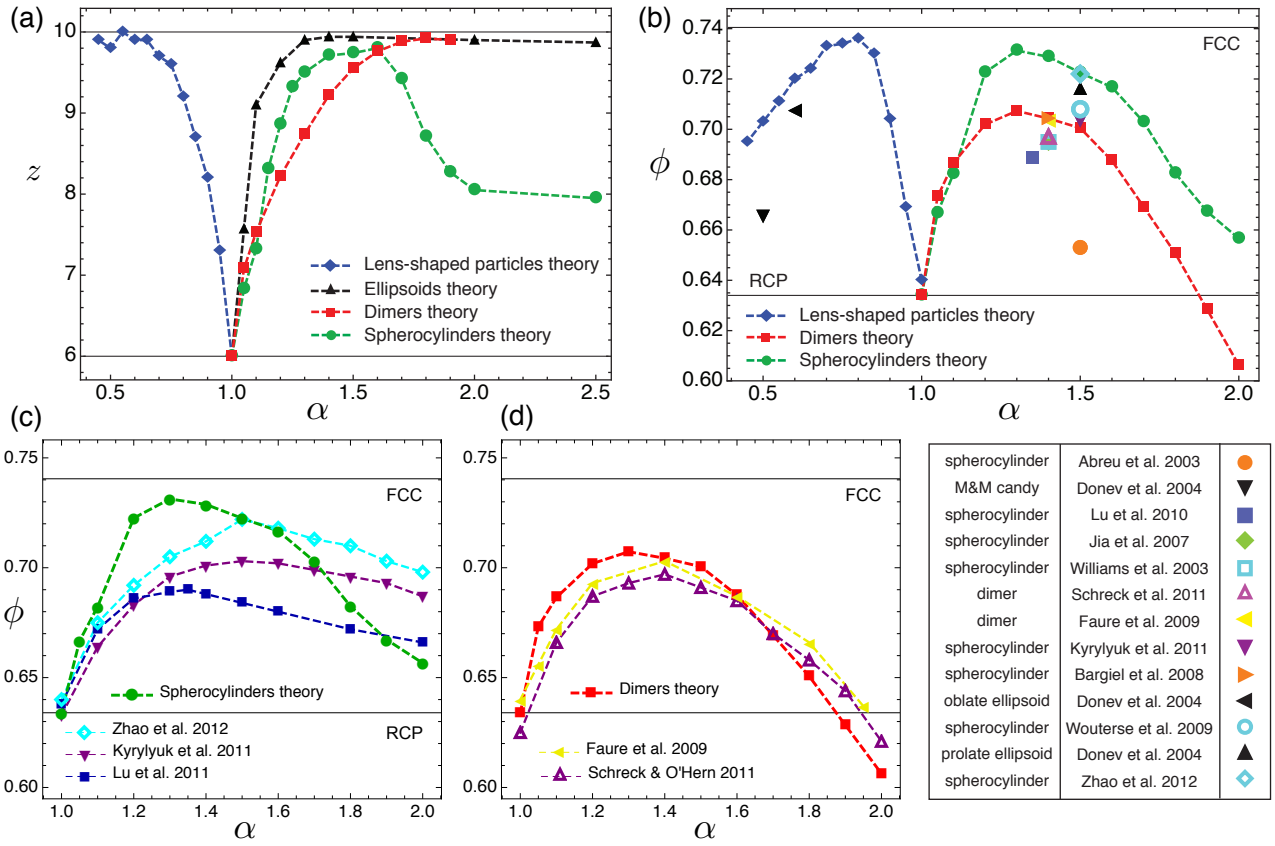

FIG. 21 (Colors online) Theoretical predictions for packings of non-spherical particles (Baule *et al.*, 2013). (a) The variation $z(\alpha)$ obtained by evaluating the occurrence of degenerate configurations for dimers, spherocylinders, ellipsoids of revolution, and lens-shaped particles. A smooth increase is obtained in agreement with simulation data. For spherocylinders, z decreases to the value 8 as $\alpha \to \infty$. (b) Combining $z(\alpha)$ with the results on $\overline{W}_\alpha$ from the volume ensemble leads to theoretical predictions for $\phi(\alpha)$ exhibiting a density peak for dimers, spherocylinders, and lens-shaped particles. Results on $\phi_{\max}$ for the three shapes from simulations are indicated by symbols. The theory captures well both the location of the peak and the maximum density. (c) Detailed comparison of theory and simulations for spherocylinders. The theoretical peak is slightly shifted to the left and more pronounced than in the empirical data. (d) Detailed comparison of theory and simulations for dimers showing excellent agreement.

to a close theoretical prediction for the packing density $\phi(\alpha) = V_0/\overline{W}_\alpha(z(\alpha))$ which does not contain any adjustable parameters. Figure 21b presents the results for dimers, spherocylinders and lenses showing that the theory is an upper bound of the maximal densities measured in simulations. The theory predicts the maximum density of spherocylinders at $\alpha = 1.3$ with a density $\phi_{\max} = 0.731$ and that of dimers at $\alpha = 1.3$ with $\phi_{\max} = 0.707$. For lens-shaped particles a density of $\phi_{\max} = 0.736$ is obtained for $\alpha = 0.8$, representing the densest random packing of an axisymmetric shape known so far. The theoretical predictions of $\phi(\alpha)$ compare quite well with the available numerical data for spherocylinders and dimers (Figs. 21c, d). By plotting z against ϕ parametrically as a function of α, we can also include our results in the z–ϕ phase diagram, which is thus extended from spheres to non-spherical particles and discussed next. By plotting (ϕ, z) the apparent cusp-like singularity at the spherical point $\alpha = 1$ in $z(\alpha)$ and $\phi(\alpha)$ (Figs. 21a, b) disappears and the spherical RCP point becomes as any other point in the phase diagram.

H. Towards an Edwards phase diagram for all jammed matter

The results from Secs. IV.B, IV.F, and IV.G.3 are combined in a phase diagram of jammed matter that can guide our understanding of how random arrangements of particles fill space as shown in Fig. 22. The representation in the z–ϕ plane is in a way the most natural choice, since both ϕ and z are macroscopic observables of the packing that characterize the thermodynamic state of the packing. They can also be measured in simulations in a straightforward way. Although Fig. 22 is far from complete, we observe clear classifications of pack-

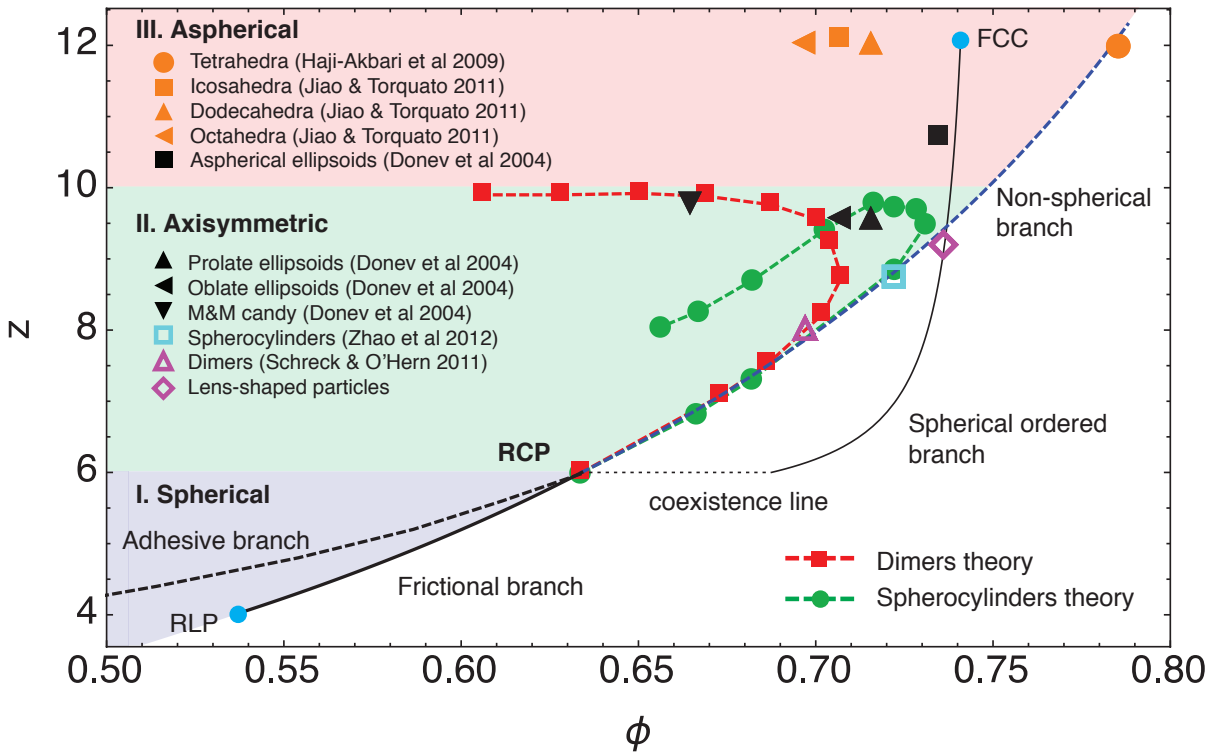

FIG. 22 (Colors online) Unifying phase diagram in the z–ϕ plane resulting from the Edwards volume ensemble theory. Theoretical results on the equations of state for spheres with and without adhesion and dimers/spherocylinders are plotted together with empirical results on maximal packing densities for non-spherical shapes from the literature (where z and ϕ have been determined in the same simulation). Different phases are identified by the symmetry of the constituents. Different equations of state due to friction, adhesion, shape, and (partial) order all come together at the RCP point.

ings based on the *symmetry* and *surface properties* of the constituents. Horizontal phase boundaries are identified by the isostatic condition for frictionless particles, predicting $z = 6$ for isotropic shapes and $z = 10$ ($z = 12$) for rotationally symmetric (fully asymmetric) shapes respectively. The frictionless RCP point at $\phi_{\rm Edw} = 0.634...$ and $z = 6$ plays a prominent role in the phase diagram, despite that it contracts the J-line. It splits up (although in a continuous manner, except for ordering) the equation of state into four different branches governed by friction, shape, adhesion, and order, as follows:

Frictional branch. The infinite compactivity RLP branch connects the RCP point $(0.634, 6)$ with the minimal RLP point at $(0.536, 4)$. This branch is the upper limit of the triangle of mechanically stable disordered sphere packings depicted in the phase diagram for 3d monodisperse spheres in Fig. 12. The RLP branch is parametrized by varying the friction μ and thus z in the equation of state (116).

Non-spherical branch. Surprisingly, we find that both dimer and spherocylinder packings appear as smooth continuations of spherical packings. The analytic form of this continuation from the spherical random branch can be derived (blue dashed line in Fig. 22) by solving the self-consistent equation (165) perturbatively for small aspect ratios (Baule *et al.*, 2013):

$$\phi(z) = \left(1 + \omega_{\rm rcp} \frac{1 + g_1(\omega_{\rm rcp}) \left(\frac{z}{z_{\rm iso}} - 1 \right) \frac{M_{\rm b}}{M_z}}{\left[\frac{z}{z_{\rm iso}} - g_2(\omega_{\rm rcp}) \left(\frac{z}{z_{\rm iso}} - 1 \right) \frac{M_{\rm b}}{M_z} \right] \left[1 + \left(\frac{z}{z_{\rm iso}} - 1 \right) \frac{M_{\rm v}}{M_z} \right]} \right)^{-1} . \tag{171}$$

Here, $\omega_{\rm rcp}$ denotes the spherical free volume at RCP, Eq. (115, $z_{\rm iso} = 6$ is the spherical isostatic value, and the functions $g_{1,2}$ can be expressed in terms of exponential integrals. The dependence of Eq. (171) on the object shape is entirely contained in the geometrical parameters $M_{\rm b}$, $M_{\rm v}$, and M_z: $M_{\rm b}$ and $M_{\rm v}$ quantify the first

order deviation from the sphere at $\alpha = 1$ of the object's hard-core boundary and its volume, respectively, while M_z measures the first order change in the coordination number upon deformation of the sphere. The inversion of Eq. (171) can be performed exactly by solving a quadratic equation for $z(\phi)$ leading to the analytic continuation of the frictional branch shown in Fig. 22.

A comparison of our theoretical results with empirical data for a large variety of shapes highlights that the analytic continuation provides an upper bound of density on the z–ϕ phase diagram for a fixed z. Maximally dense disordered packings appear to the left of this boundary, while the packings to the right of it are partially ordered. We observe that the maximally dense packings of dimers, spherocylinders, lens-shaped particles and tetrahedra all lie surprisingly close to the analytic continuation of RCP. Whether there is any deeper geometrical meaning to this remains an open question. Recent exact local expansions from the spherical RCP point to arbitrary shapes agree very well with our results and may shed further light on this question (Kallus, 2016). We also notice that the frictional and non-spherical branches are continuous at the spherical RCP point suggesting that a variation in friction might be analogous to varying shape in the phase diagram.

Adhesive branch. The non-spherical branch can also be continued into the adhesive branch of spheres, which splits off at RCP. The adhesive branch describes the universal high adhesion regime for $Ad > 1$ reaching the adhesive loose packing (ALP) point at $\phi = 1/2^3$ and $z = 2$ (see Sec. IV.F).

Spherical ordered branch. As discussed in Sec. III.A.4, the RCP point has been associated with the freezing point of a first order phase transition between a fully disordered packing of spheres and the crystalline FCC phase (Jin and Makse, 2010; Radin, 2008). The signature of this disorder-order transition is a discontinuity in the entropy density of jammed configurations as a function of the compactivity. This highlights the fact that beyond RCP, denser packing fractions of spheres can only be reached by partial crystallization up to the homogeneous FCC crystal phase (Torquato *et al.*, 2000). Experiments on hard sphere packings indeed confirm the first order transition scenario, observing the onset of crystallization at $\phi_f \approx 0.64$ at the end of the frictional branch, as well as the coexistence line (Francois *et al.*, 2013; Hanifpour *et al.*, 2015, 2014). The spherical ordered branch provides another boundary, which separates tetrahedra from all other shapes: Tetrahedra are the only shape that pack in a disordered way denser than spheres in a FCC crystal.

The picture that emerges from this phase diagram is that spherical packings can be generated on the frictional branch between the RLP and RCP limits by variation of the inter-particle friction and along the adhesion branch by varying interparticle attraction. Beyond RCP, these two lines can be continued smoothly by deforming the sphere into elongated shapes. The ordered branch does not connect smoothly to any of these branches, instead appears through a first order phase transition with a coexistence regime. It suggests that introducing order is a more drastic modification than modifying the particle interactions due to geometry or surface frictional properties. This distinction is similar to the one between discontinuous first and continuous higher-order phase transitions.

Overall, it seems that the central importance historically given to the spherical RCP point may not be justified. In the whole share of things, the spherical point appears as any other inconsequential point in a continuous variation of jammed states driven by friction, attraction or shape. It is as though each jammed state (ranging from spherical to dimers, trimers, polymers, spherocylinders, ellipsoids, tetrahedra and cubes, from frictionless to frictional and adhesive grains) carries the features of the one great single organizing principle in which all the jammed states organize, too; so that everything links to everything else, moved by the one organizing idea which is the universal physical principle in nature (Schopenhauer, 1974).

V. JAMMING SATISFACTION PROBLEM, JSP

We close our review by providing a novel understanding of the jamming criticality under the Edwards ensemble as the phase transition between the satisfiable and the unsatisfiable phases of the Jamming Satisfaction Problem. At the very end we suggest a unifying view of the Edwards ensemble of grains with the statistical mechanics of spin-glasses.

As we explained in Sec. II.A, a packing can be described as an ensemble of particles with given positions and orientations, satisfying a set of geometrical and mechanical constraints, that is, *(i)* there is no overlap between particles, and *(ii)* force and torque balances are satisfied on every particle. As such, it can be considered as an instance of a constraint satisfaction problem: the Jamming Satisfaction Problem (JSP). Thus, the full solution to the JSP requires the simultaneous determination of both: (a) Volume ensemble: the contact network of the packing, i.e., the set of normal and tangential vectors $\hat{\mathbf{n}}_a^i$ and $\hat{\boldsymbol{\tau}}_a^i$ for each particle in the packing specified by the hard-core volume constraints, and (b) Force ensemble: the magnitude of the forces $f_{a,n}^i$, $f_{a,\tau}^i$ at each contact specified by force/torque balance.

Solving the JSP, in general, is a very complicated task, and one needs to resort to some approximations. The first main approximation that we applied across this review consisted in decoupling the geometrical problem of determining the contact network of the packing from the mechanical problem of finding the force distribution.

Thus, in Sec. IV we developed the Edwards Volume Ensemble that considers in detail the volume ensemble, but do not directly considers the full force ensemble, which is only taken into account by the global isostatic constraint establishing force balance on the average coordination number.

Below, we consider another reduced JSP where one now fixes the geometry of the packing considering it as a random graph (thus, fixing the volume ensemble), and then considering the full force ensemble on these random graphs to find the force distribution. A final ensemble average over all possible random graphs consistent with prescribed (local) conditions of jamming and excluded volume on the positions of the particles is performed to obtain the final force distributions. Such a reduced JSP is therefore amenable to be solved for sparse networks by the cavity method from spin-glass theory (Mézard and Montanari, 2009; Mézard and Parisi, 2001), where one considers the geometric configuration of the particles in the packing as fixed, and then finds the force distribution.

This force distribution is nothing but the uniform Edwards' measure $\Theta_{\rm jam}$ over all possible solutions of the JSP Eq. (10) where the hard-core constraint is relaxed, being automatically satisfied because we are considering the contact network fixed. To emphasize the dependence of $\Theta_{\rm jam}$ solely on the force configuration $\{\mathbf{f}\}$ for a given realization of the contact network $\{\mathbf{d}\}$, we use the notation $\Theta_{\rm jam}(\{\mathbf{f}\}|\{\mathbf{d}\}) = P(\{\mathbf{f}\})$, and we recall here the definition for the sake of readability:

$$
\begin{aligned}
&\Theta_{\rm jam}(\{\mathbf{f}\}|\{\mathbf{d}\}) = P(\{\mathbf{f}\}) \\
&= \frac{1}{\mathcal{Z}} \prod_{i=1}^{N} \delta\left(\sum_{a\in\partial i} \mathbf{f}_a^i\right) && \text{force balance} \\
&\times \prod_{i=1}^{N} \delta\left(\sum_{a\in\partial i} \mathbf{d}_a^i \times \mathbf{f}_a^i\right) && \text{torque balance} \\
&\times \prod_{i=1}^{N} \prod_{a\in\partial i} \theta\left(\mu f_{a,n}^i - |\mathbf{f}_{a,\tau}^i|\right) && \text{Coulomb friction} \\
&\times \prod_{i=1}^{N} \prod_{a\in\partial i} \theta\left(-\mathbf{d}_a^i \cdot \mathbf{f}_a^i\right) && \text{repulsive forces} \\
&\times \prod_{\text{all contacts } a} \delta(\mathbf{f}_a^i + \mathbf{f}_a^j) && \text{Newton } 3^{\rm rd} \text{ law}, \quad (172)
\end{aligned}
$$

where the normalization or partition function $\mathcal{Z}$ is the number of solutions of this JSP. The important point is that if $\mathcal{Z} \geq 1$ then there exists a solution to the JSP, i.e., it is satisfiable (SAT). Conversely, if $\mathcal{Z} < 1$ there are no solutions to the JSP, i.e., it is unsatisfiable (UNSAT) (Kirkpatrick and Selman, 1994).

The SAT/UNSAT threshold of the JSP is marked by the coordination number $z_c^{\rm min}(\mu)$ that separates the region where solutions do exist (i.e. where $\mathcal{Z} > 1$) from the region without solutions (where $\mathcal{Z} < 1$), corresponding to an underdetermined/overdetermined set of equations, respectively. In the limiting case of frictionless particles, $z_c^{\rm min}(\mu)$ should be compared with the naive Maxwell counting isostatic condition: $z_c^{\rm min}(\mu = 0) = 2d_f$, although the JSP takes into account the full set of constraints, Eqs. (172), rather than only force balance as in Maxwell counting. The JSP thus extends this naive counting to the full set of constraints including friction μ. A jammed isostatic assembly of particles lies exactly on the edge between these two phases, i.e., where a solution to the JSP first appears as one increases the average coordination number $z(\mu)$. Figure 23 shows the average coordination number $z_c^{\rm min}(\mu)$ at the jamming transition as a function of the friction coefficient μ in a 2d sphere packing, obtained by solving the JSP through the cavity method as explained next (Bo *et al.*, 2014). Results are consistent with existing numerical simulations (Kasahara and Nakanishi, 2004; Makse *et al.*, 2000; Papanikolaou *et al.*, 2013; Shen *et al.*, 2014; Shundyak *et al.*, 2007; Silbert, 2010; Silbert *et al.*, 2002a; Song *et al.*, 2008).

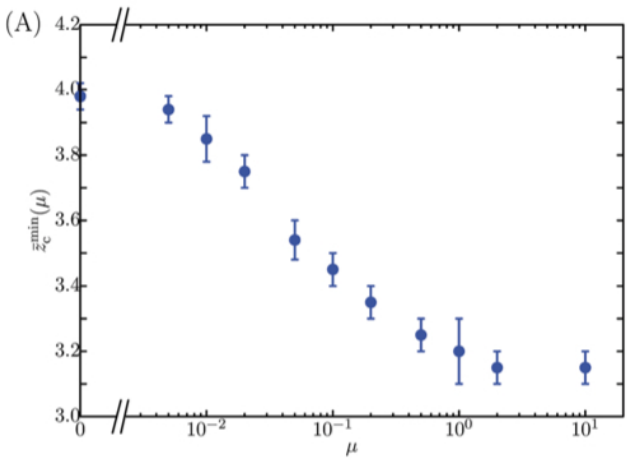

FIG. 23 Linear-log plot of average coordination number $z_c^{\rm min}(\mu)$ at the jamming transition as a function of the friction coefficient μ in 2-D sphere packing calculated with the cavity method. The curve $z_c^{\rm min}(\mu)$ separates the SAT/UNSAT phases of jamming. For $z > z_c^{\rm min}(\mu)$, the force balance equations are satisfied while they are not when $z < z_c^{\rm min}(\mu)$. At the transition $z_c^{\rm min}(\mu)$ for a given μ a jammed critical state exists separating the SAT from the UNSAT phases. $z_c^{\rm min}(\mu)$ shows a monotonic decrease with increasing μ from the isostatic Maxwell estimation $z_c^{\rm min}(\mu = 0) = 2D = 4$ to $z_c^{\rm min}(\mu = \infty) \geq D + 1 = 3$. Error bar indicates the range from the largest $z_c^{\rm min}(\mu)$ having no solution to the smallest $z_c^{\rm min}(\mu)$ having solution. Data points represents the mean of the range. (Data reprinted from (Bo *et al.*, 2014)).

A. Cavity approach to JSP

Solving the JSP amounts to compute the single force distributions $P(\mathbf{f}_a^i)$ at the contacts a's of the particle

i's. However, calculating these single force distributions $P(\mathbf{f}_a^i)$ from the joint distribution $P(\{\mathbf{f}\})$ Eq. (172) is still a very demanding computational task, which requires some additional mean-field approximations to be solved.

There are two preferred mean-field theories (both of infinite dimensional nature): the first one is the infinite range model, which assumes that each particle is in contact with every other particle in the packing. The archetypical model is the Sherrington-Kirkpatrick (SK) model of fully connected spin-glasses (Sherrington and Kirkpatrick, 1975) which has been adapted to the hard-sphere case in (Parisi and Zamponi, 2010) (see Secs. III.A.4). As a result of this approximation scheme, the real finite dimensional contact network Fig. 24a is substituted by a fully-connected network, i.e., a complete graph as shown in Fig. 24b. The solution of such a model is possible since, in a complete graph, each interaction becomes very weak, rendering a fully connected model into a weakly connected system that can be solved exactly under the hierarchy of replica symmetry breaking schemes (Mézard and Montanari, 2009). A simpler version than the SK model, yet showing all the phenomenology of jamming, is a model adapted from machine learning; the perceptron recently studied in (Franz and Parisi, 2016; Franz *et al.*, 2015).

A second mean-field theory of choice consists in approximating the contact network by a sparse random graph (Mézard and Parisi, 2001), which allows one to preserve an essential property of real finite dimensional packings: the finite coordination number z. As a consequence one may expect that the sparse random graph approximation should mimic the physics of real packings better than the fully-connected one. The sparse random graph scheme assumes that the local contact network around each particle can be approximated by a tree-like structure, i.e. it neglects the strong local correlations of loops and force chains of a real packing Fig. 24a by a locally tree-like structure, Fig. 24c. Under this approximation the JSP can be solved by a method known as cavity method (Mézard and Montanari, 2009; Mézard and Parisi, 2001), which we explain next.

It should be noticed that, although the cavity approach is a mean field theory valid for infinite dimensions, a dimensional dependence appears in the non-overlap condition in the definition of the network ensemble, see (Bo *et al.*, 2014) for details. The crucial quantity to consider in the cavity method is not the single force distribution itself $P(\mathbf{f}_a^i)$, but a modified one, called the cavity force distribution and denoted by $P_{i\to a}(\mathbf{f}_a^i)$. Physically, $P_{i\to a}(\mathbf{f}_a^i)$ is the probability distribution of the force $\mathbf{f}_a^i$ at the contact a in a modified packing where the particle j touching the particle i at the contact a has been removed (from which the name cavity). The rationale to consider $P_{i\to a}(\mathbf{f}_a^i)$ instead of the "true" force distribution $P(\mathbf{f}_a^i)$ is that for the cavity distributions it is possible to derive a set of self-consistent equations if one neglects the correlation between $P_{i\to a}(\mathbf{f}_a^i)$ and $P_{j\to a}(\mathbf{f}_a^j)$ (Bo *et al.*, 2014).

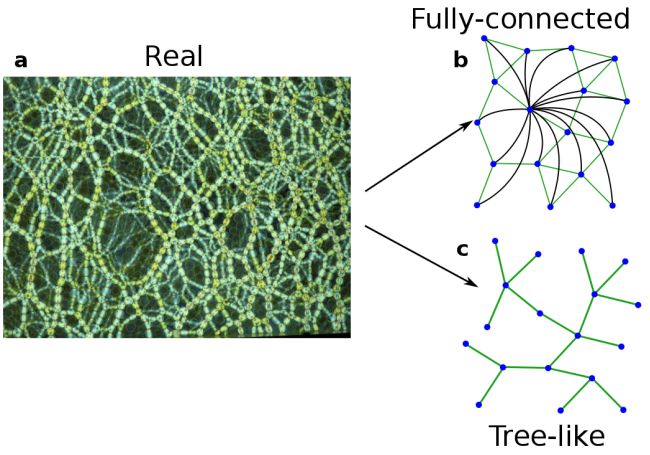

FIG. 24 (a) A real finite-dimensional packing is composed of strongly correlated force chains and geometrical loops at short scale (image reprinted with permission from the Behringer Group, Duke University). However, state-of-the-art theoretical approaches to describe this correlated structure rely upon mean-field infinite-dimensional approximate treatments of such a packing as a: (b) Fully-connected packing where every single particle is in contact with any other particle in the packing; the real network is approximated by a complete graph, i.e., each node is connected with all other nodes as shown for one of them. (c) Locally-tree like packing where the real network is approximated by a sparse random graph that locally looks like a tree structure with no loops, i.e., loops in the network are neglected, except at relatively large scales that diverge with system size, although very slowly as $\ell \sim \ln N$.

For example, the cavity equation for $P_{i\to a}(\mathbf{f}_a^i)$ can be obtained by simply convoluting the cavity force distributions $P_{k\to b}(\mathbf{f}_b^k)$ of the particles $k \neq j$ neighbors of particle i with the local mechanical constraint χ_i, as depicted in Fig. 25, and mathematically expressed as follows:

$$P_{i\to a}(\mathbf{f}_a^i) \propto \int \prod_{b\in\partial i\setminus a} d\mathbf{f}_b^k \; \chi_i \prod_{k\in\partial b\setminus i} P_{k\to b}(\mathbf{f}_b^k), \quad (173)$$

where the symbol $\propto$ implies a normalization factor, and the mechanical constraint χ_i on particle i is given by:

$$\chi_i\left(\{\mathbf{f}_a^i\}_{a\in\partial i}\right) = \delta\left(\sum_{a\in\partial i}\mathbf{f}_a^i\right)\delta\left(\sum_{a\in\partial i}\mathbf{d}_a^i\times\mathbf{f}_a^i\right) \times \prod_{a\in\partial i}\theta\left(\mu f_{a,n}^i - |\mathbf{f}_{a,\tau}^i|\right)\theta\left(-\mathbf{d}_a^i\cdot\mathbf{f}_a^i\right). \quad (174)$$

Notice that the contact directions $\{\mathbf{d}_a^i\}$ are kept fixed: they represent the "quenched" disorder introduced by the underlying contact network, which is kept fixed.

Once the set of cavity equations (173) has been solved— e.g. by iteration under the Replica Symmetric (RS) assumption (Bo *et al.*, 2014)— one can reconstruct

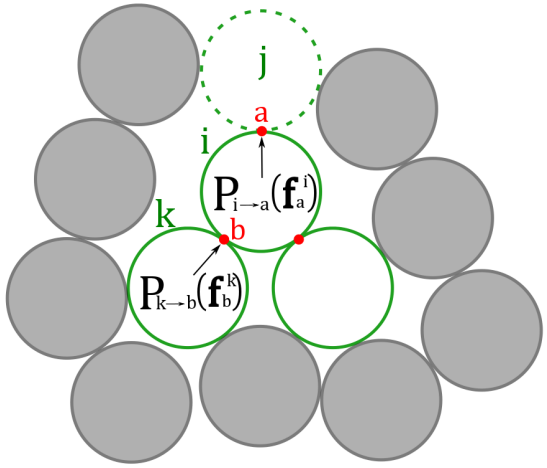

FIG. 25 Calculation of the cavity force distribution $P_{i\to a}$. First particle j (dashed contour) is virtually removed from the packing. Then $P_{i\to a}$ for particle i is computed by convoluting the distributions $P_{k\to b}$ of the neighboring particles k with the local mechanical constraint χ_i enforcing force and torque balances.

back the original force distribution at contact a by simply multiplying the cavity force distributions $P_{i\to a}(\mathbf{f}_a^i)$ and $P_{j\to a}(\mathbf{f}_a^j)$ coming from the two particles i and j in contact at a:

$$P(\mathbf{f}_a^i) \propto \; P_{i\to a}(\mathbf{f}_a^i) P_{j\to a}(\mathbf{f}_a^j). \tag{175}$$

An example of force distribution in a 3-dimensional frictionless sphere packing assessed with the cavity method is shown in Fig. 26. The result shows an exponential decay at large forces and a non-zero value for $P(f)$ at $f = 0$, i.e., it gives an exponent at the RS level

$$\theta_{\rm RS} = 0 \tag{176}$$

for the small force scaling $P(f) \sim f^\theta$, Eq. (76). This last prediction is inconsistent with simulation results, which find a value of the exponent θ in the interval $0.2 \leq \theta \leq 0.5$. It should be noted that Eq. (176) is obtained exactly at the thermodynamic limit, so no finite size effects are observed.

The discrepancy could be in principle due to the abundance of short loops in the real finite-dimensional contact network that are neglected by the locally tree-like contact network structure considered by the cavity method. However, it is known that the fraction of short force loops decreases with dimension at jamming— a results valid for any random network in infinite dimensions— yet, the non-zero weak force power-law exponent is obtained in the high dimensional calculations in the fully connected case (Charbonneau *et al.*, 2012). In this case, the complexity lost by the consideration of a uniform fully connected network is somehow overcome by the fractal complexity provided by the fullRSB solution, which in this case, gives rise to the concomitant non-zero small-force exponent. Whether a zero exponent result is the byproduct of the cavity calculation being done at the RS level or of the absence of loops in the structure is to be determined.

A similar situation appears in the replica approach to the problem: The original 1RSB calculation under the replica approach of the force distribution for hard sphere glasses done by Zamponi and Parisi (Parisi and Zamponi, 2010) led to a trivial scaling

$$\theta_{\rm 1RSB} = 0, \tag{177}$$

while the non-zero exponent was only obtained when the full RSB calculation was performed (Charbonneau *et al.*, 2014b)

$$\theta_{\rm fullRSB} = 0.42... \tag{178}$$

It should be noticed, though, that 1RSB level calculations and above are substantially more difficult to perform with the cavity method than with replicas (e.g., no calculation exists above 1RSB with the cavity method for any model).

However, the main result of the cavity approach is the detection of the SAT/UNSAT transition of the JSP for sphere packings with arbitrary friction coefficient, and a lower bound estimate of the critical coordination number $z_c^{\rm min}(\mu)$ at the jamming transition as a function of the friction coefficient μ, as shown in Fig. 23. Moreover, the cavity method seems a promising way to study JSPs for packings with particles of arbitrary shapes, which are difficult to perform with replicas.

B. Edwards flat hypothesis in the Edwards-Anderson spin-glass model

The main goal of this section is to investigate Edwards' conjecture of equiprobable jammed states in the spin-glass model first introduced by Edwards himself together with Anderson, thus, bringing together two of the most significance contributions of Edwards to science. We leverage on some rigorous results (Newman and Stein, 1999) to understand what is effectively right and what may go wrong with that hypothesis by precisely stating it in terms of metastable states in spin-glasses and jamming. We will see how this definition of metastable jammed states leads to the most precise test so far of the Edwards flat hypothesis in the exactly solvable SK model (Sherrington and Kirkpatrick, 1975), which we propose to perform in Section V.C.

The Ising spin glass on the d-dimensional cubic lattice Z^d, also known as the Edwards-Anderson model, is described by the following Hamiltonian:

$$\mathcal{H}(\vec{\sigma}) = -\sum_{\langle ij \rangle} J_{ij}\sigma_i\sigma_j \;, \tag{179}$$

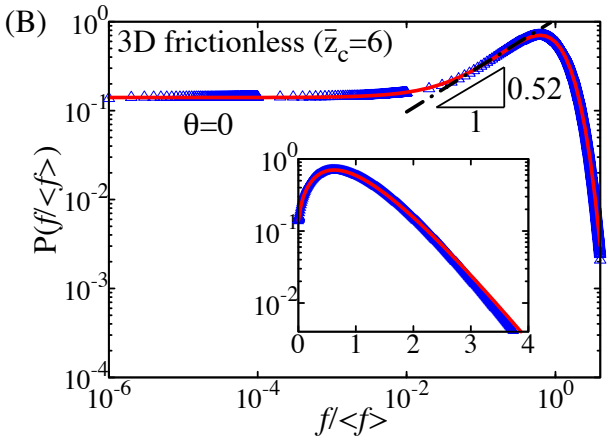

FIG. 26 Force distribution $P(f)$ in frictionless sphere packing in 3d obtained by the RS approach to JSP in (Bo *et al.*, 2014). We note that even though the cavity calculation neglects correlations between forces as in mean field infinite dimensions, the dimensional dependence appears in the non-overlap condition in the definition of the network ensemble, see (Bo *et al.*, 2014) for details. The result obtained from the cavity method (open triangles) shows a flat regime (in a log-log plot) with exponent $\theta_{\rm RS} = 0$ at small forces. In the inset, log-linear plot of the same distribution exhibits an approximate exponential tail at large forces. The red solid line corresponds to a fit through the data. (Data reprinted from (Bo *et al.*, 2014)).

where i are the sites of Z^d, the spins $\sigma_i = \pm 1$, and the sum is over nearest neighbor spins. The couplings J_{ij} are independent identically distributed random variables, and we assume their common distribution to be continuous and to have a finite mean.

A distinguishing property of spin glasses, which pertains to many complex systems including granular media, is that they feature a "rugged energy (or free energy) landscape". To give a picturesque definition of this energy landscape (we will be more precise later) let us consider a zero-temperature dynamics, where at each time step a spin is randomly chosen and flips if it lowers the energy, otherwise it does not move. An interesting question to ask is: in which regions of the energy landscape does the system wander as time elapses? The answer is that the type of walk induced by that dynamics is a very simple one: the system starts from an arbitrary spin configuration, and then, as time goes by, it moves downhill to the nearest energy minimum. At this point the dynamics will stop and no more spins will flip. At variance with a pure ferromagnet, in the spin glass this dynamics arrests very quickly, and also at a quite high-energy state, the reason being due to, precisely, the abundance of metastable states. The type of metastable states concerned in this specific case are called one-spin-flip (1SF) metastable states since they are reached following a dynamic that flips one spin at a time: when the system arrives in one of these configurations, no single spin can lower the energy by flipping, but if two neighboring spins are allowed to flip simultaneously, then lower energy states are available. In other words, 1SF states are stable against a single spin-flip, but not against two (or more) simultaneous spins-flip. An example of one-spin-flip metastable state is shown in Fig. 27 along with a possible two-spins-flip move (shown in the lowest panel) needed to escape the 1SF metastable trap. As discussed in Table I these 1SF metastable states are analogous to the locally jammed states introduced by (Torquato and Stillinger, 2001) and called 1PD in the table.

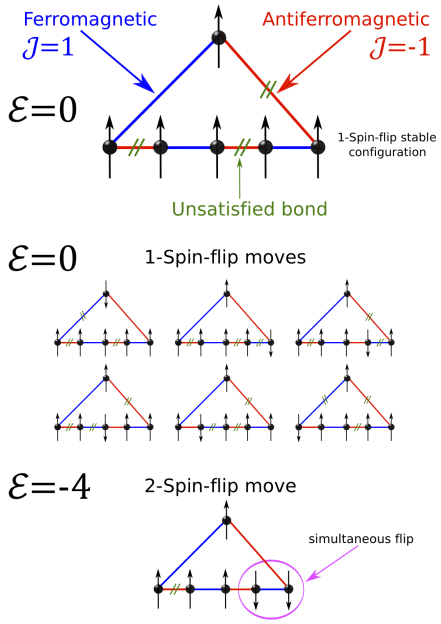

FIG. 27 Example of a 1-Spin flip stable configuration.

The concept of 1SF metastable states can be easily extended to k-spin-flip (kSF) metastable states, even without resorting to a specific dynamics, but using solely the Hamiltonian of the system Eq. (179). We define a k-spin-flip metastable state as a (infinite volume) configuration whose energy cannot be lowered by flipping any connected subset of $1, 2, \ldots, k$ spins. In particular, the ground states of the system correspond to configurations whose energy cannot be lowered by flipping any finite number of spins, i.e. they are found in the limit $k \to \infty$, that is, the ground state of the spin-glass is the ∞-SF state. The kSF metastable states are analogous to the kPD metastable collective jamming states defined in Table I that generalize the concept of collective jamming in (Torquato and Stillinger, 2001). The corresponding ground state of jamming is then the ∞-PD state. We, thus, end up with a nice analogy between spin-glasses and jamming which we can leverage to harness the nature of metastable jammed states in terms of exact results for

spin-glass metastable states obtained by (Newman and Stein, 1999).

The first important result about 1SF, 2SF, ... metastable states is that they do exist for all dimensions $d \geq 1$, and, for almost every realization of the couplings $\{J_{ij}\}$, in the thermodynamic limit, there are uncountably many kSF metastable states for all finite $k \geq 1$ (Newman and Stein, 1999). In the previous example, we saw that a one-spin-flip dynamics (i.e. a dynamics where one spin is allowed to flip at each time step) converges to 1SF metastable states. Now we may ask: how do we visit the kSF metastable states for $k > 1$? To answer this question we need to introduce more precisely the concept of *dynamics*.

Let us start by considering first the standard single-spin-flip dynamics, and then we generalize the concept to a kSF dynamics. In a 1SF dynamics, starting from an initial spin configuration $\vec{\sigma}^0$ (sampled, say, from a symmetric Bernoulli distribution), a single spin at a time is chosen uniformly at random and flips if the resulting configuration has lower energy, otherwise it does not flip. We denote by ω_1 a given realization of this zero-temperature single-spin-flip dynamics (which in principle depends on the initial configuration $\vec{\sigma}^0$ and the coupling distribution $\{J_{ij}\}$). Now, a k-spin-flips dynamics is defined in such a way that rigid flips of all lattice animals (finite connected subset of Z^d) up to k spins can occur. For example in the case $k = 2$ both single-spin flips and rigid flips of all nearest neighbor pairs of spins are allowed (see the bottom panel in Fig. 27 as an example of a 2SF move). At each step of the dynamics a lattice animal of size $\ell \leq k$ is chosen at random with probability p_ℓ and it flips if the resulting configuration has lower energy, otherwise it does not flip. The probabilities p_ℓ must satisfy $\sum_{\ell=1}^{k} p_\ell n_\ell < \infty$ for any k (including $k \to \infty$), where n_ℓ is the number of lattice animals of size ℓ (containing the origin of Z^d). We denote by ω_k a given realization of this kSF dynamics (Newman and Stein, 1999).

Having defined the kSF dynamics, we can now state two important rigorous results. The first one is that for almost every realization of the couplings $\{J_{ij}\}$, initial configuration $\vec{\sigma}^0$, and dynamics ω_k (for a fixed k), there exists a limiting configuration $\vec{\sigma}^\infty$ which is a kSF metastable state, i.e., the final state $\vec{\sigma}^\infty$ is energetically stable against the flip of any subset of k spins (Newman and Stein, 1999). We denote such a limiting configuration as $\vec{\sigma}^\infty_k$, with the subscript k stressing that it is a kSF metastable state. The second result is that *almost every* $\vec{\sigma}^\infty_k$ *has the same energy density* e_k (i.e. energy per site), which is also independent from the coupling realization (but depends on the choice of the dynamics) (Newman and Stein, 1999). This does not mean that there does not exist a spectrum of energy densities among all kSF metastable configurations. Actually a non-trivial spectrum does indeed exist for any dimension d. The point is that, once a given kSF dynamics is chosen, almost all realizations ω_k of this dynamics will produce configurations $\vec{\sigma}^\infty_k$ having the same energy density.

Let us now recall how we defined the metastable states in a granular system, i.e. the jammed configurations we introduced in the very beginning of this review and right above. In analogy with one-spin-flip metastable states, we defined the one-particle-displacement 1PD metastable states as those configurations whose volume fraction cannot be increased by displacing any single particle. However, if two particles are displaced simultaneously, the system can escape this jammed trap and reach states with higher volume fraction. More generally, we defined a k-particle-displacement kPD metastable state as a configuration whose volume fraction cannot be increased by displacing any subset of $1, 2, \ldots, k$ particles. Jammed ground states in this picture are found by taking the limit $k \to \infty$.

Equipped with this twofold view on metastability, we can formulate the following interesting question, which brings us to Edwards conjecture. Imagine to walk on the energy/volume landscape guided by a one-spin-flip/one-particle-displacement dynamics that, in turn, brings you in a 1SF/1PD metastable state. The question is: starting from a random initial configuration, will you visit with your dynamics all the available 1SF/1PD metastable states? The answer, in general, is NO, and the reason is that both 1SF and 1PD metastable states have different energies and volume fractions, respectively, while it can be proven (at least for the spin glass) that once we have fixed the dynamics, we always end up in metastable states having the same energy (in the spin glass case) or, presumably, having the same volume fraction (in the granular one). Therefore, for a given choice of the dynamics, we can never visit all the available 1SF/1PD metastable states, and, evidently, it does not make much sense to ask if we visit those states with equal probability, without further specifying their energy (or volume fraction).

So, now we come to the real meaningful question and related Edwards' conjecture, which is: *does a given dynamics, ending up always in configurations having the same energy (or volume fraction), sample uniformly ALL the available metastable states of that given energy?* Let us exemplify the question with the specific case of the spin glass. Consider again a 1SF dynamics. This dynamics converges to 1SF metastable states having the same energy density, say e^*. Then the question is: does the dynamics pick up all the available 1SF metastable states in the system with energy e^* with equal probability?

Edwards hypothesis is, basically, an affirmative answer to the previous question. However, proving this conjecture is a very difficult task, as discussed all along this review. Simulations of jammed states, for instance using Molecular Dynamics, Discrete Element Methods, Lubachevsky-Stillinger (Lubachevsky and Stillinger, 1990) or any other jamming generating algorithm may

not be able to provide an answer to this question for systems large enough to be of definitive value. Thus, in the next section we will make a little digression on the Sherrington-Kirkpatrick model (Sherrington and Kirkpatrick, 1975), which is an exactly solvable mean-field model of a spin glass where the metastable states can be mathematically and precisely defined and may allow for a rigorous proof, or disproof, of Edwards hypothesis, at least at the mean-field level.

Before explaining this calculation, there is another issue that we need to clarify, since it may generate confusion. Let us consider the set of 2SF metastable states in the spin glass. These states form a subset of the 1SF metastable states, since states which are 2SF-stable are automatically 1SF-stable, but the converse is not necessarily true. Also, the energies of 2SF metastable states may cross, in principle, the energies of 1SF metastable states. Now posit that we fix the value of the energy of the metastable states. Without further indications the metastable states with that energy may be 1SF or 2SF metastable states. However, once a dynamics is specified, for example a ω_2 dynamics, it will sample only 2SF metastable states, but it will not sample the 1SF ones. Therefore, metastable states with that given value of the energy cannot be sampled uniformly, as in the previous example where 1SF metastable states are not sampled at all.

We thus arrive at the conclusion that it does not make sense to say that metastable states with a given energy are equiprobable, without specifying also the k-spin-flip dynamics. Trying to extend this conclusion to granular system, we may reformulate Edwards' hypothesis saying that "when N grains occupy a volume V, they do so in such a way that all the k-PD metastable states corresponding to that volume V are equally weighted".

The Edwards hypothesis in a more general sense, namely the assumption that all the metastable states with given energy density are equivalent, has inspired many authors to study simple statistical models. It has been found to hold, at least in good numerical approximation, for both, the steady-state of tapped systems in the regime of weak tapping intensities (Dean and Lefèvre, 2001; Prados and Brey, 2002), and in the regime of slow relaxational dynamics of various models (Barrat *et al.*, 2000). But already in the last case a counterexample is the domain growth of a 3d random field Ising model, a case in which the properties of a long-time configuration of (low) energy is not well reproduced by the typical metastable configuration of the same energy due to domain-wall pinning by disorder. In (Godrèche and Luck, 2005) also a counterexample is found by using the analytically solvable one-spin flip dynamics of the 1d Ising chain to display qualitative discrepancies between the dynamic evolution and the averaging over an *a priori* probability measure of Edwards type (and refinements). (Camia, 2005) also gives a simple criterion for testing Edwards hypothesis in certain zero-temperature, ferromagnetic spin-flip dynamics, providing explicit examples in one and higher dimension that the limiting distributions of those dynamics do not coincide with the uniform distribution over the blocked configurations of the dynamics. (Luck and Mehta, 2007) study a finite column of N grains bearing binary orientation variables, but following a stochastic dynamics which does not obey detailed balance. The model bears two parameters in the flipping rates, namely a dimensionless vibration intensity and an activation energy. They establish a phase diagram with four dynamical phases and of particular interest is the glassy phase, where intermittency and a strong deviation from Edwards flatness assumption can be observed through the distribution of local dimer configurations.

On the mean-field level, the Sherrington-Kirkpatrick (SK) model does not admit a simple relation between configurational entropy and effective temperature either (Eastham *et al.*, 2006). These authors study the dynamics in the canonical SK model and show that the metastable states selected by dynamics are of a very special character in which the energy $2e_i$ to flip the spin at site i has a distribution $p(e)$ which is small for e close to zero. Generic metastable states have $p(0) \neq 0$. In the thermodynamic limit the dynamically selected metastable states constitute a vanishing fraction of the totality of metastable states and therefore, according to the Edwards hypothesis should not be expected to be selected. The authors of (Eastham *et al.*, 2006) also explain why the system converges onto such a tiny subset of the metastable states through a population dynamics model. In the next section we discuss precisely the case of the SK model in greater detail.

To conclude this section, we like to point out another rigorous result valid for spin glasses described by the Hamiltonian in Eq. (179), which represents a sort of "weaker" formulation of Edwards conjecture. The result is the following. We learned that each dynamics picks up always metastable states having the same energy density, which we call again e^*. Now, if we focus only on the states of energy e^* reachable by the dynamics we chose (which may not be all the available states with that energy), can we say something about the way they are sampled by the dynamics? The answer is yes, in that all these final states not only have the same energy, but they are *equiprobable*, i.e., they are reachable with the same probability (Newman and Stein, 1999).

C. Opening Pandora's box: Test of Edwards flat hypothesis in the Sherrington-Kirkpatrick spin-glass model

In this section we discuss the validity of Edwards flat hypothesis in the mean-field fully-connected exactly-solvable version of the Edwards-Anderson spin-glass model, the so-called Sherrington-Kirkpatrick (SK) spin-

glass model (Sherrington and Kirkpatrick, 1975). The interest in considering this particular model stems from the fact that it allows one to calculate analytically several observables using Edwards flat assumption, that can be compared with the corresponding quantities measured in dynamical simulations of the same model, thus providing an ideal testing ground to examine the applicability of Edwards conjecture.

The SK model is the infinite dimensional limit of the Edwards-Anderson model, whose Hamiltonian is akin to the one given in Eq. (179), but the sum runs over all $N(N-1)/2$ pairs of distinct spins. A key quantity which can be calculated exactly in the SK model is the 'complexity' $\Sigma(e)$ as a function of the energy density (we only consider the system at zero temperature) (Bray and Moore, 1980). Physically, the complexity $\Sigma(e)$ is defined as the logarithmic scaled number of metastable states $\mathcal{N}_N(e)$ of a given energy density e:

$$\Sigma(e) = \lim_{N\to\infty} \frac{\log \mathcal{N}_N(e)}{N} \ , \tag{180}$$

where N is the size of the system (i.e. the number of spins). The word 'scaled' indicates that $\Sigma(e)$ is the logarithm of $\mathcal{N}_N(e)$ scaled by N.

The type of metastable states we are talking about are precisely the 1SF metastable states defined in the previous section, and $\mathcal{N}_N(e)$ is their number. Now, let us consider a 1SF dynamics at zero temperature, starting from a random initial configuration, sampled, for example, from a symmetric Bernoulli distribution. We can then apply the general results introduced in the previous section. Specifically, we know that the 1SF dynamics will arrest always in states (i.e. configurations) having the same energy, say ϵ, and the number of such states, which we denote by $\Gamma_N(\epsilon)$, is exponentially large in the system size N. On the other side, from the 'static' point of view, we can calculate analytically the total number of available 1SF metastable states of energy ϵ under the Edwards flat assumption, which is given precisely by $\mathcal{N}_N(\epsilon) \sim e^{N\Sigma(\epsilon)}$ (Bray and Moore, 1980).

At this point, the Edwards ergodic question arises: does the dynamically generated $\Gamma_N(\epsilon)$ equal the static flat averaged $\mathcal{N}_N(\epsilon)$? And, if so, does the dynamics pick up all the $\mathcal{N}_N(\epsilon)$ states with the same probability?

If Edwards hypothesis is correct, then the answer to both these questions is affirmative. Actually, it suffices that only the first condition be true, i.e. $\Gamma_N(\epsilon) = \mathcal{N}_N(\epsilon)$, since the second claim would be automatically true according to what we said at the end of the previous section. However, measuring $\Gamma_N(\epsilon)$ from the dynamics is not an easy task, and hence we have to resort to another convenient quantity. A suitable, and easily measurable, observable to test Edwards hypothesis is the distribution of local fields $P(h)$. The local field h_i acting on spin i is defined as $h_i = \sum_{j\neq i} J_{ij}\sigma_j$, and, in a 1SF stable configuration, all these local fields satisfy the condition $h_i\sigma_i > 0$ for any i.

Thus, we are lucky to arrive to a mathematically tractable definition of metastable 1SF state in the SK model which can be incorporated into the SK partition function — as done in (Roberts, 1981), notice that this paper predates by a decade the Edwards formulation, indeed, it can be said that the Edwards problem has been debated in the spin glass community for a longer time than in the granular community — by the constraint $\Theta(\sum_{j\neq i} \sigma_i J_{ij}\sigma_j)$ to obtain the exact mean-field solution for $P(h)$ for this 1SF metastable state under the Edwards flat assumption of equiprobability. Such a prediction can be then compared with the states dynamically obtained under a 1SF dynamics from the fully connected SK model, for instance, a single-spin-flip Glauber dynamics as done in (Eastham *et al.*, 2006). Then, a precise test of Edwards ergodicity can be achieved. One would only hope that an analogous mathematical definition would exist for 1PD locally metastable states for jammed hard spheres, which eventually might be incorporated into the replica framework for hard-sphere glasses (Parisi and Zamponi, 2010) to test Edwards hypothesis in such a jammed model. However, such a mathematical definition is not available as far as we know.

On the other hand, the replica approach for hard-sphere calculates directly the ground state at ∞-PD (Parisi and Zamponi, 2010). Therefore, in such a case, the Edwards flat assumption is proved to be correct to describe the ground state of the hard-sphere glass. The pressing question is then whether Edwards ergodicity is extended to all other k-PD metastable states of hard-sphere glasses beyond the ground state.

Analogously, we wish to answer the same question for the k-SF metastable states in spin glasses. The mathematical treatment of such states is of extreme mathematical complexity. Thus, in what follows, we concentrate on answering the ergodic question on the 1SF. It might be said, though, that these 1PD/1SF states are extremely fragile since they only satisfy a local jamming condition. In the case of 1PD, they are also of little practical utility, i.e., in any realistic compaction experiment they will be completely avoided in favour of more stable states close to the ground state. In the case of 1SF, there is no real experimental system where they can be applied, anyway. Even if Edwards ergodicity might be proved wrong under 1SF/1PD, the question will remain whether the flat assumption might improve as we approach the ground state, where it is known to be exact (Parisi and Zamponi, 2010).

Putting aside these caveats, we are still interested to compare the form of $P(h)$ measured in the ending configurations of the 1SF dynamics with the one predicted by Edwards flat assumption, in particular for small values of the local fields $h \sim 0$. Assuming the scaling form:

$$P(h) \sim h^\alpha, \quad \text{for } h \to 0, \tag{181}$$

a lower bound on the exponent α can be derived by imposing the stability of 1SF metastable states with respect to single spin-flips. The argument goes as follows: consider two spins σ_i and σ_j, along with their local fields h_i and h_j and their coupling J_{ij}. The energy cost to flip one spin, say σ_i, is given by $\Delta E = 2|h_i| - 2J_{ij}\sigma_i\sigma_j$. The non trivial case is realized when the bond J_{ij} is satisfied, i.e. when $J_{ij}\sigma_i\sigma_j > 0$, so that we have $\Delta E = 2|h_i| - 2|J_{ij}|$. Since this condition must be satisfied even by the smallest possible field $h_i \sim N^{-1/(1+\alpha)}$, and since $|J_{ij}| \sim N^{-1/2}$, then the stability condition $\Delta E > 0$ of the 1SF metastable state gives $\alpha \geq 1$. Therefore, the distribution $P(h)$ must vanish at small fields like h^α with an exponent α not smaller than one. A direct dynamical measurement of $P(h)$ in the final configurations of a 1SF dynamics shows that $P(h)$ indeed vanishes linearly for $h \to 0$ (Eastham *et al.*, 2006):

$$P(h) \sim h, \quad \text{dynamics}, \tag{182}$$

i.e. the lower bound $\alpha \geq 1$ is actually saturated.

On the other side, what is the form of $P(h)$ calculated by using Edwards hypothesis on the equiprobability of all the available 1SF metastable states?

It turns out that in the SK model the exact calculation of $P(h)$ using Edwards ensemble can be carried out. At the present, the known analytical result for $P(h)$ is the Replica Symmetric (RS) solution (Roberts, 1981), which gives for $h \to 0$:

$$P(0) \propto \text{const} > 0, \quad \text{Edwards prediction at RS level.} \tag{183}$$

This is in contrast with the result of the dynamics, Eq. (182), which gives instead $P(0) = 0$ (Eastham *et al.*, 2006). Therefore, we should conclude that Edwards hypothesis is not valid for the SK model. However, there is a subtle inconsistency in the RS calculation of $P(h)$, and thus we cannot fully trust the RS analytical prediction of the intercept $P(0)$, Eq. (183). The inconsistency comes from the fact that the RS calculation is exact only above a certain energy density $e_c \sim -0.672...$ (Bray and Moore, 1980), and ceases to be valid below that energy. But the energy ϵ of the states selected by any 1SF dynamics we are aware of lies below the critical energy e_c ($\epsilon < e_c$), where the RS calculation of $P(h)$ is not correct. As a consequence, also the RS value of the intercept $P(0)$ is wrong, and thus the possibility that the right calculation under the Edwards flat assumption may give the dynamical result $P(0) = 0$ remains open.

The correct calculation of $P(h)$, for energies $e < e_c$, has to be done by taking into account the effect of Replica-Symmetry-Breaking (RSB), as in the low temperature phase of the equilibrium version of the model. This calculation has not been carried out yet (mainly because of its algebraic complexity), so we cannot draw yet definitive conclusions about the validity of Edwards flat assumption in the SK model.

Thus, we would like to propose to the jamming-glass community what could be the ultimate theoretical test of the Edwards flat assumption at the mean-field level for 1SF metastable states: the RSB calculation of the exponent α for the small-field limit of $P(h)$, Eq. (181), and its comparison with the dynamical result $\alpha = 1$ for the 1SF dynamics in the SK model. If such an heroical calculation would ever be done (heroically done because of its technical complexity), it will surely enter in the *Pantheon of Jamming* as one of the few explicit tests of Edwards ergodic assumption.

The plausible outcomes of this calculation may be the following: *i)* it is possible that the RSB effect would give only small perturbative corrections below e_c, so that the intercept of $P(0)$ may be non-zero even in the full-RSB solution; *ii)* conversely, it may be that the full-RSB effect is not small. For example, this is what happens in the model of frictionless hard-spheres in infinite dimension (Charbonneau *et al.*, 2014b). In this model, the analog of $P(h)$ is the distribution of inter-particle forces $P(f)$, Eq. (76). The model solution can be worked out by using the replica method, and it has a full-RSB structure akin to the one found in the SK model. Now, in the hard-spheres model, a RS calculation of $P(f)$ gives $P(0) > 0$, i.e., a finite intercept at zero force. Moreover, even the 1step-RSB solution (i.e. the solution accounting for just the first level in the hierarchical breaking of replica symmetry) gives $P(0) > 0$ as well, as discussed in Eq. (177). However, the full-RSB result is $P(f) \sim f^\theta$ with $\theta = 0.42...$, Eq. (178), and thus $P(0) = 0$. Therefore, in the light of the previous discussion, the full-RSB calculation of $P(h)$ in the SK model using Edwards ensemble would be a crucial result to resolve unequivocally the question on the validity of Edwards hypothesis in this model. All in all, it will always remain open the Edwards ergodic validity in the most critical case of three dimensions where real packings and humans live.

VI. CONCLUSIONS AND OUTLOOK

More than 25 years after Edwards original hypothesis on the entropy of granular matter, it becomes increasingly evident that the consequences of Edwards simple statement are far reaching. For one, it allows us to understand the properties of jammed granular matter — one of the paradigms of athermal matter states — by analogy with thermal equilibrium systems. The first-order transition of jammed spheres identified within Edwards' thermodynamics (Jin and Makse, 2010) is reminiscent of the entropy induced phase transition of equilibrium hard spheres, which is found at $\phi = 0.494$ and $\phi = 0.545$, respectively. Clearly, the physical origins of these two

transitions are fundamentally different: The equilibrium phase transition is a consequence of the maximization of the conventional entropy, while the transition at RCP of jammed spheres is driven by the competition between volume minimization and maximization of the entropy of jammed configurations, Eq. (8).

Such an analogy can probably be extended to other disorder-order phase transition observed in equilibrium systems. Anisotropic elongated particles, e.g., exhibit transitions between isotropic and nematic phases: For large α, Onsager's theory of equilibrium hard rods predicts a first order isotropic-nematic transition with freezing point at the rescaled density $\phi\alpha = 3.29$ and melting point at $\phi\alpha = 4.19$ (Onsager, 1949). By analogy with the case of jammed spheres, one might wonder whether packings of non-spherical particles exhibit similar transitions that could be characterized in the z–ϕ phase diagram. Packings of hard thin rods indeed satisfy a scaling law, where the RCP has been experimentally identified at $\phi\alpha \approx 5.4$ (Philipse, 1996).

For colloidal suspensions of more complex shapes like polyhedra, both liquid crystalline as well as plastic crystalline and even quasicrystalline phases have been found (Agarwal and Escobedo, 2011; Damasceno *et al.*, 2012; Haji-Akbari *et al.*, 2009; Marechal and Löwen, 2013). Entropic concepts based on shape are only starting to be explored even for equilibrium systems (van Anders *et al.*, 2014; Cohen *et al.*, 2016; Escobedo, 2014). In the jammed regime, the behaviour of packing density as a function of shape has been shown to be exceedingly complex (Chen *et al.*, 2014). Edwards granular entropy might be the key to understand such empirical data on a more fundamental level.

Our approach based on the self-consistent equation (165) can be applied to a large variety of both convex and non-convex shapes. The key is to parametrize the Voronoi boundary between two such shapes, which allows for the calculation of the Voronoi excluded volume and surface. In fact, analytical expressions for the Voronoi boundary can be derived following an exact algorithm for arbitrary shapes by decomposing the shape into overlapping and intersecting spheres (see Figs. 18,19). Therefore, a systematic search for maximally dense packings in the space of given object shapes can be performed using our framework. Extensions to mixtures and polydisperse packings can also be formulated. This might elucidate in particular the validity of Ulam's conjecture that the sphere is the worst packing object in 3d (Gardner, 2001), which has also been formulated in a random version (Jiao and Torquato, 2011) locally around the sphere shape (Kallus, 2016).

The Edwards' approach could help more generally to elucidate how macroscopic properties of granular matter arise from the anisotropy of the constituents – one of the central questions in present day materials science (Borzsonyi and Stannarius, 2013; Glotzer and Solomon, 2007). A better understanding of this problem will facilitate, e.g., the engineering of new functional materials with particular mechanical responses by tuning the shape of the building blocks (Jaeger, 2015) or to new ways to construct space filling tilings (Andrade *et al.*, 2005; Hermann *et al.*, 1990). Edwards statistical mechanics might be the key to tackle this problem based on theory rather than direct simulations.

We postulate that a unifying theoretical framework can predict not only the structural properties (volume fraction and coordination number), but also mechanical properties (vibrational density of states and yield stress) and dissipative properties (damping) as a function of the shape and interaction properties (e.g., friction) of the constitutive particles. If such an approach is possible, then one could envision to span the large parameter space of the problem from a theoretical point of view to obtain predictions of optimal packings with desired properties. The penalty for approaching the problem theoretically rather than by a direct numerical generation of the packings as in reverse engineering evolutionary techniques (Miskin and Jaeger, 2013) is that all results are only valid at the mean-field level. Thus, predictions of the resulting optimal shapes can only be approximate. On the other hand, it might be possible to develop a theory versatile enough to encompass a large portion of the parameter space which cannot be easily accessed by the direct simulation of packing protocols in reverse engineering. Such a theory might explore particles made of rigidly gluing spheres in arbitrary shapes, and also other generic shapes such as (a) union of spheres of arbitrary radius, (b) intersection of spheres of arbitrary radius leading to tetrahedral-like particles and in general (c) any irregular polyhedra. Another advantage is the ability to possibly span over more than one relevant property of granular materials, not only density but also yield stress and dissipation. Furthermore, such an approach would include interparticle friction, a property that was not considered before, yet, it is of crucial importance in granular packings.

On the more fundamental side of things, the controversy on the validity of Edwards statistical mechanics has been caused by different interpretations of Edwards' laconic statement (Edwards, 1994): *"We assume that when N grains occupy a volume V they do so in such a way that all configurations are equally weighted. We assume this; it is the analog of the ergodic hypothesis of conventional thermal physics."*

As regards the veracity of this statement, it is not rigorously established not disproved yet. However, one must not be fooled by believing that a statistical mechanics description of granular media is a least well-founded branch of theoretical physics, if only one remembers that almost every branch of theoretical physics is lacking 'rigorous proofs', although this is not considered as an inappropriate foundation for such branches. The main issue with

Edwards' statement, and the reason why it will be likely hard to reach an end to the diatribe, is that the statement, as it stands, is incomplete.

From a broad standpoint, the problem is whether it is possible to describe the properties of the asymptotic states of the dynamics by using only static features of the system. In Edwards' statement there is no reference at all to which are those asymptotic dynamic states. To solve this issue, we have proposed a rigorous definition of jammed states as those configurations satisfying the geometrical hard-core and mechanical force and torque balances constraints. Then we have further classified those jammed states on the basis of their stability properties under k-Particle-Displacements, inspired by an analogous characterization of (energetically) metastable states in spin glasses through the concept of k-Spin-Flips. With this definition of the asymptotic dynamic states, we redefined (in italics) Edwards' ensemble by the following proposition: "We assume that when N grains occupy a volume V they do so in such a way that all stable jammed configurations *in a given kPD jamming category* are equally weighted. We assume this; it is the analogue of the ergodic hypothesis of conventional thermal physics (*and also out-of-equilibrium spin glasses and hard-sphere glasses*)."

This statement also clarifies the role of the protocol, i.e. of the dynamics, in the Edwards' ensemble. A "legal" protocol is the one for which the asymptotic dynamic states are in a given kPD class, with a unique value of k. This is, again, motivated by a spin-glass analogy. In this case an example of correct protocol is, for instance, a single-spin-flip Glauber dynamics, for which the asymptotic dynamic states are only the 1SF metastable states, which all have the same energy. In the granular framework this is equivalent to say that the asymptotic jammed states of a legal protocol are only the kPD metastable states (with a fixed k, for instance the 1PD), and they (presumably) have the same volume. Then the question of whether these states are statistically equivalent (i.e. equiprobable) remains still open, and we have suggested a model (SK) where an end-to-end comparison between the results of dynamics and a static computation can be performed, in principle, in an exact analytical way.

An "illegal" protocol is one that mixes different kPD metastable states, i.e., whose asymptotic dynamic states have different values of k, and hence different stability properties. Nothing can be claimed for such illegal protocols. In the case of legal protocols, it has been rigorously proved in spin glasses that statistical equivalence of the asymptotic dynamic states of the given protocol holds true, i.e., the kSP visited by a given dynamics are indeed equiprobable (Newman and Stein, 1999). Whether this statement is also rigorous for jammed states is an open question, but the correctness in spin glasses points towards an affirmative answer. The stronger claim that the asymptotic dynamic states are also the totality of kPD (kSF) metastable states with given volume fraction (energy density) is not analytically proved or disproved for any model we are aware of.

Bearing in mind the previous caveats about the correct Edwards' ensemble and the corresponding flat assumption, we finally discuss the important problem of how to prepare a granular system adequate for properly testing Edwards' statistics.

The granular system explores the configurational landscape by the external tapping introduced by the experimentalist. During tapping, after each tap, the grains relax in a different final kPD configuration, generally with a different value of k. According to the previous discussion, in this general tapping experiment, it is not clear whether the Edwards' measure is valid or not, because the assumptions at the basis of Edwards' ensemble (i.e. fixed V and fixed k) are violated from the very beginning of the experiment. Indeed, for a protocol that widely mixes many kPD configurations, the analogy with spin glasses does not suggest that the resulting states have any chance to be equiprobable (also it is not even clear whether a smooth invariant measure does exist at all). Likewise, the numerical results of (Gao *et al.*, 2006) should be probably re-analyzed under this novel viewpoint as well.

Therefore, to test Edwards' measure in an appropriate experimental setup, the motions of grains must be well-controlled, since the configurations available to the system depend upon the amount of energy/power put into the system. By well-controlled we mean that the tapping must be gentle, ideally infinitesimally small, as discussed in (Edwards *et al.*, 2004). In this regime, the tapping causes small changes in the contact network, according to the strength of the tap. A particle will move or not depending on the magnitude of the forces exerted by the surrounding particles in mechanical equilibrium and its confinement in the container. More precisely, the criterion of whether a particular grain in the system will move in response to the perturbation will be the Coulomb condition of a threshold force, above which sliding of contacts can occur and below which there can be no changes.

Roughly speaking we can say that a rearrangement will occur between those grains in the system whose configuration and neighbours produce a force which is overcome by the external disturbance. This threshold force necessary to move the particles is different for different grains. If the tapping is small, this implies that there are regions in the sample in which the contact network changes and other regions which are unperturbed. The picture at any moment in time will contain pockets of particles in motion encircled by static ones. Each of these pockets has a perimeter, defined by the immobile grains. The present derivation assumes the existence of these regions. It is equivalent to the assumption of a dilute gas in the classical Boltzmann equation (Edwards *et al.*, 2004).

The crucial point is that the energy input must be on the level of noise, and thus the tapping must be relatively gentle, such that the grains largely remain in contact with one another, but are able to explore the energy landscape over a long period of time. In the case of external vibrations, the appropriate frequency and amplitude can be determined experimentally for different grain types, by investigating the motion of the individual grains or by monitoring the changes in the overall volume fraction over time. For example, it is important that the amplitude of the tapping does not exceed the gravitational force, or else the grains are free to fly up in the air, re-introducing the problem of initial creation just as they would if they were simply poured into another container. Thus, if the same small amount of energy is put in the system at each tap, it is reasonable to expect that this protocol is the closest possible one to a k-particle-displacement dynamics which explores the kPD jammed states approximatively with the same k with equal probability (Edwards *et al.*, 2004).

Conversely, in the strong tapping regime, the statistical equivalence of the asymptotic dynamic states cannot be claimed. Notwithstanding, this does not preclude the use of Edwards' ensemble as a very principled approximation supposedly more justified than other mean-field approaches. *A fortiori*, the great advantage of Edwards' approach is that it leads to concrete quantitative predictions for realistic packing scenarios. As we discuss in detail in Sec. IV, the volume ensemble in the Voronoi convention allows us to treat packings of frictional and frictionless particles, adhesive and non-adhesive, granular and colloidal sizes, mono-disperse and poly-disperse, in 2d, 3d and beyond, as well as spherical and non-spherical shapes within a unified framework. Such a comprehensive treatment is currently out of reach for any other approach that can treat glassy and/or jammed systems analytically, such as mode-coupling theory (Götze, 2009) or replica theory (Parisi and Zamponi, 2010). Moreover, the analytical efforts needed to extend these theories to incorporate, for instance, friction or anisotropies are unsurmountable. The verdict on Edwards' Alexandrian solution to this Gordian Knot, as on every physical theory, should be returned, ultimately, on the goodness of its predictions when compared with experimental data and practical applications.

ACKNOWLEDGMENTS

AB acknowledges funding under EPSRC grant EP/L020955/1. FM and HAM acknowledge funding from NSF (Grant No. DMR-1308235) and DOE Geosciences Division (Grant No. DE-FG02-03ER15458). We are grateful to the following scientists whom, over the years, have shaped our vision of the granular problem: J. S. Andrade Jr., L. Bo, T. Boutreux, J. Brujić, S. F. Edwards, P.-G. de Gennes, N. Gland, S. Havlin, J. T. Jenkins, Y. Jin, D. L. Johnson, J. Kurchan, S. Li, G. Parisi, R. Mari, L. La Ragione, M. Shattuck, C. Song, H. E. Stanley, M. S. Tomassone, J. J. Valenza, K. Wang, and P. Wang. We are grateful for comments on the review by: R. Blumenfeld, J.-P. Bouchaud, B. Chakraborty, P. Charbonneau, G. Gradenigo, M. Moore, C. O'Hern, G. Parisi, M. Saadatfar, M. Shattuck, M. Sperl, M. Wyart, A. Zaccone, and F. Zamponi. We also thank T. Aste, B. Behringer, R. Blumenfeld, and S. Nagel for the permission to use their images.

REFERENCES

Abreu, C., F. Tavares, and M. Castier (2003), Powder Technol. **134**, 167.
Agarwal, U., and F. A. Escobedo (2011), Nature Mater. **10**, 230.
Alexander, S. (1998), Phys. Rep. **296**, 65 .
Alonso-Marroquín, F., and H. J. Herrmann (2004), Phys. Rev. Lett. **92**, 054301.
van Anders, G., D. Klotsa, N. K. Ahmed, M. Engel, and S. C. Glotzer (2014), Proc. Nat. Acad. Sci. **111**, E4812.
Andrade, J. S., H. J. Herrmann, R. F. S. Andrade, and L. R. da Silva (2005), Phys. Rev. Lett. **94**, 018702.
Anikeenko, A. V., and N. N. Medvedev (2007), Phys. Rev. Lett. **98**, 235504.
Anikeenko, A. V., N. N. Medvedev, and T. Aste (2008), Phys. Rev. E **77**, 031101.
Arevalo, R., L. A. Pugnaloni, I. Zuriguel, and D. Maza (2013), Phys. Rev. E **87**, 022203.
Aristoff, D., and C. Radin (2009), J. Stat. Phys. **135**, 1.
Asenjo, D., F. Paillusson, and D. Frenkel (2014), Phys. Rev. Lett. **112**, 098002.
Aste, T. (2005), J. Phys. Cond. Mat. **17**, S2361.
Aste, T. (2006), Phys. Rev. Lett. **96**, 018002.
Aste, T., and A. Coniglio (2004), Europhys. Lett. **67**, 165.
Aste, T., and T. Di Matteo (2008), Phys. Rev. E **77**, 021309.
Aste, T., T. Di Matteo, M. Saadatfar, T. J. Senden, M. Schröter, and H. L. Swinney (2007), Europhys. Lett. **79**, 24003.
Aste, T., M. Saadatfar, A. Sakellariou, and T. Senden (2004), "Investigating the geometrical structure of disordered sphere packings," in *Proceedings of the International Conference New Materials and Complexity*, Vol. 339, pp. 16 – 23.
Aste, T., M. Saadatfar, and T. Senden (2005), Phys. Rev. E **71**, 061302.
Aste, T., M. Saadatfar, and T. J. Senden (2006), J. Stat. Mech. , P07010.
Athanassiadis, A. G., M. Z. Miskin, P. Kaplan, N. Rodenberg, S. H. Lee, J. Merritt, E. Brown, J. Amend, H. Lipson, and H. M. Jaeger (2014), Soft Matter **10**, 48.
Atkinson, S., F. H. Stillinger, and S. Torquato (2014), Proc. Nat. Acad. Sci. **111**, 18436.
Aurenhammer, F. (1991), ACM Computing Surveys **23**, 345.
Bagi, K. (1997), "Analysis of micro-variables through entropy principles," in *Powders and Grains 97*, edited by R. P. Behringer and J. T. Jenkins, pp. 251–254.
Bagi, K. (2003), Granular Matter **5**, 45.

Ball, R., and R. Blumenfeld (2002), Phys. Rev. Lett. **88**, 115505.

Baranau, V., S.-C. Zhao, M. Scheel, U. Tallarek, and M. Schröter (2016), Soft Matter **12**, 3991.

Bargiel, M. (2008), Computational Science–ICCS2008 **5102**, 126.

Barrat, A., J. Kurchan, V. Loreto, and M. Sellitto (2000), Phys. Rev. Lett. **85**, 5034.

Baule, A., and H. A. Makse (2014), Soft Matter **10**, 4423.

Baule, A., R. Mari, L. Bo, L. Portal, and H. A. Makse (2013), Nature Commun. **4**, 2194.

Bellon, L., and S. Ciliberto (2002), Physica D **168–169**, 325 .

Berg, J., S. Franz, and M. Sellitto (2002), Eur. Phys. J. B **26**, 349.

Bernal, J. D. (1960), Nature **185**, 68.

Bernal, J. D. (1964), Proc. Roy. Soc. London Ser. A **280**, 299.

Bernal, J. D., and J. Mason (1960), Nature **188**, 910.

Berryman, J. G. (1983), Phys. Rev. A **27**, 1053.

Berthier, L., J.-L. Barrat, and J. Kurchan (2000), Phys. Rev. E **61**, 5464.

Bi, D., S. Henkes, K. E. Daniels, and B. Chakraborty (2015), Annual Review of Condensed Matter Physics **6**, 63.

Biazzo, I., F. Caltagirone, G. Parisi, and F. Zamponi (2009), Phys. Rev. Lett. **102**, 195701.

Blum, J., R. Schräpler, B. J. R. Davidsson, and J. M. Trigo-Rodríguez (2006), The Astrophysical Journal **652**, 1768.

Blumenfeld, R., S. Amitai, J. F. Jordan, and R. Hihinashvili (2016), Phys. Rev. Lett. **116**, 148001.

Blumenfeld, R., and S. Edwards (2003), Phys. Rev. Lett. **90**, 10.1103/PhysRevLett.90.114303.

Blumenfeld, R., and S. Edwards (2006), Eur. Phys. J. E **19**, 23.

Blumenfeld, R., and S. F. Edwards (2009), J. Phys. Chem. B **113**, 3981.

Blumenfeld, R., J. F. Jordan, and S. F. Edwards (2012), Phys. Rev. Lett. **109**, 238001.

Bo, L., R. Mari, C. Song, and H. A. Makse (2014), Soft Matter **10**, 7379.

Boissonat, J. D., C. Wormser, and M. Yvinec (2006), in *Effective Computational Geometry for Curves and Surfaces*, Mathematics and Visualization, edited by J. D. Boissonnat and M. Teillaud (Springer) p. 67.

Borzsonyi, T., and R. Stannarius (2013), Soft Matter **9**, 7401.

Bouchaud, J.-P. (2002), "Granular media: Some ideas from statistical physics," in *Slow Relaxations and Nonequilibrium Dynamics in Condensed Matter*, Les Houches Lecture Notes, Vol. 77, edited by J.-L. Barrat, M. Feigelman, J. Kurchan, and J. Dalibard, Chap. 4 (Springer-Verlag) pp. 131–197.

Bowles, R. K., and S. S. Ashwin (2011), Phys. Rev. E **83**, 031302.

Bray, A. J., and M. A. Moore (1980), Journal of Physics C: Solid State Physics **13** (19), L469.

Brey, J., A. Prados, and B. Sanchez-Rey (2000), Physica A **275**, 310 .

Briscoe, C., C. Song, P. Wang, and H. A. Makse (2008), Phys. Rev. Lett. **101**, 188001.

Briscoe, C., C. Song, P. Wang, and H. A. Makse (2010), Physica A **389**, 3978.

Brouwers, H. J. H. (2006), Phys. Rev. E **74**, 031309.

Brujić, J., S. Edwards, D. Grinev, I. Hopkinson, D. Brujić, and H. Makse (2003a), Farad. Disc. **123**, 207.

Brujić, J., S. Edwards, I. Hopkinson, and H. Makse (2003b), Physica A **327**, 201.

Brujić, J., C. Song, P. Wang, C. Briscoe, G. Marty, and H. A. Makse (2007), Phys. Rev. Lett. **98**, 248001.

Brujić, J., P. Wang, C. Song, D. L. Johnson, O. Sindt, and H. A. Makse (2005), Phys. Rev. Lett. **95**, 128001.

Caglioti, E., V. Loreto, H. Herrmann, and M. Nicodemi (1997), Phys. Rev. Lett. **79**, 1575.

Camia, F. (2005), Eur. Phys. J. B **47**, 239.

Cates, M., J. Wittmer, J. Bouchaud, and P. Claudin (1998), Phys. Rev. Lett. **81**, 1841.

Cavagna, A. (2009), Physics Reports **476**, 51.

Chaikin, P. M., A. Donev, W. Man, F. H. Stillinger, and S. Torquato (2006), Ind. Eng. Chem. Res. **45**, 6960.

Chakraborty, B. (2010), Soft Matter **6**, 2884.

Chakravarty, A., S. Edwards, D. Grinev, M. Mann, T. Phillipson, and A. Walton (2003), in *Proceedings of the Workshop on the Quasi-static Deformations of Particulate Materials*.

Charbonneau, P., E. I. Corwin, G. Parisi, A. Poncet, and F. Zamponi (2015a), ArXiv e-prints arXiv:1512.09100 [cond-mat.dis-nn].

Charbonneau, P., E. I. Corwin, G. Parisi, and F. Zamponi (2012), Phys. Rev. Lett. **109**, 205501.

Charbonneau, P., E. I. Corwin, G. Parisi, and F. Zamponi (2015b), Phys. Rev. Lett. **114**, 125504.

Charbonneau, P., J. Kurchan, G. Parisi, P. Urbani, and F. Zamponi (2014a), J. Stat. Mech. **2014**, P10009.

Charbonneau, P., J. Kurchan, G. Parisi, P. Urbani, and F. Zamponi (2014b), Nature Commun. **5**.

Chaudhuri, P., L. Berthier, and S. Sastry (2010), Phys. Rev. Lett. **104**, 165701.

Chen, E. R., D. Klotsa, M. Engel, P. F. Damasceno, and S. C. Glotzer (2014), Phys. Rev. X **4**, 011024.

Ciamarra, M. P. (2007), Phys. Rev. Lett. **99**, 089401.

Ciamarra, M. P., and A. Coniglio (2008), Phys. Rev. Lett. **101**, 10.1103/PhysRevLett.101.128001.

Ciamarra, M. P., A. Coniglio, and A. de Candia (2010), Soft Matter **6**, 2975.

Ciamarra, M. P., A. Coniglio, and M. Nicodemi (2006), Phys. Rev. Lett. **97**, 158001.

Ciesla, M., G. Pajak, and R. M. Ziff (2015), Phys. Chem. Chem. Phys. **17**, 24376.

Cinacchi, G., and S. Torquato (2015), The Journal of Chemical Physics **143**, 224506.

Clarke, A. S., and H. Jónsson (1993), Phys. Rev. E **47**, 3975.

Clusel, M., E. I. Corwin, A. O. N. Siemens, and J. Brujić (2009), Nature **460**, 611.

Cohen, A. P., S. Dorosz, A. B. Schofield, T. Schilling, and E. Sloutskin (2016), Phys. Rev. Lett. **116**, 098001.

Coniglio, A., A. de Candia, A. Fierro, M. Nicodemi, and M. Tarzia (2004), Physica A **344**, 431.

Coniglio, A., A. Fierro, and M. Nicodemi (2002), Eur. Phys. J. E **9**, 219.

Coniglio, A., and H. Herrmann (1996), Physica A **225**, 1 .

Coniglio, A., and M. Nicodemi (2000), J. Phys. Cond. Mat. **12**, 6601.

Coniglio, A., and M. Nicodemi (2001), Physica A **296**, 451.

Conway, J., and N. J. A. Sloane (1999), *Sphere packings, Lattices and Groups*, 3rd ed., A series of comprehensive mathematics, Vol. 290 (Springer, New York).

Corwin, E., H. Jaeger, and S. Nagel (2005), Nature **435**, 1075.

Corwin, E. I., M. Clusel, A. O. N. Siemens, and J. Brujić (2010), Soft Matter **6**, 2949.

Cremona, L. (1890), *Graphical statics: two treatises on the*

graphical calculus and reciprocal figures in graphical statics (Clarendon Press).
Crisanti, A., and F. Ritort (2003), J. Phys. A **36**, R181.
Cugliandolo, L. F. (2011), J. Phys. A **44**, 483001.
Cugliandolo, L. F., J. Kurchan, and L. Peliti (1997), Phys. Rev. E **55**, 3898.
Damasceno, P. F., M. Engel, and S. C. Glotzer (2012), Science **337**, 453.
Danisch, M., Y. Jin, and H. A. Makse (2010), Phys. Rev. E **81**, 051303.
Dauchot, O. (2007), "Glassy behaviours in a-thermal systems, the case of granular media: A tentative review," in *Ageing and the Glass Transition*, Lecture Notes in Physics, Vol. 716, edited by M. Henkel, M. Pleimling, and R. Sanctuary (Springer) pp. 161–206.
Dean, D. S., and A. Lefèvre (2001), Phys. Rev. Lett. **86**, 5639.
DeGiuli, E., E. Lerner, C. Brito, and M. Wyart (2014), Proc. Nat. Acad. Sci. **111**, 17054.
Delaney, G. W., and P. W. Cleary (2010), EPL **89**, 34002.
Delaney, G. W., T. Di Matteo, and T. Aste (2010), Soft Matter **6**, 2992.
Delaney, G. W., D. Weaire, S. Hutzler, and S. Murphy (2005), Philos. Mag. Lett. **85**, 89.
Desmond, K. W., and E. R. Weeks (2014), Phys. Rev. E **90**, 022204.
Dieterich, E., J. Camunas-Soler, M. Ribezzi-Crivellari, U. Seifert, and F. Ritort (2015), Nature Phys. **11**, 971.
Digby, P. J. (1981), Journal of Applied Mechanics **48**, 803.
Donev, A., I. Cisse, D. Sachs, E. Variano, F. Stillinger, R. Connelly, S. Torquato, and P. Chaikin (2004), Science **303**, 990.
Donev, A., R. Connelly, F. H. Stillinger, and S. Torquato (2007), Phys. Rev. E **75**, 051304.
Donev, A., F. H. Stillinger, and S. Torquato (2005a), Phys. Rev. Lett. **95**, 090604.
Donev, A., S. Torquato, and F. Stillinger (2005b), Phys. Rev. E **71**, 011105.
Drocco, J. A., M. B. Hastings, C. J. O. Reichhardt, and C. Reichhardt (2005), Phys. Rev. Lett. **95**, 088001.
Eastham, P. R., R. A. Blythe, A. J. Bray, and M. A. Moore (2006), Phys. Rev. B **74**, 020406.
Edwards, S., and D. Grinev (1999a), Phys. Rev. Lett. **82**, 5397.
Edwards, S., and D. Grinev (2001a), Chem. Eng. Sci. **56**, 5451 .
Edwards, S., and R. Oakeshott (1989), Physica A **157**, 1080.
Edwards, S. F. (1991), "The aging of glass forming liquids," in *Disorder in Condensed Matter Physics*, edited by J. Blackman and J. Taguena (Oxford University Press, Oxford) pp. 147–154.
Edwards, S. F. (1994), "The role of entropy in the specification of a powder," in *Granular matter: an interdisciplinary approach*, edited by A. Mehta (Springer, New York) pp. 121–140.
Edwards, S. F. (2008), J. Phys. A **41**, 324019.
Edwards, S. F., J. Brujić, and H. A. Makse (2004), "A basis for the statistical mechanics of granular systems," in *Unifying Concepts in Granular Media and Glasses*, edited by A. Coniglio, A. Fierro, H. Herrmann, and M. Nicodemi (Elsevier Science BV) pp. 9–23.
Edwards, S. F., and D. Grinev (2001b), Physica A **302**, 162 .
Edwards, S. F., and D. V. Grinev (1999b), Chaos **9**, 551.
van Eerd, A. R. T., W. G. Ellenbroek, M. van Hecke, J. H. Snoeijer, and T. J. H. Vlugt (2007), Phys. Rev. E **75**, 060302.
Ellenbroek, W. G., M. van Hecke, and W. van Saarloos (2009), Phys. Rev. E **80**, 061307.
Ellenbroek, W. G., E. Somfai, M. van Hecke, and W. van Saarloos (2006), Phys. Rev. Lett. **97**, 258001.
Erikson, J. M., N. W. Mueggenburg, H. M. Jaeger, and S. R. Nagel (2002), Phys. Rev. E **66**, 040301.
Escobedo, F. A. (2014), Soft Matter **10**, 8388.
Farrell, G. R., K. M. Martini, and N. Menon (2010), Soft Matter **6**, 2925.
Faure, S., A. Lefebvre-Lepot, and B. Semin (2009), "Dynamic numerical investigation of random packing for spherical and nonconvex particles," in *ESAIM: Proceedings*, Vol. 28, edited by M. Ismail, B. Maury, and J.-F. Gerbeau, pp. 13–32.
Fierro, A., M. Nicodemi, and A. Coniglio (2002a), Europhys. Lett. **59**, 642.
Fierro, A., M. Nicodemi, and A. Coniglio (2002b), Phys. Rev. E **66**, 061301.
Fierro, A., M. Nicodemi, and A. Coniglio (2003), J. Phys. Cond. Mat. **15**, S1095.
Finney, J. L. (1970), Proc. Roy. Soc. London A **319**, 479.
Francois, N., M. Saadatfar, R. Cruikshank, and A. Sheppard (2013), Phys. Rev. Lett. **111**, 148001.
Franz, S., and G. Parisi (2016), J. Phys. A of Physics A: Mathematical and Theoretical **49**, 145001.
Franz, S., G. Parisi, P. Urbani, and F. Zamponi (2015), Proc. Nat. Acad. Sci. **112**, 14539.
Frenkel, G., R. Blumenfeld, Z. Grof, and P. R. King (2008), Phys. Rev. E **77**, 10.1103/PhysRevE.77.041304.
Gago, P. A., D. Maza, and L. A. Pugnaloni (2016), Papers in Physics **8**, 080001.
Gantapara, A. P., J. de Graaf, R. van Roij, and M. Dijkstra (2013), Phys. Rev. Lett. **111**, 015501.
Gao, G.-J., J. Blawzdziewicz, and C. S. O'Hern (2006), Phys. Rev. E **74**, 061304.
Gao, G.-J., J. Blawzdziewicz, C. S. O'Hern, and M. Shattuck (2009), Phys. Rev. E **80**, 061304.
Gardner, M. (2001), *The Colossal Book of Mathematics: Classic Puzzles, Paradoxes, and Problems* (Norton).
Gendelman, O., Y. G. Pollack, I. Procaccia, S. Sengupta, and J. Zylberg (2016), Phys. Rev. Lett. **116**, 078001.
Glotzer, S. C., and M. J. Solomon (2007), Nature Mater. **6**, 557.
Goddard, J. (2004), Int. J. Solids Struct. **41**, 5851 .
Godrèche, C., and J. M. Luck (2005), J. Phys. Cond. Mat. **17**, S2573.
Goldbart, P. M., N. Goldenfeld, and D. Sherrington (2005), *Stealing the gold: A celebration of the pioneering physics of Sam Edwards*.
Götze, W. (2009), *Complex Dynamics of Glass-Forming Liquids: A Mode-Coupling Theory* (Oxford University Press).
Gradenigo, G., E. E. Ferrero, E. Bertin, and J.-L. Barrat (2015), Phys. Rev. Lett. **115**, 140601.
Haji-Akbari, A., M. Engel, A. S. Keys, X. Zheng, R. G. Petschek, P. Palffy-Muhoray, and S. C. Glotzer (2009), Nature **462**, 773.
Hales, T. C. (2005), Ann. Math. **162**, 1065.
Hanifpour, M., N. Francois, V. Robins, A. Kingston, S. M. Vaez Allaei, and M. Saadatfar (2015), Phys. Rev. E **91**, 062202.
Hanifpour, M., N. Francois, S. M. Vaez Allaei, T. Senden,

and M. Saadatfar (2014), Phys. Rev. Lett. **113**, 148001.
van Hecke, M. (2010), J. Phys. Cond. Mat. **22**, 033101.
Henkes, S., and B. Chakraborty (2005), Phys. Rev. Lett. **95**, 198002.
Henkes, S., and B. Chakraborty (2009), Phys. Rev. E **79**, 061301.
Henkes, S., M. van Hecke, and W. van Saarloos (2010), Europhys. Lett. **90**, 14003.
Henkes, S., C. S. O'Hern, and B. Chakraborty (2007), Phys. Rev. Lett. **99**, 038002.
Hermes, M., and M. Dijkstra (2010), EPL **89**, 38005.
Herrmann, H. J. (1993), Physica A **191**, 263.
Herrmann, H. J., G. Mantica, and D. Bessis (1990), Phys. Rev. Lett. **65**, 3223.
Hiwatari, Y., T. Saito, and A. Ueda (1984), J. Chem. Phys. **81**, 6044.
Hsu, C.-J., D. L. Johnson, R. A. Ingale, J. J. Valenza, N. Gland, and H. A. Makse (2009), Phys. Rev. Lett. **102**, 058001.
Hu, Y., D. L. Johnson, J. J. Valenza, F. Santibanez, and H. A. Makse (2014a), Phys. Rev. E **89**.
Hu, Y., H. A. Makse, J. J. Valenza, and D. L. Johnson (2014b), Geophysics **79**, L41.
Huang, K. (1987), *Statistical Mechanics* (Wiley).
Ikeda, A., L. Berthier, and P. Sollich (2012), Phys. Rev. Lett. **109**, 018301.
Ikeda, A., and K. Miyazaki (2010), Phys. Rev. Lett. **104**, 255704.
Jaeger, H. M. (2015), Soft Matter **11**, 12.
Jaeger, H. M., S. R. Nagel, and R. P. Behringer (1996), Rev. Mod. Phys. **68**, 1259.
Jaoshvili, A., A. Esakia, M. Porrati, and P. M. Chaikin (2010), Phys. Rev. Lett. **104**, 185501.
Jaynes, E. T. (1957a), Phys. Rev. **106**, 620.
Jaynes, E. T. (1957b), Phys. Rev. **108**, 171.
Jenkins, J., D. Johnson, L. L. Ragione, and H. Makse (2005), J. Mech. Phys. Solids **53**, 197 .
Jia, X., G. M., R. A. Williams, and D. Rhodes (2007), Powder Technol. **174**, 10.
Jiao, Y., F. H. Stillinger, and S. Torquato (2010), Phys. Rev. E **81**, 041304.
Jiao, Y., and S. Torquato (2011), Phys. Rev. E **84**, 041309.
Jin, Y., P. Charbonneau, S. Meyer, C. Song, and F. Zamponi (2010), Phys. Rev. E **82**.
Jin, Y., and H. A. Makse (2010), Physica A **389**, 5362.
Jin, Y., J. G. Puckett, and H. A. Makse (2014), Phys. Rev. E **89**, 052207.
Johnson, D. L., Y. Hu, and H. Makse (2015), Phys. Rev. E **91**, 062208.
Johnson, K. L. (1985), *Contact Mechanics* (Cambrdige University Press).
Jorjadze, I., L.-L. Pontani, K. A. Newhall, and J. Brujić (2011), Proc. Nat. Acad. Sci. **108**, 4286.
Kadanoff, L. P. (1999), Rev. Mod. Phys. **71**, 435.
Kadau, D., and H. J. Herrmann (2011), Phys. Rev. E **83**, 031301.
Kallus, Y. (2016), Soft Matter **12**, 4123.
Kallus, Y., and V. Elser (2011), Phys. Rev. E **83**, 036703.
Kamien, R. D., and A. J. Liu (2007), Phys. Rev. Lett. **99**, 155501.
Kapfer, S. C., W. Mickel, K. Mecke, and G. E. Schröder-Turk (2012), Phys. Rev. E **85**, 030301.
Kasahara, A., and H. Nakanishi (2004), Phys. Rev. E **70**, 051309.
Kepler, J. (1611), *Strena seu de nive sexangula (The six-cornered snowflake)* (http://www.thelatinlibrary.com/kepler/strena.html).
Kirkpatrick, S., and B. Selman (1994), Science **264**, 1297.
Kirkpatrick, T. R., and P. G. Wolynes (1987), Phys. Rev. A **35**, 3072.
Kirkwood, J. G. (1935), J. Chem. Phys. **3**, 300.
Klumov, B. A., Y. Jin, and H. A. Makse (2014), The J. Phys. Chem. B **118**, 10761.
Klumov, B. A., S. A. Khrapak, and G. E. Morfill (2011), Phys. Rev. B **83**, 184105.
Knight, J. B., C. G. Fandrich, C. N. Lau, H. M. Jaeger, and S. R. Nagel (1995), Phys. Rev. E **51**, 3957.
Krapivsky, P. L., and E. BenNaim (1994), The Journal of Chemical Physics **100**, 6778.
Kruyt, N., and L. Rothenburg (2002), Int. J. Solids. Struct. **39**, 571.
Krzakala, F., and J. Kurchan (2007), Phys. Rev. E **76**, 021122.
Kurchan, J. (2000), Journal of Physics: Condensed Matter **12**, 6611.
Kurchan, J. (2001), "Rheology and how to stop aging," in *Jamming and Rheology: Constrained Dynamics on Microscopic and Macroscopic Scales*, edited by A. Liu and S. R. Nagel (Taylor & Francis, London).
Kyrylyuk, A. V., M. A. van de Haar, L. Rossi, A. Wouterse, and A. P. Philipse (2011), Soft Matter **7**, 1671.
Landau, L. D., and E. M. Lifshitz (1980), *Statistical Physics* (Butterworth-Heinemann).
Landau, L. D., L. P. Pitaevskii, A. M. Kosevich, and E. M. Lifshitz (1986), *Theory of Elasticity* (Butterworth-Heinemann).
de Larrard, F. (1999), "Concrete mixture proportioning: A scientific approach," (CRC Press).
Lechenault, F., F. da Cruz, O. Dauchot, and E. Bertin (2006), J. Stat. Mech. , P07009.
Lefevre, A. (2002), J. Phys. A **35**, 9037.
Lefèvre, A., and D. S. Dean (2002), Phys. Rev. B **65**, 220403.
Lerner, E., E. DeGiuli, G. During, and M. Wyart (2014), Soft Matter **10**, 5085.
Lerner, E., G. During, and M. Wyart (2013), Soft Matter **9**, 8252.
Leuzzi, L. (2009), J. Non-Crystall. Solids **355**, 686 .
Li, S.-Q., and J. Marshall (2007), J. Aeros. Sci. **38**, 1031 .
Lieou, C. K. C., and J. S. Langer (2012), Phys. Rev. E **85**, 061308.
Liu, A. J., and S. R. Nagel (2010), Annu. Rev. Cond. Matt. Phys. **1**, 347.
Liu, C. h., S. R. Nagel, D. A. Schecter, S. N. Coppersmith, S. Majumdar, O. Narayan, and T. A. Witten (1995), Science **269**, 513.
Liu, W., S. Li, A. Baule, and H. A. Makse (2015), Soft Matter **11**, 6492.
Loi, D., S. Mossa, and L. F. Cugliandolo (2008), Phys. Rev. E **77**, 051111.
Lois, G., J. Blawzdziewicz, and C. S. O'Hern (2008), Phys. Rev. Lett. **100**, 028001.
Løvoll, G., K. J. Måløy, and E. G. Flekkøy (1999), Phys. Rev. E **60**, 5872.
Lu, K., E. E. Brodsky, and H. P. Kavehpour (2008a), Nature Phys. **4**, 404.
Lu, P., S. Li, J. Zhao, and L. Meng (2010), Science China **53**, 2284.
Lu, P. J., E. Zaccarelli, F. Ciulla, A. B. Schofield, F. Sciortino,

and D. A. Weitz (2008b), Nature **453**, 499.
Lubachevsky, B. D., and F. H. Stillinger (1990), J. Stat. Phys. **60**, 561.
Luchnikov, V. A., N. N. Medvedev, L. Oger, and J.-P. Troadec (1999), Phys. Rev. E **59**, 7205.
Luck, M. J., and A. Mehta (2007), Europ. Phys. J. B **57**, 429.
Magnanimo, V., L. L. Ragione, J. T. Jenkins, P. Wang, and H. A. Makse (2008), EPL **81**, 34006.
Mailman, M., and B. Chakraborty (2011), J. Stat. Mech. **2011**, L07002.
Mailman, M., and B. Chakraborty (2012), J. Stat. Mech. **2012**, P05001.
Majmudar, T. S., and R. P. Behringer (2005), Nature **435**, 1079.
Majmudar, T. S., M. Sperl, S. Luding, and R. P. Behringer (2007), Phys. Rev. Lett. **98**, 10.1103/PhysRevLett.98.058001.
Makse, H., and J. Kurchan (2002), Nature **415**, 614.
Makse, H. A., J. Brujić, and S. F. Edwards (2005), "Statistical mechanics of jammed matter," in *The Physics of Granular Media*, edited by H. Hinrichsen and D. E. Wolf (Wiley-VCH).
Makse, H. A., N. Gland, D. L. Johnson, and L. Schwartz (2004), Phys. Rev. E **70**, 061302.
Makse, H. A., N. Gland, D. L. Johnson, and L. M. Schwartz (1999), Phys. Rev. Lett. **83**, 5070.
Makse, H. A., D. L. Johnson, and L. M. Schwartz (2000), Phys. Rev. Lett. **84**, 4160.
Man, W., A. Donev, F. H. Stillinger, M. T. Sullivan, W. B. Russel, D. Heeger, S. Inati, S. Torquato, and P. M. Chaikin (2005), Phys. Rev. Lett. **94**, 198001.
Marconi, U. M. B., A. Puglisi, L. Rondoni, and A. Vulpiani (2008), Phys. Rep. **461**, 111 .
Marechal, M., and H. Löwen (2013), Phys. Rev. Lett. **110**, 137801.
Mari, R., F. Krzakala, and J. Kurchan (2009), Phys. Rev. Lett. **103**, 025701.
Marshall, J. S., and S. Li (2014), *Adhesive Particle Flow* (Cambridge University Press).
Martin, C. L., and R. K. Bordia (2008), Phys. Rev. E **77**, 031307.
Matsushima, T., and R. Blumenfeld (2014), Phys. Rev. Lett. **112**, 098003.
Maxwell, J. C. (1864), Philosophical Magazine **26**, 250.
Maxwell, J. C. (1870), Transactions of the Royal Society of Edinburgh **26**, 1.
McNamara, S., and H. Herrmann (2004), Phys. Rev. E **70**, 061303.
McNamara, S., P. Richard, S. K. de Richter, G. Le Caer, and R. Delannay (2009a), Phys. Rev. E **80**, 031301.
McNamara, S., P. Richard, S. K. de Richter, G. Le Caer, and R. Delannay (2009b), "Overlapping histogram method for testing edward's statistical mechanics of powders," in *Powders and Grains 2009*, AIP Conference Proceedings, Vol. 1145, edited by M. Nakagawa and S. Luding (AIP) pp. 465–468.
Medvedev, N., and Y. Naberukhin (1987), J. Non-Crystall. Solids **94**, 402 .
van Meel, J. A., B. Charbonneau, A. Fortini, and P. Charbonneau (2009a), Phys. Rev. E **80**, 061110.
van Meel, J. A., D. Frenkel, and P. Charbonneau (2009b), Phys. Rev. E **79**, 030201.
Mehta, A., and S. Edwards (1990), Physica A **168**, 714.
Metzger, P. (2004), Phys. Rev. E **70**, 051303.
Metzger, P., and C. Donahue (2005), Phys. Rev. Lett. **94**, 148001.
Meyer, S., C. Song, Y. Jin, K. Wang, and H. A. Makse (2010), Physica A **389**, 5137.
Mézard, M., and A. Montanari (2009), *Information, Physics, and Computation* (Oxford University Press).
Mézard, M., and G. Parisi (2001), Eur. Phys. J. B **20**, 217.
Mindlin, R. D. (1949), Journal of Applied Mechanics (ASME) **71**, 259.
Miskin, M. Z., and H. M. Jaeger (2013), Nature Mater. **12**, 326.
Miskin, M. Z., and H. M. Jaeger (2014), Soft Matter **10**, 3708.
Moukarzel, C. F. (1998), Phys. Rev. Lett. **81**, 1634.
Moukarzel, C. F. (2005), "Response functions in isostatic packings," in *The Physics of Granular Media*, edited by H. Hinrichsen and D. E. Wolf (Wiley-VCH).
Mounfield, C., and S. Edwards (1994), Physica A **210**, 279.
Mueth, D. M., H. M. Jaeger, and S. R. Nagel (1998), Phys. Rev. E **57**, 3164.
Müller, M., and M. Wyart (2015), Annu. Rev. Cond. Matt. Phys. **6**, null.
Neudecker, M., S. Ulrich, S. Herminghaus, and M. Schröter (2013), Phys. Rev. Lett. **111**, 028001.
Newhall, K. A., I. Jorjadze, E. Vanden-Eijnden, and J. Brujić (2011), Soft Matter **7**, 11518.
Newman, C. M., and D. L. Stein (1999), Phys. Rev. E **60**, 5244.
Ngan, A. (2004), Physica A **339**, 207 .
Ngan, A. H. W. (2003), Phys. Rev. E **68**, 011301.
Nicodemi, M. (1999), Phys. Rev. Lett. **82**, 3734.
Nicodemi, M., A. Coniglio, A. de Candia, A. Fierro, M. Ciamarra, and M. Tarzia (2004), "Statistical mechanics of jamming and segregation in granular media," in *Unifying Concepts in Granular Media and Glasses*, edited by A. Coniglio, A. Fierro, H. Herrmann, and M. Nicodemi (Elsevier) pp. 47–61.
Nicodemi, M., A. Coniglio, and H. Herrmann (1997a), Physica A **240**, 405.
Nicodemi, M., A. Coniglio, and H. J. Herrmann (1997b), J. Phys. A **30**, L379.
Nicodemi, M., A. Coniglio, and H. J. Herrmann (1997c), Phys. Rev. E **55**, 3962.
Nicodemi, M., A. Coniglio, and H. J. Herrmann (1999), Phys. Rev. E **59**, 6830.
Norris, A. N., and D. L. Johnson (1997), J. App. Mech. **64**, 39.
Nowak, E., J. Knight, E. Ben-Naim, H. Jaeger, and S. Nagel (1998), Phys. Rev. E **57**, 1971.
Nowak, E., J. Knight, M. Povinelli, H. Jaeger, and S. Nagel (1997), Powd. Tech. **94**, 79.
O'Hern, C., A. Liu, and S. Nagel (2004), Phys. Rev. Lett. **93**, 165702.
O'Hern, C., L. Silbert, A. Liu, and S. Nagel (2003), Phys. Rev. E **68**, 011306.
O'Hern, C. S., S. A. Langer, A. J. Liu, and S. R. Nagel (2001), Phys. Rev. Lett. **86**, 111.
O'Hern, C. S., S. A. Langer, A. J. Liu, and S. R. Nagel (2002), Phys. Rev. Lett. **88**, 075507.
Okabe, A., B. Boots, K. Sugihara, and S. Nok Chiu (2000), *Spatial Tessellations: Concepts and Applications of Voronoi Diagrams* (Wiley-Blackwell).
Olsson, P., and S. Teitel (2007), Phys. Rev. Lett. **99**, 178001.

Ono, I., C. O'Hern, D. Durian, S. Langer, A. Liu, and S. Nagel (2002), Phys. Rev. Lett. **89**, 095703.

Onoda, G. Y., and E. G. Liniger (1990), Phys. Rev. Lett. **64**, 2727.

Onsager, L. (1949), Ann. N. Y. Acad. Sci. **51**, 627.

Oron, G., and H. Herrmann (1999), Physica A **265**, 455 .

Oron, G., and H. J. Herrmann (1998), Phys. Rev. E **58**, 2079.

Paillusson, F. (2015), Phys. Rev. E **91**, 012204.

Paillusson, F., and D. Frenkel (2012), Phys. Rev. Lett. **109**, 208001.

Palásti, I. (1960), Publ. Math. Res. Inst. Hung. Acad. Sci. **5**, 353.

Papanikolaou, S., C. S. O'Hern, and M. D. Shattuck (2013), Phys. Rev. Lett. **110**, 198002.

Parisi, G. (1988), *Statistical Field Theory* (Addison-Wesley).

Parisi, G., and F. Zamponi (2010), Rev. Mod. Phys. **82**, 789.

Parteli, E. J. R., J. Schmidt, C. Blumel, K.-E. Wirth, W. Peukert, and T. Poschel (2014), Sci. Rep. **4**.

Pathria, R. K., and P. D. Beale (2011), *Statistical Mechanics* (Elsevier).

Philippe, P., and D. Bideau (2002), Europhys. Lett. **60**, 677.

Philipse, A. (1996), Langmuir **12**, 1127.

Phillips, C. L., J. A. Anderson, G. Huber, and S. C. Glotzer (2012), Phys. Rev. Lett. **108**, 198304.

Portal, L., M. Danisch, A. Baule, R. Mari, and H. A. Makse (2013), J. Stat. Mech. , P11009.

Potiguar, F., and H. Makse (2006), Eur. Phys. J. E **19**, 171.

Pouliquen, O., M. Nicolas, and P. D. Weidman (1997), Phys. Rev. Lett. **79**, 3640.

Prados, A., J. Brey, and B. Sanchez-Rey (2000), Physica A **284**, 277.

Prados, A., and J. J. Brey (2002), Phys. Rev. E **66**, 041308.

Puckett, J. G., and K. E. Daniels (2013), Phys. Rev. Lett. **110**, 058001.

Puckett, J. G., F. Lechenault, and K. E. Daniels (2011), Phys. Rev. E **83**, 041301.

Qiong, C., and H. Mei-Ying (2014), Chin. Phys. B **23**, 074501.

Radeke, C., K. Bagi, B. Paláncz, and D. Stoyan (2004), Granular Matter **6**, 17.

Radin, C. (2008), J. Stat. Phys. **131**, 567.

Radjai, F., M. Jean, J.-J. Moreau, and S. Roux (1996), Phys. Rev. Lett. **77**, 274.

Radjai, F., and V. Richefeu (2009), Mech. Mater. **41**, 715 .

Rainone, C., and P. Urbani (2015), ArXiv e-prints arXiv:1512.00341 [cond-mat.soft].

Rényi, A. (1958), Publ. Math. Res. Inst. Hung. Acad. Sci. **3**, 109.

Ribiere, P., P. Richard, P. Philippe, D. Bideau, and R. Delannay (2007), Eur. Phys. J. E **22**, 249.

Richard, P., M. Nicodemi, R. Delannay, P. Ribiere, and D. Bideau (2005), Nature Mater. **4**, 121.

Richard, P., P. Philippe, F. Barbe, S. Bourles, X. Thibault, and D. Bideau (2003), Phys. Rev. E **68**, 020301.

Roberts, S. A. (1981), Journal of Physics C: Solid State Physics **14** (21), 3015.

Roth, L. K., and H. M. Jaeger (2016), Soft Matter **12**, 1107.

Rothenburg, L., and N. P. Kruyt (2009), J. Mech. Phys. Solids **57**, 634.

Roux, J.-N. (2000), Phys. Rev. E **61**, 6802.

Satake, M. (1993), Mech. Mater. **16**, 65 .

Schaller, F. M., S. C. Kapfer, M. E. Evans, M. J. F. Hoffmann, T. Aste, M. Saadatfar, K. Mecke, G. W. Delaney, and G. E. Schröder-Turk (2013), Philos. Mag. **93**, 3993.

Schaller, F. M., S. C. Kapfer, J. E. Hilton, P. W. Cleary, K. Mecke, C. D. Michele, T. Schilling, M. Saadatfar, M. Schröter, G. W. Delaney, and G. E. Schröder-Turk (2015a), EPL **111**, 24002.

Schaller, F. M., M. Neudecker, M. Saadatfar, G. W. Delaney, G. E. Schröder-Turk, and M. Schröter (2015b), Phys. Rev. Lett. **114**, 158001.

Schopenhauer, A. (1974), "Transcendent speculation on the apparent deliberateness in the fate of the individual," in *Parerga and Paralipomena: Short Philosophical Essays*, Vol. I (Oxford University Press) pp. 199–225.

Schreck, C. F., M. Mailman, B. Chakraborty, and C. S. O'Hern (2012), Phys. Rev. E **85**, 061305.

Schreck, C. F., N. Xu, and C. S. O'Hern (2010), Soft Matter **6**, 2960.

Schröder-Turk, G. E., W. Mickel, M. Schröter, G. W. Delaney, M. Saadatfar, T. J. Senden, K. Mecke, and T. Aste (2010), EPL **90**, 34001.

Schröter, M., D. Goldman, and H. Swinney (2005), Phys. Rev. E **71**, 030301.

Schwarz, J. M., A. J. Liu, and L. Q. Chayes (2006), EPL **73**, 560.

Scott, G. D. (1960), Nature **188**, 908.

Scott, G. D. (1962), Nature **194**, 956.

Shen, T., S. Papanikolaou, C. S. O'Hern, and M. D. Shattuck (2014), Phys. Rev. Lett. **113**, 128302.

Sherrington, D., and S. Kirkpatrick (1975), Phys. Rev. Lett. **35**, 1792.

Shum, H. C., A. R. Abate, D. Lee, A. R. Studart, B. Wang, C.-H. Chen, J. Thiele, R. K. Shah, A. Krummel, and D. A. Weitz (2010), Macromol. Rapid Commun. **31**, 108.

Shundyak, K., M. van Hecke, and W. van Saarloos (2007), Phys. Rev. E **75**, 010301.

Silbert, L., A. Liu, and S. Nagel (2005), Phys. Rev. Lett. **95**, 098301.

Silbert, L. E. (2010), Soft Matter **6**, 2918.

Silbert, L. E., D. Ertas, G. S. Grest, T. C. Halsey, and D. Levine (2002a), Phys. Rev. E **65**, 031304.

Silbert, L. E., G. S. Grest, and J. W. Landry (2002b), Phys. Rev. E **66**, 061303.

Silbert, L. E., A. J. Liu, and S. R. Nagel (2006), Phys. Rev. E **73**, 041304.

Silbert, L. E., A. J. Liu, and S. R. Nagel (2009), Phys. Rev. E **79**, 021308.

Skoge, M., A. Donev, F. H. Stillinger, and S. Torquato (2006), Phys. Rev. E **74**, 041127.

Smith, K. C., T. S. Fisher, and M. Alam (2011), Phys. Rev. E **84**, 030301.

Snoeijer, J., T. Vlugt, W. Ellenbroek, M. van Hecke, and J. van Leeuwen (2004), Phys. Rev. E **70**, 061306.

Sohn, H. Y., and C. Moreland (1968), Canad. J. Chem. Eng. **46**, 162.

Somfai, E., M. van Hecke, W. G. Ellenbroek, K. Shundyak, and W. van Saarloos (2007), Phys. Rev. E **75**, 020301.

Song, C., P. Wang, Y. Jin, and H. A. Makse (2010), Physica A **389**, 4497 .

Song, C., P. Wang, and H. Makse (2005), Proc. Nat. Acad. Sci. **102**, 2299.

Song, C., P. Wang, and H. A. Makse (2008), Nature **453**, 629.

Srebro, Y., and D. Levine (2003), Phys. Rev. E **68**, 061301.

Tarjus, G., and P. Viot (2004), Phys. Rev. E **69**, 011307.

Thue, A. (1892), Forand. Skand. Natur. **14**, 352.

Tian, J., Y. Xu, Y. Jiao, and S. Torquato (2015), Sci. Rep.

5, 16722 EP .
Tighe, B. P., A. R. T. van Eerd, and T. J. H. Vlugt (2008), Phys. Rev. Lett. **100**, 238001.
Tighe, B. P., J. H. Snoeijer, T. J. H. Vlugt, and M. van Hecke (2010), Soft Matter **6**, 2908.
Tighe, B. P., and T. J. H. Vlugt (2010), J. Stat. Mech. , P01015.
Tighe, B. P., and T. J. H. Vlugt (2011), J. Stat. Mech. , P04002.
Tkachenko, A. V., and T. A. Witten (2000), Phys. Rev. E **62**, 2510.
Toninelli, C., G. Biroli, and D. S. Fisher (2006), Phys. Rev. Lett. **96**, 035702.
Tonks, L. (1936), Phys. Rev. **50**, 955.
Torquato, S., and Y. Jiao (2009), Nature **460**, 876.
Torquato, S., and Y. Jiao (2010), Phys. Rev. E **82**, 061302.
Torquato, S., and Y. Jiao (2012), Phys. Rev. E **86**, 011102.
Torquato, S., and F. Stillinger (2010), Rev. Mod. Phys. **82**, 2633.
Torquato, S., and F. H. Stillinger (2001), J. Phys. Chem. B **105**, 11849.
Torquato, S., and F. H. Stillinger (2003), Phys. Rev. E **68**, 041113.
Torquato, S., and F. H. Stillinger (2006), Phys. Rev. E **73**, 031106.
Torquato, S., T. M. Truskett, and P. G. Debenedetti (2000), Phys. Rev. Lett. **84**, 2064.
Trappe, V., V. Prasad, L. Cipelletti, P. N. Segre, and D. A. Weitz (2001), Nature **411**, 772.
Unger, T., J. Kertesz, and D. Wolf (2005), Phys. Rev. Lett. **94**, 178001.
Valverde, J. M., M. A. S. Quintanilla, and A. Castellanos (2004), Phys. Rev. Lett. **92**, 258303.
Walton, K. (1987), J. Mech. Phys. Solids **35**, 213 .
Wang, C., K. Dong, and A. Yu (2015), Phys. Rev. E **92**, 062203.
Wang, K., C. Song, P. Wang, and H. A. Makse (2010a), EPL **91**, 68001.
Wang, K., C. Song, P. Wang, and H. A. Makse (2012), Phys. Rev. E **86**, 10.1103/PhysRevE.86.011305.
Wang, P., C. Song, C. Briscoe, and H. A. Makse (2008), Phys. Rev. E **77**, 10.1103/PhysRevE.77.061309.
Wang, P., C. Song, C. Briscoe, K. Wang, and H. A. Makse (2010b), Physica A **389**, 3972.
Wang, P., C. Song, Y. Jin, and H. A. Makse (2011), Physica A **390**, 427.
Wang, P., C. Song, Y. Jin, K. Wang, and H. A. Makse (2010c), J. Stat. Mech. 10.1088/1742-5468/2010/12/P12005.
Wang, P., C. Song, and H. A. Makse (2006), Nature Phys. **2**, 526.
Weaire, D., and T. Aste (2008), *The pursuit of perfect packing* (CRC Press).
Williams, S. R., and A. P. Philipse (2003), Phys. Rev. E **67**, 051301.
Wouterse, A., S. Luding, and A. P. Philipse (2009), Granular Matter **11**, 169.
Wyart, M. (2005), Annales de Physique **30**, 1.
Wyart, M. (2010), EPL **89**, 64001.
Wyart, M. (2012), Phys. Rev. Lett. **109**, 125502.
Wyart, M., S. Nagel, and T. Witten (2005a), EPL **72**, 486.
Wyart, M., L. Silbert, S. Nagel, and T. Witten (2005b), Phys. Rev. E **72**, 051306.
Xia, C., J. Li, Y. Cao, B. Kou, X. Xiao, K. Fezzaa, T. Xiao, and Y. Wang (2015), Nature Commun. **6**.
Xu, N., J. Blawzdziewicz, and C. O'Hern (2005), Phys. Rev. E **71**, 061306.
Xu, N., D. Frenkel, and A. J. Liu (2011), Phys. Rev. Lett. **106**, 245502.
Yang, R., R. Zou, and A. Yu (2000), Phys. Rev. E **62**, 3900.
Yi, G.-R., D. J. Pine, and S. Sacanna (2013), J. Phys. Cond. Mat. **25**, 193101.
Zaccarelli, E. (2007), J. Phys. Cond. Mat. **19**, 323101.
Zaccone, A., and E. Scossa-Romano (2011), Phys. Rev. B **83**, 184205.
Zhang, H., and H. Makse (2005), Phys. Rev. E **72**, 011301.
Zhao, J., S. Li, R. Zou, and A. Yu (2012), Soft Matter **8**, 1003.
Zhou, J., S. Long, Q. Wang, and A. D. Dinsmore (2006), Science **312**, 1631.